EQUILIBRIUM $^{2}H/^{1}H$ FRACTIONATIONS IN ORGANIC MOLECULES

Thesis by

Ying Wang

In Partial Fulfillment of the Requirements for the degree of

Doctor of Philosophy

CALIFORNIA INSTITUTE OF TECHNOLOGY

Pasadena, California

2010

(Defended September 30, 2009)

To my family

献给我的家人

ACKNOWLEDGEMENTS

In the winter of 2004, as a first-year graduate student, I was looking for the opportunity for the second proposal to fulfill my Ph.D. qualification exam. After talking to Prof. Paul Wennberg about my background and interests, he decided to introduce me to the next-door office. “But I do not have a biology background,” I worried before he knocked at the door. “Alex does not have one either.” said Paul. Thus I met Prof. Alex Sessions, who later became my Ph.D. advisor. During that first talk with Alex, to my surprise, he generously provided four potential projects. Now I remember only two of them: slice a long sediment core into fine layers and analyze the organic hydrogen isotopes, maybe also carbon, of each layer; or investigate the equilibrium fractionation of hydrogen isotopes in organic molecules using some innovative — at least to me — ab initio QM calculations. Without hesitation, I chose the latter. All I thought was: “It is at Caltech.”

Today, when that second proposal has evolved into this thesis, I want to express my most sincere appreciations to Alex, not only for his guidance, support, and tremendous patience that helped me complete this thesis, but also for his inspiring ways of doing scientific research that had a big impact on my transition from a student to a scientist. His open mind and versatility which actively generate ideas from both theoretical and experimental aspects have encouraged me to keep learning and exploring fields of great diversity. His pursuits of details and questioning on “coincidences” have taught me the attitudes of a real scientist. I am also grateful to Prof. George Rossman, my academic advisor and a good friend, whose encouragement, mentoring, and superb enthusiasm helped me adapt to the challenging and intensive life at Caltech throughout my graduate study. I want to thank Prof. Willian Goddard and Prof. John Eiler, who have been extraordinarily generous with their time and thoughts to offer me insightful advice. I also want to thank Prof. Arndt Schimmelmann at Indiana University, who kindly analyzed the organic standards used in this study.

The work presented in this thesis also benefited greatly from my colleagues within Prof. Sessions’ group, Prof. Goddard’s group, and Prof. Eiler’s group, including Megnas

Eek, Li Chao, Alon Amrani, Sarah Feakins, Ashley Jones, Xinning Zhang, Sky Rashby, Anne Dekas, Maggie Osburn, Lichun Zhang, Ling Gao, Robert Nielsen, Adri van Duin, Julie O'Leary, Weifu Guo, Zhengrong Wang, Hagit Affek, Laurent Remusat, and Nivedita Thiagarajan.

My life and study at Caltech were made unforgettable by my precious friends. They are Kendra Turk, Ben Harrison, Ben Hickey, Jie Cheng, Xin Guo, Min Chen, Kaveh Pahlevan, Gretchen Aleks, Margarita Marinova, Lingsen Meng, Le Kuai, Lijun Liu, Daoyuan Sun, Ting Chen, William Amidon, Ravi Kanda, Zhaoyan Zhu, Ling Zheng, Fei Wang, Athena Trentin, Yujiu Wang, Bo Li, Dongping Zhuang, Yue Zou, Yi Liu, Jigang Wu, Molei Tao, Chunhui Gu, Mo Li, Ru He, Yun-hsueh Rita Liu, and Yizhou Liu.

At last, I would like to present my most special thanks to my parents, Jianqiong Wang and Qiongma Xiong, and my husband, Hua Wang. Their unconditional love and support have always been the greatest treasure in my life.

ABSTRACT

Compound-specific H isotope analysis has become widespread over the past decade and stimulated a variety of studies using the H isotopic composition (δ^2H values) of sedimentary organic molecules as paleoenvironmental proxies. Since alkyl H can be affected by a variety of exchange processes that lead to δ^2H changes on geological timescales, interpretation of empirical δ^2H data must account for these changes, which requires quantitative knowledge regarding the endpoint of the isotopic exchange, i.e., equilibrium fractionation factor (α_{eq}). Nevertheless, to date relevant data have been lacking for molecules larger than methane. This is because the conventional isotope exchange experiments suffer from the slow exchange rates of C-bound H (half-life ~ 10^5–10^6 years), whereas theoretical calculations — a convenient way to cover many organic structures over wide temperature ranges — are restricted by systematic biases for the H isotope system.

To remedy the situation, this project was proposed to use experimental equilibration data to calibrate ab initio calculations of α_{eq}. To accurately measure the value of α_{eq} within reasonable experimental timescale, I utilized the keto-enol tautomerism that leads to fast equilibration between H positions adjacent to carbonyl groups (denoted as H_α) and water. By equilibrating ketones with waters of varying δ^2H values, the values of α_{eq} were measured for H_α positions in a variety of acyclic and cyclic molecular structures at different temperatures. On the other hand, statistical thermodynamics and ab initio QM computations (B3LYP/6-311G**) were applied to calculate α_{eq} values for the same ketone molecules. Comparison between experimental and theoretical results yields a temperature-dependent linear calibration curve for linear molecules with slope = 1.081−0.00376T and intercept = 8.404−0.387T (T is temperature in degrees Celsius). For cyclic structures, the calibration is slightly different with slope of 1.44±0.05 and intercept of 32.8±5.1. Application of these calibration curves to more ab initio calculations generates the α_{eq} values for various H sites in alkanes, alkenes, ketones, carboxylic acids, esters, alcohols, and ethers, with the uncertainties estimated to be 10–25‰. The effects of functional groups were found to increase the value of α_{eq} for H next to electron-donating groups, e.g., −OR, −OH or −O(C=O)R, and to decrease the value of α_{eq} for H next to electron-withdrawing

groups, e.g., −(C=O)R or −(C=O)OR. It is analogous to the well-known substituent effects in the aromatic ring system.

Our results provide a modular dataset to calculate equilibrium $^{2}H/^{1}H$ fractionations for common molecules found in sediments and oils. By summing over individual H positions, the equilibrium fractionation relative to water between 0 and 100°C is estimated to be −70‰ to −90‰ for *n*-alkanes, around −100‰ for acyclic isoprenoids and −75 to −100‰ for steroids and hopanoids. The temperature dependence of these molecular fractionations is very weak within the relevant temperature range. The results agree well with field data for thermally mature hydrocarbons ($\delta^{2}H$ values between -80‰ and -110‰ relative to water; Schimmelmann et al., 2006), suggesting that the observed $\delta^{2}H$ changes in sedimentary organic matter can be confidently attributed to H exchange towards an equilibrium state.

Because of the need to accurately measure the widely-ranging $\delta^{2}H$ values encountered in natural and isotopically-exchanged samples, a side project was conducted to quantitatively investigate the isotopic memory effects in compound-specific $^{2}H/^{1}H$ analysis by gas chromatography/pyrolysis/isotope-ratio mass spectrometry (GC/P/IRMS), i.e., the situation in which the $^{2}H/^{1}H$ ratio of a given chromatographic peak affects that of the following peak(s). Through a series of experiments that employed synthesized esters with $\delta^{2}H$ varying by up to 1000‰, we were able to estimate the isotopic memory to be typically 2–4% of the nominal $\delta^{2}H$ difference between two adjacent peaks. It increases with decreasing time separation, increasing analyte abundance of the preceding peak, or increasing age of the pyrolysis reactor. Roughly half of the memory effect can be attributed to the H_2-adsorption process in the pyrolytic reactor, and the other half to unknown processes within the GC. Finally, based on our experimental and model study, modifications in routine analyses were proposed to mitigate memory effects.

TABLE OF CONTENTS

LIST OF FIGURES

LIST OF TABLES

INTRODUCTION

Aligned with my great interests in isotope geochemistry and biogeochemistry, the main thread of my PhD research has been focusing on the quantitative investigation of equilibrium $^2H/^1H$ fractionation (α_{eq}) of organic H, with the goal of providing building blocks to calculate accurate fractionation factors for geo-relevant organic molecules. Based on the need in this project to accurately measure the δ^2H value of highly ^2H-enriched molecules, I also completed a side project to quantitatively evaluate the isotopic memory effects in compound-specific $^2H/^1H$ analysis by gas chromatography/pyrolysis/isotope-ratio mass spectrometry (GC/P/IRMS). Therefore, my thesis is composed of two parts: I. Equilibrium $^2H/^1H$ fractionation in organic molecules (consisting of Chapters 1, 2, and 3); and II. Memory effects in compound-specific $^2H/^1H$ analysis by GC/P/IRMS (consisting of Chapter 4). The background and relevance of this study are presented below, followed by brief introduction of each chapter.

Recent advances in compound-specific H isotope methodology and instrumentation (Sessions et al., 1999; Sessions and Hayes, 2005) have stimulated great interests in using compound-specific $^2H/^1H$ analysis to study sedimentary organic matter (SOM) and fossil fuels (Xie et al., 2000; Huang et al., 2002; Dawson et al., 2005). Most researchers tend to view δ^2H data as another isotopic fingerprint, analogous to $\delta^{13}C$, to track sources of SOM, extract paleoenvironmental information, etc. But unlike organic C, organic H is exchangeable during diagenetic and catagenic reactions that leave the carbon skeleton intact (Sessions et al., 2004). The rate of isotopic exchange between an organic H atom and other available H (e.g., water, mineral H) is highly dependent on the organic structure. Alkyl H that is covalently bonded to C is normally considered the most isotopically conservative moiety. However, reduced bond strength and increased polarity of bonds can be introduced by nearby electron-withdrawing groups, which will increase the acidity and hence exchangeability of the alkyl H. Structures that stabilize charged transition states, such as aromatic rings and tertiary center, also tend to increase the rate of exchange (Schimmelmann et al., 2006). Consequently, the exchange half-life for alkyl H in SOM is

estimated to be on the order of 10^5–10^6 years below 100°C (Sessions et al. 2004), which is slow but geologically relevant.

In fact, concrete evidence for extensive H exchange in SOM has been widely observed in the field: (i) Fatty acids in fresh biomass are ubiquitously more ^{2}H-enriched relative to phytol by more than 100‰ (Sessions et al., 1999; Zhang and Sachs, 2007), but this biosynthetic fractionation is often missing or greatly reduced in sediments and oils. (ii) Systematic increases in δ^2H values with higher thermal maturation are widely observed for bulk SOM samples, extractable fractions (e.g., aliphatic, aromatic, and polar fractions) and individual molecules (Sessions et al. 2004; Schimmelmann et al., 2006). The increase is larger where the ambient water and organic matter differ more wildly, and is negligible where they differ by 80–110‰, a situation typically associated with high maturity (dos Santos and Hayes, 1999). Moreover, the changes in aromatic and isoprenoid molecules are faster than *n*-alkanes (Dawson et al., 2004; Pedentchouk et al., 2006). These patterns highlight the proposed mechanism that the exchange with relatively ^{2}H-enriched waters is the most important process controlling the post-burial δ^2H changes in SOM and petroleum, and that the distinctive δ^2H change patterns for different types of compounds arise from the variations in their equilibrium fractionation factor (α_{eq}) and exchange rate (Schimmelmann et al., 1999; Sessions et al. 2004; Schimmelmann et al., 2006). Moreover, it implicitly suggests that the equilibrium fractionation between alkyl H and water must lie in the range −80 to −110‰, a hypothesis ready to test if we know the value of equilibrium fractionation factor. On the other hand, to use the exchangeability of H as a process recorder of the thermal maturation, one needs to know the exchange "endpoint", again, the equilibrium fractionation factor and its temperature dependence.

In principle, equilibrium fractionation factors can be predicted from the partition function ratios of the two substances in equilibrium (Bigeleisen and Mayer, 1947; Urey, 1947). However, this method is implicitly restricted by several necessary approximations, which are potentially significant for hydrogen isotopic exchange at room temperature. Moreover, the calculation requires the value of molecular vibrational frequencies, for which spectroscopic measurements are scarce for ^{2}H-substituted molecules (Richet et al., 1977), while ab initio modeling is accompanied by unknown systematic uncertainties. The

alternative approach, isotope exchange experiments, suffered from extremely slow exchange rates of normal alkyl H in hydrocarbons (reviewed by Sesssions et al., 2004). Even though a variety of mineral catalysts and enzymes can be used to accelerate the exchange, they are likely to promote rearrangement, cleavage, and oxidation reactions that alter the molecular structure. Partial-exchange with ^2H_2O can amplify the change in δ^2H but does not reach the equilibrium state. Consequently, the overall uncertainty in reported theoretical estimates is typically ±100‰, almost equally large as the fractionation factors (Knyazev et al., 1992).

To circumvent the above difficulties, we measured the value of α_{eq} for relatively active H positions via isotope exchange experiments. The results are then used as anchor points to calibrate theoretical α_{eq} values of varying organic structures and eventually provide a modular dataset for organic moieties common to sedimentary organic matter. This type of compendium took experimentalist several decades to compile for O isotope system in minerals. With the assistance of computational chemistry, it can be done in just a few years for organic H.

The results of this study should enable a variety of new types of geochemistry investigation. Most immediately, we will be able to discern whether sedimentary hydrocarbons are in isotopic equilibrium with water or between different compounds, and thus to judge when they should be used to infer original environmental conditions. This would have a big impact on the paleoclimate community. More relevant to energy research, when isotopic equilibrium is attained, the temperature-dependence of equilibrium fractionations could contribute to basin thermal models, which would be most useful for temperatures < 200°C, much lower than the effective temperature range of most other geochemical thermometers. Also, $^2H/^1H$ ratios of source-rock formation water might be inferred from that of the hydrocarbons, which could help distinguish between potential source rocks. In cases where isotopic equilibrium is not reached, the approach to equilibrium can be used to quantitatively understand the kinetics of H exchange, e.g., the catalytic properties of different geochemical environments. It could also improve our understanding about the kinetics of hydrocarbon generation, especially the extent of H

transfer between kerogen and water in maturing source rocks. This is thought to be a key process in petroleum generation (Schimmelmann et al., 2006).

Chapter 1 focuses on the experimental and theoretical methodologies that were used to obtain α_{eq} values of organic H. We utilized the keto-enol tautomerism that leads to fast equilibration between H_α and water. By equilibrating linear ketones with waters of varying δ^2H values, the value of α_{eq} for H_α positions in a variety of molecular structures at different temperatures was measured and used to calibrate theoretical α_{eq} values for the same ketone molecules. Comparison between experimental and theoretical results yields a temperature-dependent linear calibration curve.

In Chapter 2, this calibration curve was applied to ab initio calculations for various H sites in linear alkanes, alkenes, ketones, carboxylic acids, esters, alcohols, and ethers, with the uncertainties estimated to be 10–20‰. The data provide a complete set of building blocks to calculate equilibrium $^2H/^1H$ fractionations for common linear molecules found in sediments and oils. Moreover, comparison of different H positions substantially improved our understanding of the relationship between chemical environments and the value of α_{eq}. Equilibrium fractionation was estimated for common linear biomarkers. The results agree well with field data for thermally mature hydrocarbons, providing strong evidence for the hypothesis that the post-burial δ^2H changes are primarily caused by H exchange towards an equilibrium state.

In Chapter 3, similar experimental and theoretical studies were conducted on cyclic ketones to investigate fractionations in the ring system. According to the stereochemistry that differentiates the axial and equatorial positions in cyclic ketones, the regression between experimental and theoretical α_{eq} values produces a calibration curve that is distinctive from the calibration based on acyclic ketones.

Chapter 4 is an investigation of the isotopic memory effect in compound-specific $^2H/^1H$ analyses by GC/P/IRMS, i.e., the situation in which the $^2H/^1H$ ratio of a given chromatographic peak affects that of the following peak(s). This effect can introduce significant errors to measurements with large inter-peak δ^2H variations and systematically bias the estimation of fractionation factors based on measurements of ^2H-enriched

compounds. We designed a series of experiments to quantitatively evaluate the memory effect in the GC/P/IRMS system and to investigate the potential mechanisms. In the end, modifications in routine analyses are proposed to mitigate memory effects.

REFERENCES

Dawson D., Grice K., Wang S. X., Alexander R. and Radke J. (2004) Stable hydrogen isotopic composition of hydrocarbons in torbanites (Late Carboniferous to Late Permian) deposited under various climatic conditions. *Org. Geochem.* **35**, 189–197.

Dawson D., Grice K. and Alexander R. (2005) Effect of maturation on the indigenous delta D signatures of individual hydrocarbons in sediments and crude oils from the Perth Basin (Western Australia). *Org. Geochem.* **36**, 95–104.

dos Santos Neto E. V. and Hayes J. M. (1999) Use of hydrogen and carbon stable isotopes characterizing oils from the Potiguar Basin (onshore) Northeastern Brazil. *AAPG Bulletin.* **83**, 496–18.

Huang Y. S., Shuman B., Wang Y. and Webb T. (2002) Hydrogen isotope ratios of palmitic acid in lacustrine sediments record late Quaternary climate variations. *Geology* **30**, 1103–1106.

Knyazev D. A., Myasoedov N. F. and Bochkarev A. V. (1992) The theory of the equilibrium isotope effects of hydrogen. *Russ. Chem. Rev.* **61**, 204–220.

Pedentchouk N., Freeman K. H. and Harris N. B. (2006) Different response of delta D values of n-alkanes, isoprenoids, and kerogen during thermal maturation. *Geochim. Cosmochim. Acta* **70**, 2063–2072.

Richet P., Bottinga Y. and Javoy M. (1977) Review of hydrogen, carbon, nitrogen, oxygen, sulfur, and chlorine stable isotope fractionation among gaseous molecules. *Ann. Rev. Earth Planet. Sci.* **5**, 65–110.

Schimmelmann A., Sessions A. L. and Mastalerz M. (2006) Hydrogen isotopic composition (D/H) of organic matter during diagenesis and thermal maturation. *Ann. Rev. Earth Planet. Sci.* **34**, 501–533.

Sessions A. L. and Hayes J. M. (2005) Calculation of hydrogen isotopic fractionations in biogeochemical systems. *Geochim. Cosmochim. Acta* **69**, 593–597.

Sessions A. L., Burgoyne T. W., Schimmelmann A. and Hayes J. M. (1999) Fractionation of hydrogen isotopes in lipid biosynthesis. *Org. Geochem.* **30**, 1193–1200.

Sessions A. L., Sylva S. P., Summons R. E. and Hayes J. M. (2004) Isotopic exchange of carbon-bound hydrogen over geologic timescales. *Geochim. Cosmochim. Acta* **68**, 1545–1559.

Xie S., Nott C. J., Avsejs L. A., Volders F., Maddy D., Chambers F. M., Gledhill A., Carter J. F. and Evershed R. P. (2000) Palaeoclimate records in compound-specific delta D values of a lipid biomarker in ombrotrophic peat. *Org. Geochem.* **31**, 1053–1057.

Zhang Z. and Sachs J. P. (2007) Hydrogen isotope fractionation in freshwater algae: I. Variations among lipids and species. *Org. Geochem.* **38**, 582–608

C h a p t e r 1

EQUILIBRIUM $^{2}H/^{1}H$ FRACTIONATIONS IN ORGANIC MOLECULES.

I. EXPERIMENTAL CALIBRATION OF AB INITIO CALCULATIONS

Ying Wang[1], Alex L. Sessions[1], Robert J. Nielsen[2] and William A. Goddard III[2]

[1]Division of Geological and Planetary Sciences,
[2]Materials and Process Simulation Center,
California Institute of Technology, Pasadena, CA, USA

(*Geochimica et Cosmochimica Acta*, 2009, *in press*)

ABSTRACT

Carbon-bound hydrogen in sedimentary organic matter can undergo exchange over geologic timescales, altering its isotopic composition. Studies investigating the natural abundance distribution of ^{1}H and ^{2}H in such molecules must account for this exchange, which in turn requires quantitative knowledge regarding the endpoint of exchange, i.e., the equilibrium isotopic fractionation factor (α_{eq}). To date, relevant data have been lacking for molecules larger than methane. Here we describe an experimental method to measure α_{eq} for C-bound H positions adjacent to carbonyl group (H_{α}) in ketones. H at these positions equilibrates on a timescale of days as a result of keto-enol tautomerism, allowing equilibrium $^{2}H/^{1}H$ distributions to be indirectly measured. Molecular vibrations for the same ketone molecules are then computed using Density Functional Theory at the B3LYP/6-311G** level and used to calculate α_{eq} values for H_{α}. Comparison of experimental and computational results for six different straight and branched ketones yields a temperature-dependent linear calibration curve with slope = 1.081 − 0.00376T and intercept = 8.404 − 0.387T, where T is temperature in degrees Celsius. Since the dominant systematic error in the calculation — omission of anharmonicity — is of the same size for ketones and C-bound H in most other linear compounds, we propose that this calibration can be applied to analogous calculations for a wide variety of organic molecules with linear carbon skeletons for temperatures below 100°C. In Chapter 2 we use this new calibration dataset to calculate the temperature-dependent equilibrium isotopic fractionation factors for a range of linear hydrocarbons, alcohols, ethers, ketones, esters, and acids.

1. INTRODUCTION

Studies of the natural abundance distribution of the stable isotopes of hydrogen (^{1}H and ^{2}H) have facilitated many important scientific findings, ranging from the fundamental basis for isotope effects (Urey et al., 1932; Urey and Rittenberg, 1933) to ecological studies (Estep and Hoering, 1981; Sternberg et al., 1984), paleoclimate reconstructions (Feng and Epstein, 1994), and the origins of petroleum hydrocarbons (Schoell and Whiticar, 1982; Whiticar et al., 1985). More recently, the ability to measure ^{2}H/^{1}H ratios in individual lipid compounds has enabled many new applications, including the biochemical basis for biosynthetic fractionations (Sessions et al., 1999; Chikaraishi et al., 2004 a,b; Zhang and Sachs, 2007; Zhang et al., 2009), apportioning marine versus terrestrial sources of lipids (Chikaraishi and Naraoka, 2003; Li et al., 2009), reconstruction of paleoenvironment (Dawson et al., 2004; Krull et al., 2006), more detailed paleoclimate studies (Pagani et al., 2006; Sachs et al., 2009), the role of H transfer in source rock maturation and petroleum generation processes (Schimmelmann et al., 1999; Schimmelmann et al., 2004), and the origin of extremely ^{2}H-enriched compounds in carbonaceous meteorites (Huang et al., 2005; Gourier et al., 2008).

Hydrogen in organic molecules is affected by a variety of exchange processes that can lead to changes in isotopic composition without concomitant changes in molecular structure (Sessions et al., 2004; Schimmelmann et al., 2006). The timescale for such exchange is highly dependent on organic structure, and ranges from seconds for loosely bound H (such as in OH and NH moieties) to millions of years for aliphatic C-bound H at room temperature (Schimmelmann et al., 2006). For studies of individual lipids seeking to reconstruct original biotic or environmental variables, identifying and avoiding such exchange is key (e.g., Andersen et al., 2001; Pedentchouk et al., 2006). For other studies seeking to understand the diagenesis and thermal maturation of sedimentary organic matter (e.g., Schimmelmann et al., 1999; Dawson et al., 2005), the extent and results of exchange are of primary interest. Regardless, in all cases interpreting empirical data requires knowledge of the ^{2}H/^{1}H distribution expected to result from exchange, i.e., the temperature-dependent equilibrium isotopic fractionation factor (α_{eq}). To cite just one example, observations that sedimentary leaf-wax lipids have very different δ^2H values than co-

occurring water have been used to argue that H exchange in *n*-alkanes is very slow (Yang and Huang, 2003). However, such arguments cannot be developed quantitatively unless the resulting equilibrium fractionation is accurately known.

Estimates of equilibrium $^{2}H/^{1}H$ fractionations are also relevant to isotopic studies of bulk organic hydrogen, where the contribution from rapidly exchanging H positions must be accounted for (Schimmelmann, 1991). This is typically achieved experimentally by forcing isotopic exchange with water vapors having different $^{2}H/^{1}H$ values (Schimmelmann et al., 1999; Sauer et al., 2009). The results of this differential exchange allow the contribution of exchangeable positions to the bulk H pool to be calculated. However, further calculation of the $^{2}H/^{1}H$ ratio of nonexchangeable H by mass balance requires knowledge of the equilibrium fractionation factors for exchangeable H positions, which are difficult to obtain experimentally. Only a few estimates for essentially pure substances (e.g., cellulose) are currently available (Schimmelmann, 1991).

To date, there have not been any precise estimates for α_{eq} values in organic compounds larger than methane. Isotope exchange experiments proceed far too slowly for most aliphatic H, with exchange half-lives typically 10^{5}–10^{6} years at 200°C for aromatic and saturated hydrocarbons without catalysis (reviewed by Sessions et al., 2004). Partial exchange with $^{2}H_{2}O$ is commonly employed to amplify $\delta^{2}H$ shifts (Koepp, 1978; Larcher et al., 1986), but this approach precludes measuring equilibrium fractionations because equilibrium is not reached. Similarly, mineral catalysts and/or high temperatures which speed equilibration often promote side reactions, including rearrangement and oxidation, which confound measurements of pure equilibrium partitioning (Sessions et al., 2004). A few experimental studies have employed isomerase enzymes to catalyze ^{3}H incorporation into the methyl group of malate (Thomson, 1960) and pyruvate (Meloche et al., 1977) at 35°C and thus deduced the equilibrium fractionation for $^{2}H/^{1}H$ exchange. While useful for some organic species, this approach is not suitable for many molecules that interest organic geochemists, particularly hydrocarbons.

Theoretical calculation of α_{eq}, the alternative approach, was first developed by Urey (1947) and Bigeleisen and Mayer (1947) based on the vibrational energy differences

between isotopologues. Although proven to yield accurate results for many isotopic systems, theoretical calculations have not generally been applied to hydrogen isotopes in organic molecules for several reasons. Calculation of the reduced partition function ratio (β factor) requires known molecular vibrational frequencies — generally based on spectroscopic measurements — which are not available for most ^{2}H-substituted organic molecules relevant to natural systems (Richet et al., 1977; O'Neil, 1986). Computational methods based on molecular simulations, including empirical force fields (Hartshorn and Shiner, 1972) and ab initio modeling (Liu and Tossell, 2005; Hill and Schauble, 2008; Otake et al., 2008) do not require measured vibrational frequencies as inputs, but are accompanied by unknown, and potentially large, systematic errors. This is primarily due to several necessary approximations, including the omission of anharmonicity, rotational corrections, and rotation-vibration coupling terms, which are potentially significant for hydrogen isotopic exchange at room temperature (Richet et al., 1977). Finally, the theory is based on ideal gases, whereas many natural fractionation processes take place in aqueous solution where interactions with solvent molecules could significantly affect internal vibrational modes and contribute to uncertainty (Jancso and Van Hook, 1974).

As a consequence of these difficulties, theoretical estimates for α_{eq} values reported to date are of high precision but poor or unknown accuracy. For example, the overall uncertainty in reported α_{eq} values between aliphatic H and water is typically ±100‰ (Van Hook, 1968; Knyazev et al., 1992; Sessions et al., 2004), almost as large as the fractionation itself. Nevertheless, theoretical calculations provide the only plausible means for estimating α_{eq} values in the huge number of varying organic structures that are encountered in the natural environment. Thus the most efficient way forward is to use empirical and/or experimental data to calibrate a subset of theoretical calculations, which can then be used to efficiently evaluate a much larger range of related structures.

Here we demonstrate one approach to using experimental equilibration data to calibrate theoretical estimates of α_{eq} values. Organic H positions adjacent to carbonyl groups (denoted as H_{α}) undergo rapid equilibration with water H via keto-enol tautomerism under acid or base catalysis (Appendix 1), with exchange half-lives varying from minutes to a few years depending on temperature and pH (Amyes and Richard, 1996; Richard et al.,

2001). By equilibrating ketones with waters of varying δ^2H values and measuring the resulting δ^2H values of the ketones at equilibrium, the value of α_{eq} for H_α positions can be derived. Multiple experiments using different molecular structures and different temperatures yield an appropriate calibration dataset for theoretical calculations.

In this chapter, we describe the experimental and theoretical methods used to obtain α_{eq} values for exchangeable H in ketones, and report the values of α_{eq} between 0–100°C in seven different structures. We discuss potential sources of error in the experimental measurements and theoretical calculations, and possible applications of the experimental-theoretical calibration. In Chapter 2, we use the calibration dataset presented here to calculate α_{eq} values for C-bound H in a much wider range of organic molecules with *n*-alkyl skeletons that are relevant to natural environments.

2. NOTATION AND NOMENCLATURE

Throughout this paper, H without superscripts is used to denote hydrogen atoms irrespective of isotopic species, whereas ^1H and ^2H indicate a specific isotope. Hydrogen isotopic data ($^2H/^1H$ ratios) are reported as δ^2H values relative to the Vienna Standard Mean Ocean Water (VSMOW) international standard:

$$\delta^2H = \frac{(^2H/^1H)_{sample}}{(^2H/^1H)_{VSMOW}} - 1 \tag{1-1}$$

The permil (‰) symbol used in conjunction with δ^2H values implies a factor of 10^3 which is then omitted from Eq. 1-1. Differences in isotopic abundance between two species (e.g., organic compound and water) are described by the isotopic fractionation factor (α) and/or isotopic enrichment factor (ε):

$$\alpha_{A,B} = \frac{(^2H/^1H)_A}{(^2H/^1H)_B}, \quad \varepsilon_{A,B} = (\alpha_{A,B} - 1)$$

An organic molecule often contains H atoms in different groups which are not chemically equivalent and thus must be characterized by different fractionations (Knyazev et al., 1992; Criss, 1999). When equilibrium has been established between two organic molecules AH_m and BH_n, each containing q_A and q_B groups of equivalent H atoms, the fractionation factor between the two molecules can be estimated as (Galimov, 1971):

$$\alpha_{eq} = \frac{n\sum_{i}^{q_A} p_i \beta^i_{AH_m}}{m\sum_{j}^{q_B} p_j \beta^j_{BH_n}} \tag{1-2}$$

where β^i_{AHm} and β^j_{BHn} are the β factor of the *i*th group in AH_m and the β factor of the *j*th group in BH_n, respectively, and p_i and p_j are the number of equivalent H atoms in the *i*th and *j*th group. Eq. 1-2 shows that the β factor of the whole molecule takes on the form of the arithmetic mean of the individual beta factors weighted by the number of equivalent H atoms in each group.

Potential for confusion arises because our experiments compare isotopic compositions measured for entire molecules, inferred for certain molecular positions (e.g., all H adjacent to a carbonyl group), and calculated for specific, individual atoms. In the interest of clarity, we adopt the following conventions. (*i*) All δ^2H values refer to measured isotopic compositions for entire molecules. (*ii*) Values of α_{eq} (and ε_{eq} refer to $^2H/^1H$ fractionations between organic substrate and water in equilibrium at the specified temperature. The isotope ratio of water is always placed in the denominator, such that a normal isotope effect yielding organic matter depleted in ^2H relative to water results in α_{eq} values < 1, and ε_{eq} values < 0. Note that, when reporting experimental results, α_{eq} refers to all H_α atoms undergoing exchange even if they are not equivalent, such as would be measured in the asymmetric molecule 2-methyl-3-heptanone. In contrast, when reporting theoretical results, α_{eq} refers to the fractionation calculated only for equivalent hydrogen atoms (i.e., the two secondary H_α atoms in 2-methyl-3-heptanone). In each case, the meaning is specified in the text. (*iii*) In ab initio calculations, H_α positions normally thought to be equivalent (i.e., the three primary H_α atoms on the methyl group of 2-heptanone) yield slightly different

fractionations because the molecule is held in a static conformation for the calculations, ignoring the molecular rotations around C−C bonds that occur at ambient temperature. In these cases, we average the fractionations for all nominally equivalent positions to yield a single fractionation factor, which is reported.

The Greek letters α and β are conventionally used to denote the position of carbon atoms relative to a functional group. Unfortunately, they are also used by geochemists to refer to the fractionation factor (α) and reduced partition function ratio (β), respectively. To minimize confusion, we use Greek letters as subscripts to indicate molecular positions, e.g., H_α is the hydrogen atom attached to the first carbon center adjacent to the carbonyl group, H_β is one additional C−C bond further removed, etc. Greek letters not used as subscripts always refer to isotopic fractionations (α_{eq}) or reduced partition function ratios (β).

3. METHODS

3.1. Experimental methods

Seven different volatile ketones were selected as substrates for experimental equilibration with water. Each ketone was fully dissolved in deionized water, sealed in closed vessels with minimal headspace and incubated at constant temperature. At selected time points, samples were removed and the ketone extracted into hexane. The δ^2H values of both ketone and water were then analyzed. The value of α_{eq} between exchangeable H and water at equilibrium can be derived from the slope of a regression between δ^2H values of the ketone and the corresponding waters. Detailed descriptions of each step are presented below.

3.1.1. Materials

Selection of organic substrates is constrained by several factors. Molecules containing a carbonyl functional group are required for rapid equilibration. Given that aldehydes tend to oxidize and esters tend to hydrolyze in basic and acidic conditions, we chose ketones as the

substrates for equilibration. To achieve sufficient concentration for isotopic analysis, the aqueous solubility of the substrate must be higher than ~2.5 mM (assuming 100% extraction efficiency), which excludes ketones of carbon number ≥ 10. Small molecules are also preferred because they contain relatively more exchangeable H and thus can produce greater δ^2H shifts during equilibration. However, as size decreases the molecule becomes more hydrophilic and harder to extract. Chromatographic resolution from the solvent peak also becomes more difficult, which thus excludes ketones of carbon number ≤ 4.

Consequently, we chose 7 ketones ranging from C_6 to C_9, including 2-heptanone (99%), 4-heptanone (98%), 5-nonanone (98%), 2-methyl-3-hexanone (99%), 2,4-dimethyl-3-pentanone (98%), 3,5-dimethyl-4-heptanone (97%) and cyclohexanone (99%). All were obtained from Sigma-Aldrich. They contain primary, secondary, and tertiary H_α in linear (straight and branched) ketones and secondary H_α in a cyclic ketone. Fig. 1-1 gives ball and stick depictions of the optimized structure of each molecule resulting from ab initio modeling (see 3.2.2.). A large amount of ^2H-enriched water was prepared from distilled water by addition of ^2H_2O (99.5%, Cambridge Isotope Laboratories), and was then mixed with ^2H-depleted water (obtained from a melted Antarctic ice core) at varying volume ratios to produce series of 7–9 waters with evenly spaced δ^2H values between −286‰ and +480‰. This range brackets the δ^2H values of the unexchanged ketone substrates so that equilibrium can be approached from both directions.

3.1.2. Isotope exchange experiments

Ketones were individually dissolved in each of the 7–9 waters to form 51 different ketone-water solutions. Concentrations of the solutions ranged between 10 and 22 mM, depending on the solubility of the ketone. Solution pH was adjusted to either 12 or 1 with NaOH or HCl, determined at 25°C using an EC500 pH Meter (Extech).

Experiments were conducted in two stages, with the first designed to estimate exchange rates and the second to accurately measure equilibrium fractionations. In the first stage of experiments, 100 mL aliquots of each solution were sealed in separate glass bottles with

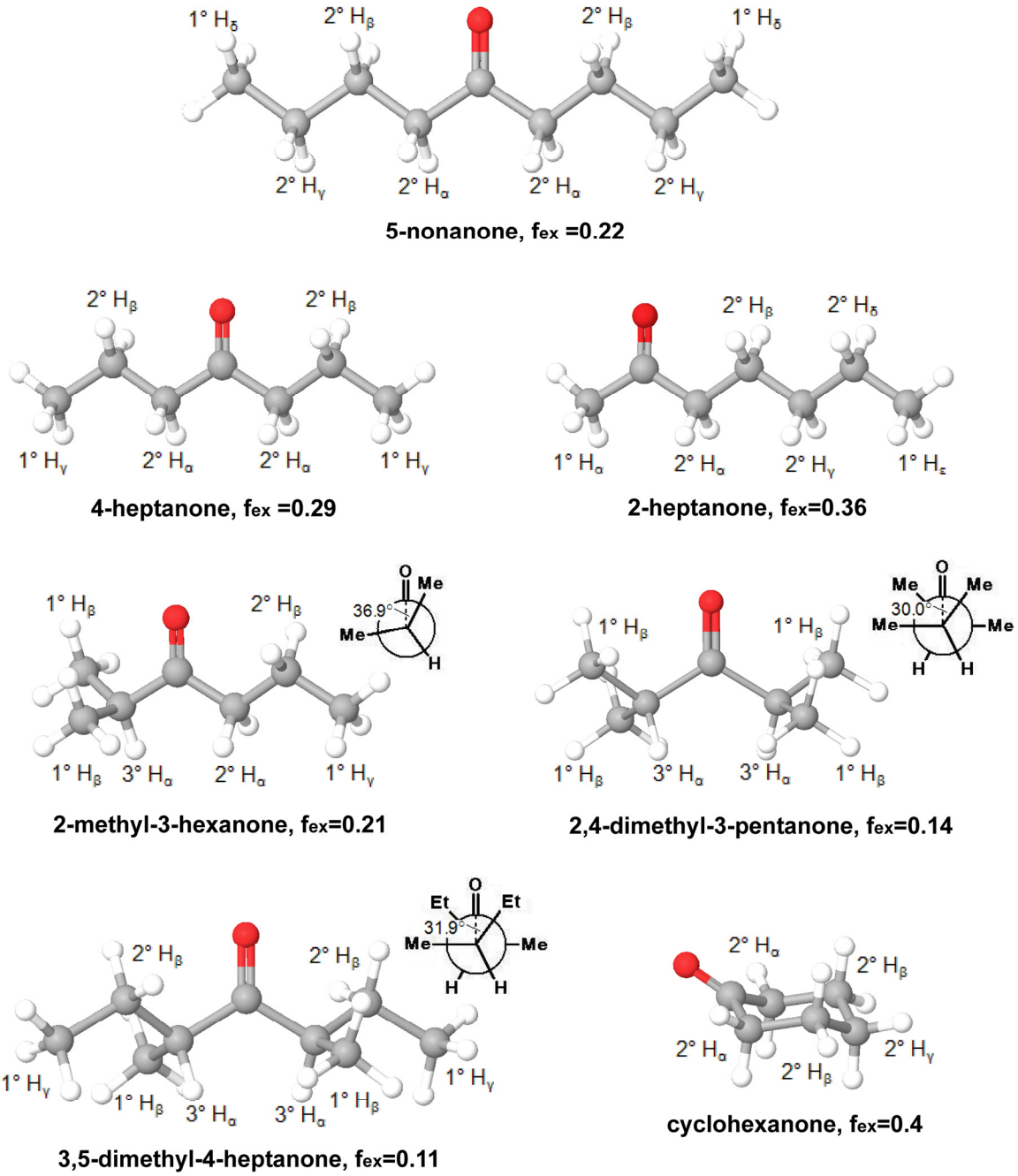

Figure 1-1. Optimized geometries of the 7 substrate ketone molecules (● = O, ● = C, ○ = H). H is labeled according to the relative distance from the carbonyl group (subscript Greek letters) and the configuration of the C atom (1° = primary, 2° = secondary, 3° = tertiary). f_{ex} is the fraction of exchangeable H in each molecule, assumed to be exclusively H_α (see 3.1.5.). The O=C-C_α-C_β dihedral angle is indicated for 2-methyl-3-hexanone, 2,4-dimethyl-3-pentanone and 3,5-dimethyl-4-heptanone.

rubber septa and incubated in a water bath (Model 202, Napco) at 25, 50 or 70°C. Aliquots (2 mL) were taken from each bottle at successive time intervals using a glass syringe. Each aliquot was immediately extracted by shaking with 6 mL of cold (−18°C) hexane, with extraction efficiencies of 80–95%. The extract was then analyzed without further concentration. From the temporal evolution of substrate δ^2H values and solution pH, exchange rates can be estimated according to the kinetics of second-order reactions (see 3.1.6.). Rate constants were measured for selected combinations of ketone substrate, temperature and pH (see Table 1-1) so as to estimate the time needed for each of the 7 substrates to reach equilibrium.

Although consecutive sampling of a single bottle yields an exchange profile for the substrate that demonstrates the achievement of equilibrium, repeatedly penetrating the rubber septum over a period of days to weeks can also lead to contamination of the sample with atmospheric water vapor and/or evaporation of the sample. Both effects will bias the measured fractionation factor. This is especially problematic at the highest temperature (70°C) employed here. Therefore, in the second stage of experiments three 2 mL aliquots of each solution were flame-sealed in glass ampoules so as to exclude any possible evaporation or exchange of water vapor. They were incubated at pH 12.00 in the water bath at 25 ± 0.5°C, 50 ± 0.8°C, or 70 ± 1.0°C, respectively. The length of incubation was determined according to rate constants from the first set of experiments, and was always at least 80 exchange half-lives to ensure equilibrium was reached. Following incubation, ampoules were removed from the water bath and quenched in a dry ice/hexane mixture to form ice-water slurry in less than 8 s. Each ampoule was then thawed at room temperature, cracked open, and extracted by shaking with 6 mL cold hexane. The purity of the extracted ketones was checked with a ThermoFinnigan Trace GC equipped with a DB-5ms column (30 m × 0.25 mm × 0.25 μm) and coupled to a DSQ mass spectrometer (GC/MS). In all cases one peak of greater than 99% purity was observed. The δ^2H value and pH of the water in three randomly selected ampoules were measured before and after the incubation, and no significant change was observed.

3.1.3. Isotopic analysis of ketones

The δ^2H value of each ketone substrate was measured before and after exchange on a ThermoFinnigan Trace GC coupled to a Delta^{plus}XP isotope-ratio mass spectrometer via a pyrolysis reactor (GC/P/IRMS). No Nafion drier was employed. The GC was equipped with a 30 m × 0.32 mm I.D. × 1.0 μm film-thickness EC^{TM}-1 column (Alltech) and a programmable temperature vaporization (PTV) injector that was operated in splitless mode. The pyrolysis tube (Al_2O_3, 0.8 mm I.D. x 305 mm long) was operated at 1440ºC. The flow rate of the carrier gas (He) was 1.4 mL/min. The temperature of the GC oven was initially kept at 40°C for 4 min, followed by three sequential ramps: 8°C/min to 100°C, 20°C/min to 200°C, and 6°C/min to 320°C. Methane reference gas (δ^2H = −148‰) introduced between the downstream end of the GC column and the pyrolysis reactor was used as the internal calibration standard (Wang and Sessions, 2008). Mass-2 and -3 signals were processed using ISODAT NT 2.5 software (ThermoElectron), and data were reported as δ^2H values relative to VSMOW in permil units. The H_3^+ factor was determined daily by measuring the mass 3/2 signal ratio of 10 injections of H_2 reference gas at varying peak height. The value of the H_3^+ factor was very stable at 3.0–3.3 ppm/mV.

Our GC/P/IRMS system exhibits a memory effect of 1–5% between successive peaks separated by 100 s (Wang and Sessions, 2008). If uncorrected, this memory could lead to errors up to 10‰ in the measurements of exchanged ketones, for which δ^2H ranges from −260‰ to +70‰. Moreover, these errors systematically increase with the value of δ^2H and hence will bias the derived fractionation factors. To avoid these problems, a combined calibration-normalization strategy was employed as follows. Three *n*-alkane standards, C_{17} (−142‰), C_{22} (−62.2‰), and C_{27} (−226.5‰), were co-injected with each ketone sample, and a group of four methane reference peaks spaced at 50 s intervals was inserted at 50 s before each of the analyte peaks (Fig. 1-2a). The last methane peak in each group was used to calibrate the δ^2H value of the following analyte. Since the peak area (mass-2) was identical (±7%) for each *n*-alkane standard and the ketone analyte, all of them were subject to equivalent memory effects from the preceding methane peaks. Therefore a normalization curve based on the three *n*-alkane standards can be used to correct for memory effects. δ^2H values for the seven exchanged samples of 2-methyl-3-heptanone and for the three *n*-alkane

standards in these measurements are plotted in Fig. 1-2b as an example. Each ketone sample was measured 2–5 times with standard deviation typically of 1–4‰ (complete δ^2H data are in Appendix Table 1-A1). The overall standard deviation for 306 measurements of the *n*-alkane standards was 4‰ for C_{17}, 3‰ for C_{22}, and 3‰ for C_{27}.

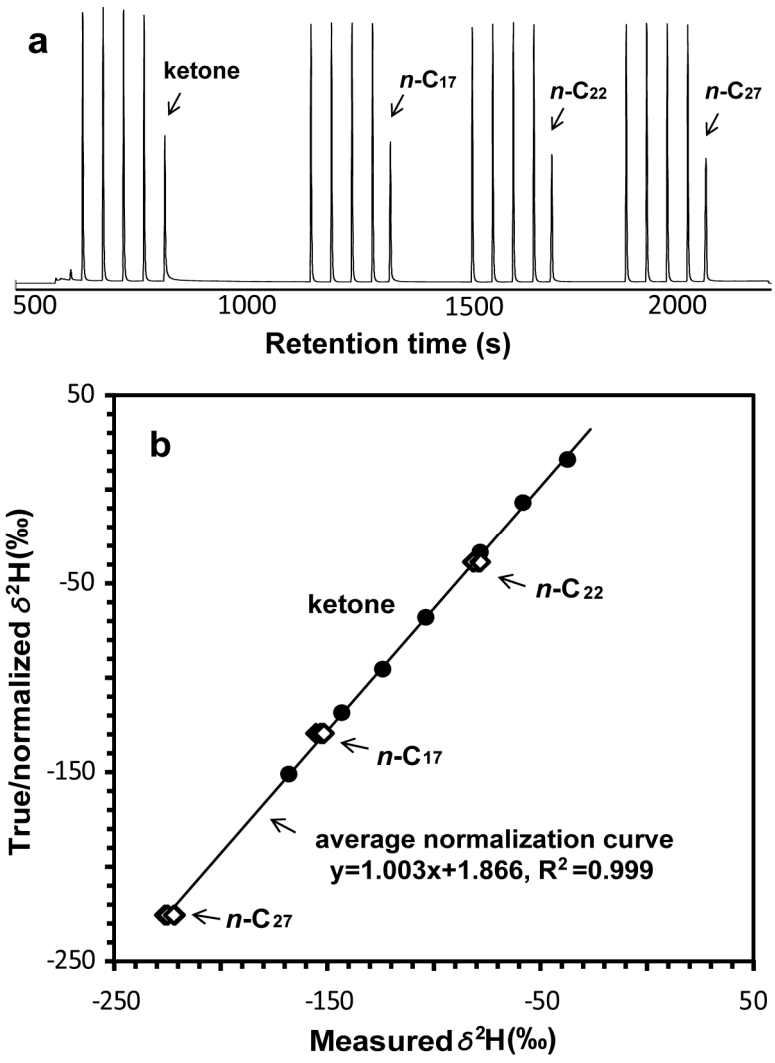

Figure 1-2. (a) GC/IRMS chromatogram (*m/z* 2) from a typical analysis of a ketone sample. Unlabelled peaks are methane reference gas. (b) Normalization curve constructed for analyses of 2-methyl-3-heptanone. The solid circles are data for the 2-methyl-3-heptanone samples exchanged with seven waters of varying δ^2H values. Open diamonds are for the three *n*-alkane standards associated with each analysis and largely overlap.

3.1.4. Isotopic analysis of water

The δ^2H value of water from each sample was analyzed with a DLT-100 liquid-water isotope analyzer (Los Gatos Research, Inc.). A constant volume of 0.65 μL was injected into a heated (70˚C) injection port, and 25 scans were averaged to produce the measured $^2H/^1H$ ratio. A flush cycle of 100 s was adopted between injections to purge residual water vapor from the laser cavity. Six consecutive injections of each sample or standard were measured, with the mean of the last three injections accepted as the final result. Six working standards spanning a similar δ^2H range (−275.2‰ to 457.6‰) as the samples were used for calibration. Since the samples are highly basic (pH 12), we ran the fresh standard every other sample to avoid base precipitates accumulating in the syringe or injection port (Lis et al., 2007). This procedure yielded standard deviations for measured δ^2H values typically of 0.2–0.4‰.

Because the water and ketone samples were analyzed by independent analytical systems with different standards, it is essential to insure that they are calibrated to the same δ^2H scale to avoid introducing systematic bias into derived fractionation factors. Both the water and organic standards used here were measured by Dr. A. Schimmelmann (Indiana University, Bloomington) using dual-inlet isotope-ratio mass spectrometry. Organic standards were first combusted to water in quartz tubes, and all waters were then reduced to H_2 over hot uranium metal (Schimmelmann and Deniro, 1993). In this way the analyses of both organic and water working standards were calibrated against the same IAEA water standards (VSMOW, SLAP, and GISP).

3.1.5. Calculation of equilibrium fractionation factors

At $^2H/^1H$ exchange equilibrium, the isotopic mass balance for a ketone molecule can be expressed as (Sessions and Hayes, 2005):

$$\delta_T = f_{ex}(\alpha_{eq}\delta_W + \alpha_{eq} - 1) + (1 - f_{ex})\delta_N \tag{1-3}$$

where δ_T, δ_W, and δ_N are the δ^2H values of the total organic molecule, water, and non-exchangeable H, respectively. f_{ex} is the fraction of exchangeable H in the ketone molecule.

α_{eq} is the average equilibrium fractionation factor between all exchangeable H in the molecule and water. By regressing δ_T on δ_W, the value of α_{eq} can be obtained from the value of the regression slope divided by f_{ex}, and δ_N can be calculated from the value of the intercept.

Since alkyl H typically exchanges on timescales of millions of years (Koepp, 1978), and keto-enol tautomerism only involves the carbonyl group and C_α position, we assume that only H_α in the ketone molecules is exchangeable during our experiments. The value of f_{ex} thus can be directly determined from the molecular structures (Fig. 1-1). This assumption can be tested by observing the constancy of δ_N for a ketone incubated at different temperatures.

3.1.6 Calculation of rate constants and activation energy for H_α exchange

Isotope exchange reactions between an organic molecule and water can be described by the first-order rate equation (Roberts and Urey, 1939; Wedeking and Hayes, 1983):

$$\frac{F_t - F_e}{F_i - F_e} = e^{-kt}$$

where k is the pseudo-first-order rate constant and F_i, F_t, and F_e are the fractional abundance of ^2H for the organic molecules *i*nitially, at time *t*, and at *e*quilibrium. At natural ^2H abundances, δ^2H values can be approximately substituted for Fs (Roberts and Urey, 1939; Sessions et al., 2004). Therefore by regressing $\ln[(\delta^2H_t-\delta^2H_e)/(\delta^2H_i-\delta^2H_e)]$ versus time, the apparent first-order rate constant (k_{obsd}) can be obtained as the negative slope. For base-catalyzed H_α exchange, $k_{obsd} = k_{OH}\,[OH^-]$, where k_{OH} is the second-order rate constant (see Appendix 1). Moveover, the substitution to give monodeuterated product proceeds p times faster than to exchange all the H_α atoms, where p is the number of equivalent H_α atoms in the molecule. Therefore the true value of k_{OH} is equal to $p\cdot k_{obsd}/[OH^-]$. Knowing k_{OH}, k_{obsd} can then be estimated at various pH values.

Activation energy was obtained according to the Arrhenius relationship,

$$k_{OH} = Ae^{-\frac{E_a}{RT}}$$

where E_a is the activation energy; T is temperature in Kelvin; R is the gas constant; A is a constant. By regressing the natural log of k_{OH} (measured at 25°C, 50°C and 70°C) versus reciprocal temperature, E_a can be calculated from the regression slope.

3.2. Computational methods

3.2.1. Estimation of equilibrium fractionation factors

$^2H/^1H$ exchange between two compounds, AH and BH, can be described by the reaction:

$$A^1H + B^2H = A^2H + B^1H$$

For the exchange of a single H atom, the value of α_{eq} is equal to that of the equilibrium constant, K_{eq}, which can be expressed as the ratio of the total partition function ratios between the compounds in equilibrium:

$$\alpha_{eq} = K_{eq} = \frac{Q(A^2H)/Q(A^1H)}{Q(B^2H)/Q(B^1H)} \quad (1\text{-}4)$$

where Q is the total partition function of the indicated species. It was first shown by Urey (1947) and Bigeleisen and Mayer (1947) that the total partition function ratio can be approximately described by molecular vibrations in the form of the reduced partition function ratio, known as the β factor. Therefore α_{eq} can be written as

$$\alpha_{eq} = \frac{\beta(AH)}{\beta(BH)} \quad (1\text{-}5)$$

The value of β, under the Born-Oppenheimer and Harmonic Oscillator approximations and the Redlich-Teller Product Rule, is calculated as:

$$\beta = \prod_{i}^{3N-6} \frac{u_{2i}}{u_{1i}} \cdot \frac{exp(-u_{2i}/2)}{exp(-u_{1i}/2)} \cdot \frac{(1-exp(-u_{1i}))}{(1-exp(-u_{2i}))} \tag{1-6}$$

in which

$$u_i = \frac{h\nu_i}{k_B T} \tag{1-7}$$

3*N*-6 is the number of normal modes for nonlinear molecules, ν_i is the vibrational frequency of the *i*th normal-mode, *h* is Planck's constant, k_B is Boltzmann's constant, and *T* is temperature in Kelvin. Symmetry numbers that would otherwise clutter the expression of β are omitted because they cancel in the calculation of α_{eq} (Eq. 1-5).

3.2.2. Ab initio modeling

Vibrational frequencies of each organic molecule were calculated using the Density Functional theory (DFT) approximation (Greeley et al., 1994) to quantum mechanics, performed using Jaguar 7.0 (Schrödinger Inc.). In particular we use the B3LYP flavor of DFT (Lee et al., 1988; Becke, 1993) which has been established to provide systematically accurate energetics, structures, and vibrational frequencies for a wide range of organic molecules (Xu et al., 2005). The B3LYP calculations used the 6-311G** basis set, a triple split-valence basis set with polarization functions on all atoms. The solvation effect for organic molecules was simulated using the Poisson-Boltzmann continuum solvation model (Tannor et al.1994) as implemented in Jaguar. These computations were carried out using the following procedures.

Starting with a best-guess molecular geometry, an optimized geometry was first calculated in the gaseous phase and then re-optimized in the aqueous phase. For molecules with branched carbon chains, we first performed a conformation scan of internal torsion with 15° increments (see 4.2.1.). The conformation with the minimum energy on the potential surface was then used as the initial guess for geometry optimization. The convergence criterion for the DFT electronic structure calculations was 5×10^{-5} hartree for energy and 5×10^{-6} hartree/Bohr for root-mean-squared (RMS) change in density matrix. The convergence criterion for optimization of the structures was 5×10^{-5} hartree for energy.

The convergence criteria for optimization in solution are three times larger than in the gas phase.

The Hessian matrix (second derivatives with respect to atom positions) was calculated numerically for the optimized geometry. The same Hessian matrix was then used to calculate vibrational frequencies for isotopologues. No scaling factor was applied. Using these frequencies, the β factor was calculated (Eq. 6) with respect to ^{2}H-substitution at individual H_{α} positions in an aqueous environment over the range of 0–100°C.

Calculation of the β factor for water was first performed on isolated molecules, i.e., as an ideal gas, following the same method (B3LYP/6-311G**) as above. The solvation effect, however, was not treated in the same way. On one hand, implicit solvation methods cannot account for the external modes in condensed phase which are more important for water molecules that are affected by hydrogen bonding than for large organic molecules with hydrophobic chains. On the other hand, explicit hydration models are limited by the number of water molecules and the configuration of the water cluster, and are thus inadequate to describe the bulk liquid water (Felipe et al., 2003). To avoid such issues, we therefore chose to multiply the ideal-gas β factor by the experimentally measured liquid-vapor fractionation factor (Horita and Wesolowski, 1994) to obtain β factors for liquid water. This approach is presumably more accurate than calculations based on solvation models of liquid water. The value of α_{eq} was then calculated as the ratio of β factors between the organic molecule in aqueous phase and liquid water.

4. RESULTS AND DISCUSSION

4.1. Isotope exchange experiments

4.1.1. Exchange kinetics

In time-series experiments, ^{2}H/^{1}H exchange profiles were measured for all substrates at 70°C, pH 12. They were also measured for cyclohexanone at 25 and 50°C, pH 12; for

cyclohexanone at 25°C, pH 1; and for 2-heptanone at 70°C, pH 1.2. Exchange rates, half-lives ($t_{1/2}$) and activation energy (E_a) were estimated (see 3.1.6. for kinetic calculations). The results are summarized in Table 1-1.

Table 1-1. Second-order rate constant and exchange half-life for base-catalyzed H_α exchange

T (°C)	k_{OH}[a] ($M^{-1}s^{-1}$)	$t_{1/2}$[b] (hr, pH=12)	$t_{1/2}$[b] (yr, pH=7)	E_a[c] (kJ/mol)
		cyclohexanone		
25	0.0188 (0.0003)	1.0	11.7	
50	0.114 (0.011)	0.2	1.9	45.2 (9.0)
70	0.196 (N/A)	0.1	1.1	
		2-heptanone		
70	0.180 (0.023)	0.1	1.2	
		4-heptanone		
70	0.058 (N/A)	0.3	3.8	
		2,4-dimethyl-3-pentanone		
70	0.016 (0.001)	1.2	14.1	

(a) Second-order rate constant for base-catalyzed H_α substitution, corrected for the number of H_α atoms in each molecule. Uncertainties (1σ) are given in parentheses.

(b) Exchange half-life calculated at pH 12 or 7

(c) Activation energy calculated according to the Arrhenius relationship

Selected data for cyclohexanone are plotted in Fig. 1-3 as an example (data for other ketones are shown in Appendix Fig. 1-A3). The δ^2H values of the ketone changed systematically with time, clearly recording the progress of $^2H/^1H$ exchange between ketone and water. At a specific temperature and pH, all incubations reached equilibrium simultaneously, as indicated by stable δ^2H values with time. At 25°C and pH 12, equilibrium was achieved within four days (~$5x10^3$ min). Exchange was faster at 50°C and pH 12, with equilibrium reached in less than 12 hours (~$5x10^2$ min). In contrast, exchange at 25°C and pH 1 was much slower, where $t_{1/2}$ was estimated to be 6 days and equilibrium was not reached within two months. The attainment of isotopic equilibrium under acid

catalysis was confirmed for 2-heptanone (Fig. 1-A3). In this case, measured ketone δD values at equilibrium and the calculated fractionation factor are equivalent to those measured under basic conditions. Since apparent exchange rate is proportional to the concentration of H^+ or OH^- (Appendix 1), our data indicate that OH^- is much more efficient than H^+ at catalyzing H_α substitution. Basic conditions (pH 12) were thus employed in most experiments.

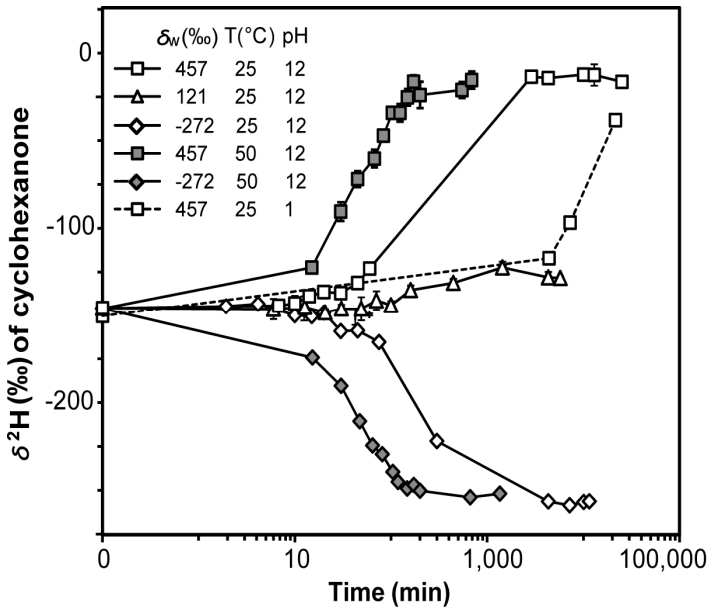

Figure 1-3. Cyclohexanone δ^2H values over time during incubations with waters of varying δ^2H values, temperature, and pH (shown in legend). Note the logarithmic x-axis. Error bars represent standard deviations from 3–5 measurements of the same sample and are generally smaller than the symbols.

At 70°C, the exchange rate for secondary H_α in 4-heptanone is faster than for tertiary H_α in 2,4-dimethyl-3-pentanone, while the rate for primary H_α in 2-heptanone, estimated from the results of 2-heptanone and 4-heptanone, is even faster. The decrease of exchange rate with increasing alkyl substitution on C_α is probably related to steric hindrance of the alkyl group(s) on the H_α position. The activation energy for base-catalyzed H_α exchange is calculated to be 45.2 ± 9.0 $kJmol^{-1}$ for cyclohexanone. Approximate rate constants for linear ketones at 50°C and 25°C can be estimated by assuming the same activation energy as for cyclohexanone.

When extrapolated to neutral pH, $t_{1/2}$ is estimated to be several years for temperatures comparable to those of diagenesis (Table 1-1). Exchange in natural environments is probably much faster, because of the presence of enzymes (Richard et al., 2001) and mineral surfaces (Alexander et al., 1982) that are potent catalysts. H_α substitution in carbonyl compounds other than ketones, e.g., carboxylic acids and their derivatives [R(C=O)X, where X = OH/O^-/OR/SR/NH_2…], also proceeds via keto-enol tautomerism and facilitates many diagenetic transformation reactions such as the racemization of amino acids. At neutral pH, H_α in oxy- and thiol-esters exchanges on timescales of 10^1–10^2 years (Amyes and Richard, 1996), comparable to ketones, while H_α in amides and the anions of carboxylic acids exchanges slowly, with $t_{1/2}$ on the order of 10^7 years. Under conditions typical of certain lab procedures, e.g., the demineralization of sediments to isolate organic matter, where organic compounds are exposed to strong acids and elevated temperatures, H_α exchange will be considerably faster. However, the impact of this exchange on isotopic analysis should — in most cases — be minimal due to the low fraction of exchangeable H in most lipids.

4.1.2. Experimental measurements of equilibrium fractionation factors.

During the second stage of $^2H/^1H$ exchange experiments, incubations were carried out with all substrates at pH 12 for 7 days, 22 days, and 85 days at 70°C, 50°C, and 25°C respectively, more than 80 times longer than the estimated $t_{1/2}$ at each temperature. Equilibrium fractionation factors for H_α are derived from the regression slope between δ^2H values of the ketone and water at equilibrium (Eq. 1-3). This yields a single value of α_{eq} that applies to all exchanging H_α positions, regardless of whether they are equivalent. R^2 values for these regressions are all greater than 0.99. Data for 2,4-dimethyl-3-pentanone are plotted as an example in Fig. 1-4. Complete δ^2H data for incubated ketones and water are presented in Appendix Table 1-A1.

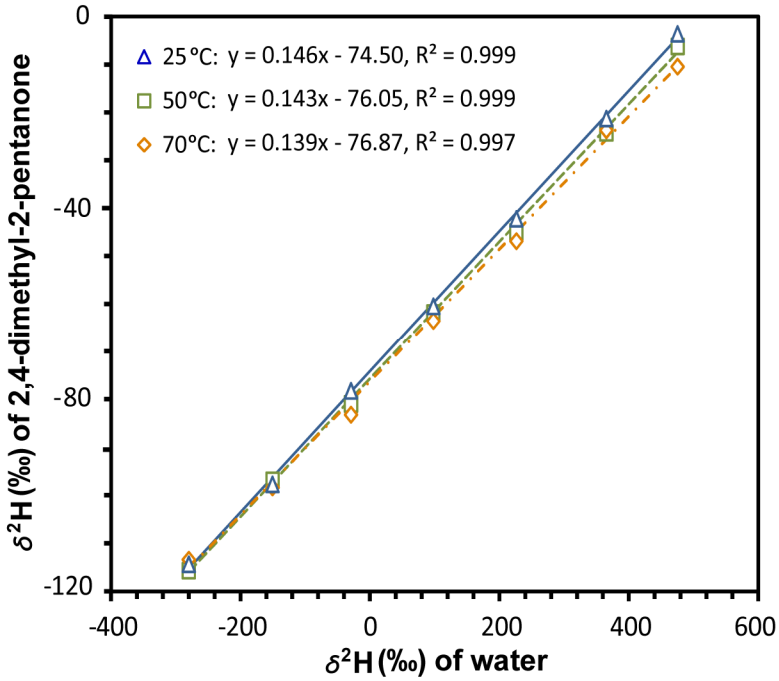

Figure 1-4. Regression of δ^2H values between 2,4-dimethyl-3-pentanone and water in equilibrium at pH 12 and 25°C (solid line), 50°C (dashed line), and 70°C (dot-and-dash line). Analytical uncertainties for each data point are smaller than the symbols.

Derived values of the equilibrium fractionation (expressed as the isotopic enrichment factor, ε_{eq}) for exchanging H_α positions of the ketone substrates are summarized in Table 1-2 and Fig. 1-5. The uncertainty in ε_{eq} values, generally between 10 and 20‰, is estimated from the standard deviation of the regression. The relatively large uncertainty for 5-nonanone at 70°C is due to the loss of two samples, while that for 2-heptanone at 25 and 50°C is probably related to variation in analyte abundance during GC/P/IRMS analysis. The values of δ_N in each ketone are statistically identical at different temperatures, confirming our assumption that only H_α is undergoing appreciable exchange during the incubations.

The two ketones that contain only tertiary H_α atoms, 3,5-dimethyl-4-heptanone and 2,4-dimethly-3-pentanone, yield similar ε_{eq} values ranging between +27‰ and −32‰ and negative temperature dependence with a crossover of $\varepsilon_{eq} = 0$ at about 55°C (Fig. 1-5). Ketones containing only secondary H_α atoms, 4-heptanone and 5-nonanone, have similar ε_{eq} values between −130‰ and −112‰ with little temperature dependence. The value of ε_{eq}

for 2-methyl-3-hexanone, a molecule containing one tertiary and two secondary H_α atoms, agrees well with the weighted average of tertiary H_α and secondary H_α. ε_{eq} for primary H_α is difficult to measure directly because the appropriate substrate — acetone — is both highly soluble in water and volatile. Instead, it was calculated by mass balance from ε_{eq} values for 2-heptanone and for secondary H_α in 4-heptanone and 5-nonanone. The result is −172‰ at 25°C, −167‰ at 50°C and −148‰ at 70°C. H_α in cyclohexanone has ε_{eq} values (Table 1-2) between those for primary and secondary H_α in linear ketones.

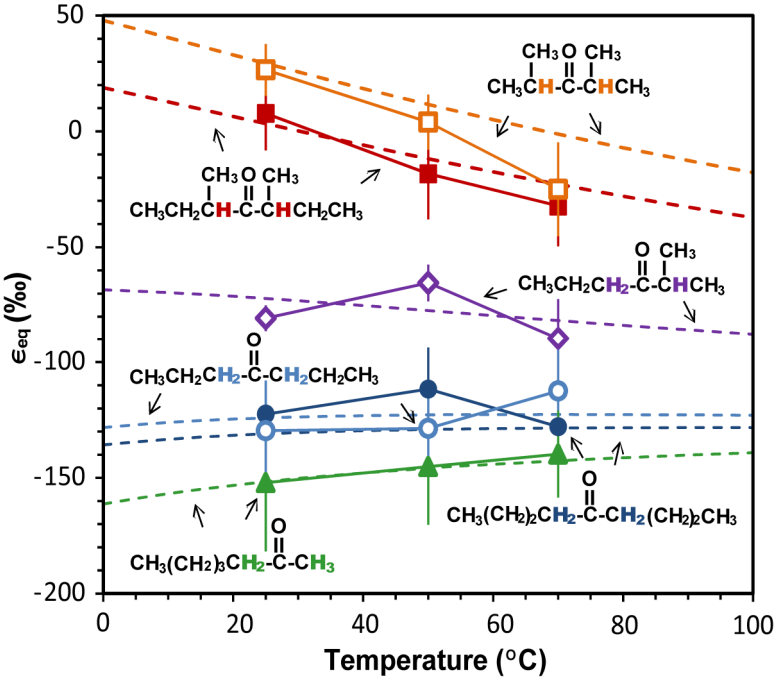

Figure 1-5. Equilibrium isotopic enrichment factors (ε_{eq}) for H_α in linear ketones as a function of temperature. Symbols represent experimental results measured at 25, 50, and 70°C with error bars of ±1σ. Dashed lines represent theoretical results from 0–100°C for the same molecules (see 4.2.2.). Data represent the weighted average for all H_α atoms in each ketone.

The value of ε_{eq} for H_α increases substantially with more alkyl substituents attached to C_α. This is likely due to the electron-donating effect of alkyl groups, with methyl groups being the strongest donor. It acts to enhance the electron density of the C_α–H_α bond and thus increases bond strength. As an example, the calculated force constants for the C_α–H_α

Table 1-2. Experimental isotopic enrichment factors (ε_{eq}) for H_α and δ^2H values for non-exchangeable H (δ_N) in the seven ketones

ketone substrate	25°C		50°C		70°C	
	ε_{eq} (‰)	δ_N (‰)	ε_{eq} (‰)	δ_N (‰)	ε_{eq} (‰)	δ_N (‰)
2,4-Dimethyl-3-pentanone	27 (11)	-91 (2)	4 (12)	-89 (2)	-25 (20)	-85 (4)
3,5-Dimethyl-4-heptanone	8 (16)	-54 (2)	-18 (20)	-45 (3)	-32 (17)	-47 (5)
2-Methyl-3-hexanone	-81 (6)	-111 (2)	-65 (8)	-109 (2)	-90 (17)	-109 (5)
4-Heptanone	-130 (22)	-69 (9)	-129 (17)	-55(7)	-112 (21)	-79 (9)
5-Nonanone	-122 (12)	-74 (3)	-112 (18)	-76 (5)	-128 (29)	-80 (9)
2-Heptanone	-152 (30)	-58 (17)	-145 (25)	-42 (14)	-140 (19)	-39 (11)
Cyclohexanone	-161 (11)	-171 (8)	-155 (10)	-182 (7)	-138 (10)	-198 (7)

Uncertainties (1σ) are given in parentheses. They are propagated from the standard error of the regression slope and intercept.

stretching mode are 1.01, 1.39, 2.31, and 2.42 mDyne/Å for acetone, 4-heptanone, 3,5-dimethyl-4-pentanone, and 2,4-dimethyl-3-pentanone, respectively. Since heavier isotopes partition preferentially into stiffer bonds (Bigeleisen and Mayer, 1947), the value of ε_{eq} is thus larger for an H bonded to C with more alkyl substitution. Hartshorn and Shiner (1972) fitted force fields to published vibrational frequencies for a series of small organic molecules (< C_3) and their ^2H-isotopologues, and then used those force fields to calculate α_{eq} relative to acetylene H at 25°C. They found that the successive replacement of H by C on a CH_3 group will result in a α_{eq} ratio of about 1.10 between the two molecules. Our results give a ratio of 1.055 between secondary H_α and primary H_α and 1.174 between tertiary H_α and secondary H_α, generally consistent with their results. In addition, their calculations revealed that α_{eq} for secondary H in cyclic hydrocarbons is lower than that in linear hydrocarbons by a ratio of 0.93, also consistent with the corresponding ratio of 0.959 in our study. Meloche et al. (1977) and Thomason (1960) used isomerase enzymes to catalyze ^3H incorporation at 35°C and thereby deduced the value of α_{eq} to be −160‰ for

the primary H_α in pyruvate and −70‰ for the secondary H_α in malate, both comparable to our results.

Another noteworthy feature is that equilibrium $^2H/^1H$ fractionation is mainly affected by atoms directly bound to the same C atom, and is only slightly affected by more remote structures. This "cutoff effect" has been demonstrated in several theoretical studies of isotope effects in organic molecules (Stern and Wolfsberg, 1966a,b; Hartshorn and Shiner, 1972), and is discussed further in Section 4.4.2.

4.2. Theoretical calculations

4.2.1. Optimized molecular geometries

Optimized geometries for the 7 ketone substrates in the gas phase are shown in Fig. 1-1. Selected bond lengths and bond angles are given in Appendix Table 1-A2. For ketones with branched carbon chains, including 2-methyl-3-hexanone, 2,4-dimethyl-3-pentanone and 3,5-dimethyl-4-heptanone, a conformation scan of internal torsion about the $O{=}C{-}C_\alpha{-}C_\beta$ dihedral shows that they are most stable when one alkyl branch is at 30°–37° to the carbonyl group (Fig. 1-6 and inserts of Fig. 1-1). Similar stable conformations were found by Langley et al. (2001) for 3-methyl-2-butanone and 2,4-dimethyl-3-pentanone using B3LYP/6-31G* and molecular mechanics (MM3 and MM4) methods.

4.2.2. Theoretical estimates of equilibrium fractionation factors

Values of the β factor were calculated from 0 to 100°C for each H_α position in the incubated ketone molecules and for water (complete β factor values are in Table 1-A3 and -4). For each ketone molecule, the reported value of ε_{eq} is the weighted average for all individual H_α positions.

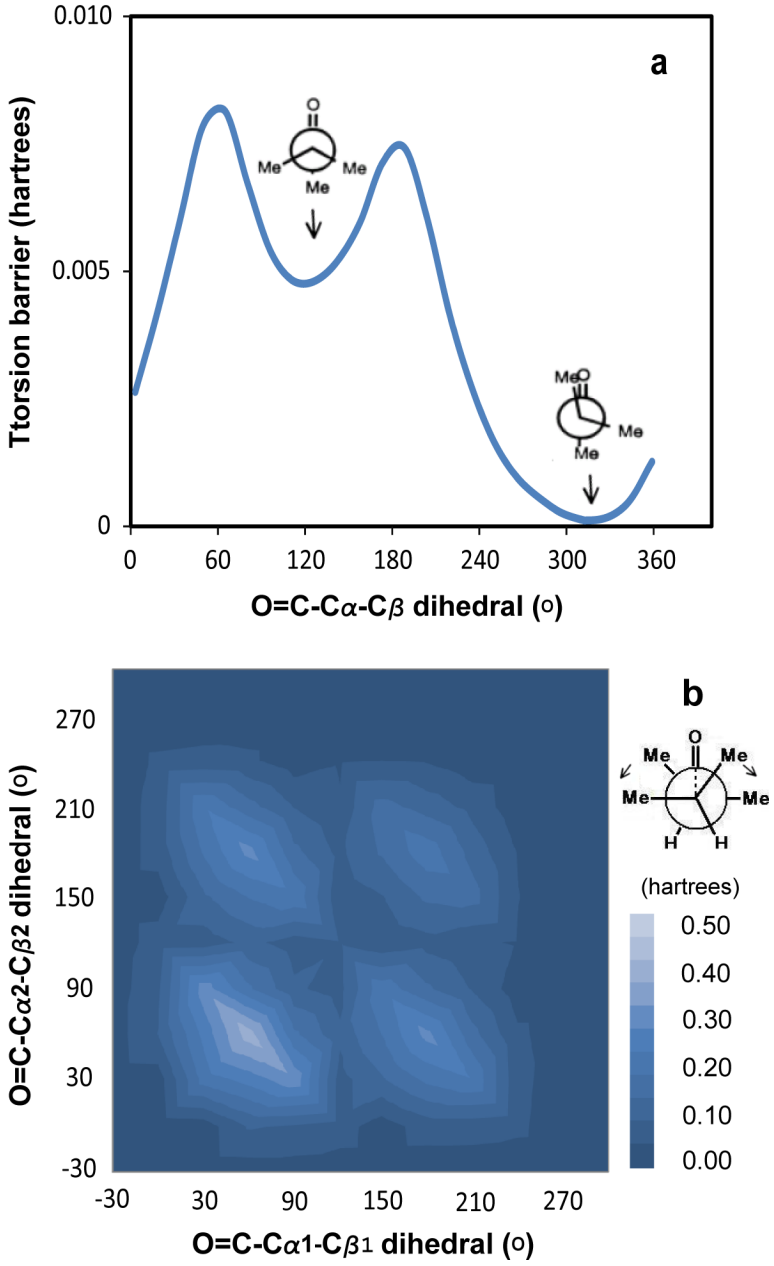

Figure 1-6. Molecular potential curve of the internal torsion about the O=C-C_α-C_β dihedral with 15° increments for (a) 2-methyl-3-hexanone and (b) 2,4-dimethyl-3-pentanone

Calculated values of ε_{eq} for the six linear ketone substrates are plotted together with the corresponding experimental results in Fig. 1-5. They agree well in both magnitude and temperature dependence. As for the experimental results, calculated ε_{eq} values for H_α in structurally similar molecules are consistent. At 25°C, the standard deviation (σ) of ε_{eq} values for secondary H_α in 4-heptanone, 5-nonanone, 2-heptanone, and 2-methyl-3-

hexanone is 3‰. Tertiary H_α in 2,4-dimethly-3-pentanone and 2-methyl-3-hexanone has consistent ε_{eq} values ($\sigma = 2$‰) that are 20–30‰ higher than the tertiary H_α in 3,5-dimethly-4-heptanone. This is consistent with the experimental results and is likely due to the stronger electron-donating ability of methyl groups than that of other alkyl groups (the C_α at C-2 in 2,4-dimethly-3-pentanone and 2-methyl-3-hexanone has two methyl branches, whereas the C_α at C-3 in 3,5-dimethly-4-heptanone has only one methyl branch).

In contrast, theoretical ε_{eq} values for cyclohexanone (based on unscaled frequencies) are ~60‰ higher than the experimental results. It thus seems that while our computational approach does an excellent job of reproducing experimental data for linear ketones, that approach does not yield accurate results for cyclic compounds (see 4.4.3. for more discussion).

4.3. Comparison of experimental and theoretical equilibrium fractionations

Experimental versus theoretical isotopic enrichment factors (ε_{eq}) for H_α in the 6 linear ketones are plotted in Fig. 1-7. In general, experiment and theory agree quite well. As temperature increases, there is a general trend towards slightly lower slope (0.982 ± 0.035 at 25°C, 0.904 ± 0.072 at 50°C, and 0.811 ± 0.038 at 70°C), i.e., the calibration curve is temperature-dependent. The trend is driven primarily by variations in tertiary H_α positions, and presumably indicates some aspect of the experiments that was not fully captured by the ab initio calculations (see discussion in 4.4.2.).

We therefore adopt a temperature-dependent calibration curve by fitting the regression slope and intercept, respectively, to temperature (Fig. 1-8). This approach gives slope = 1.081 – 0.00376T and intercept = 8.404 – 0.387T, where T is temperature in degrees Celsius. This temperature-dependent calibration scheme is then used in Chapter 2 to correct the calculated isotope enrichment factor for other organic molecules. As a simpler alternative, and considering the 10–20‰ experimental errors, one could use a temperature-averaged calibration curve (slope = 0.914 ± 0.032, intercept = −8.86 ± 3.22) derived from

all 18 data points in Fig. 1-7. The two approaches yield calibrated isotopic enrichment factors that differ by less than 12‰ between 0–100°C.

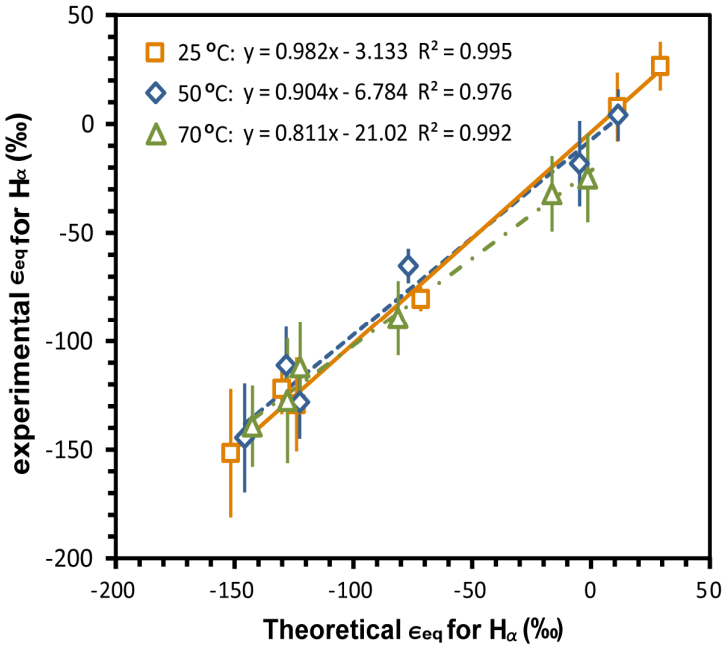

Figure 1-7. Regressions between experimental and theoretical ε_{eq} values for H_α in six linear ketones at 25°C (solid), 50°C (dash), and 70°C (dot-and-dash), respectively. Error bars represent ±1σ in experimental ε_{eq} values.

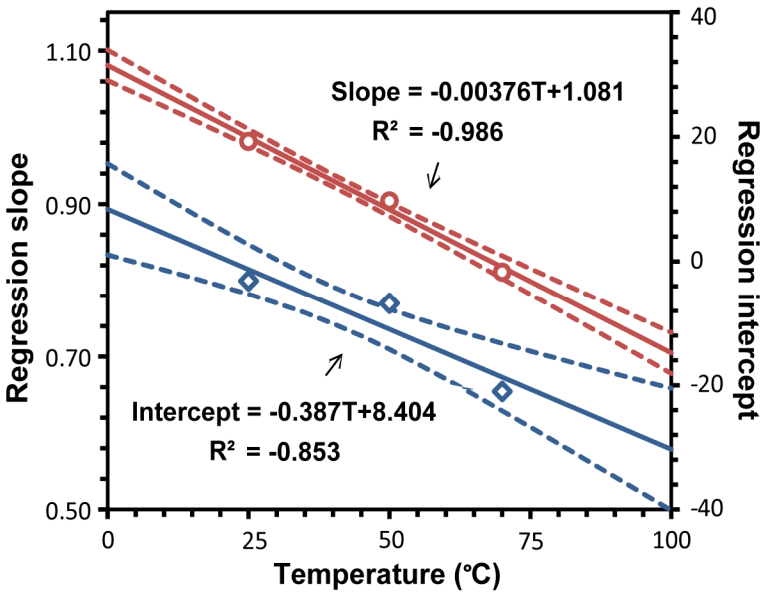

Figure 1-8. Regression of the calibration slope (circles) and intercept (diamonds) against temperature. Dashed lines indicate ±1σ for the estimated slope or intercept at any temperature between 0 and 100°C.

4.4. Sources of error

Uncertainty in the calibration represented by Fig. 1-7, and in its application to other molecules, encompasses potential systematic errors in both experimental measurements and ab initio calculations. Here we attempt to describe and quantify those uncertainties.

4.4.1. Experimental uncertainties

For the experimental dataset, the most likely potential sources of error are (*i*) failure to achieve true equilibrium, (*ii*) fractionations arising during sample extraction and handling, and (*iii*) systematic biases in measured δ^2H values. The attainment of equilibrium in our samples is demonstrable in two ways. First, equilibrium was approached from both directions by using waters of varying $^2H/^1H$ ratios. While it is true that partial equilibration of samples could still lead to a linear relationship between δ^2H values for the substrate and water, this would yield consistent fractionations for different molecules only if they exchanged at exactly the same rate, which is demonstrably untrue. Second, isotopic exchange of 2-heptanone under both acidic and basic conditions (Fig. 1-A3) — which catalyze very different exchange rates — yielded indistinguishable fractionations, strongly supporting the attainment of equilibrium.

To evaluate potential isotopic fractionations of ketones during sample extraction and handling, we conducted control experiments in which cyclohexanone, 4-heptanone and 2-heptanone were each dissolved in neutral deionized water at 25°C and then extracted without any equilibration. The resultant δ^2H values of the ketones were indistinguishable from those measured for the pure substances.

Because the measured δ^2H values for waters and ketones cover a large range of isotopic compositions, there is also a possibility for systematic biases in their measured values to arise. Such an effect is commonly referred to as "scale compression", and is known to vary between individual mass spectrometers (Coplen, 1988). Our extensive use of multiple organic and water working standards which span the range of measured δ^2H values and are both calibrated to the IAEA SMOW/SLAP scale, should largely mitigate such effects. Although minor artifacts of scale compression may still remain, they are likely < 10‰.

Thus we believe that systematic errors in the experimental data are likely to be small, and the uncertainties stated in Table 1-2 (which are based solely on the statistics of linear regression) provide an adequate estimate of both precision and accuracy for this dataset.

4.4.2 Uncertainties in ab initio calculations

Approximations adopted in the calculation of β factors, primarily the omission of anharmonicity, rotational correction, and rotation-vibration coupling, are generally expected to result in significant systematic errors for hydrogen isotopic fractionations. The excellent agreement between theoretical and experimental ε_{eq} values for linear ketones was thus unexpected. An important point is that only the ratios of partition functions and β factors enter into the calculation of α_{eq} and ε_{eq}. Since the same calculation methods (except for the solvation model) were applied to both water and ketone molecules, systematic errors in their β factors are expected to be positively correlated and tend to cancel, as pointed out by Hartshorn and Shiner (1972) and Liu and Tossell (2005).

To help pinpoint the importance of various error sources, we compared our calculated β factor for water to the result of Richet et al. (1977), who calculated various small molecules by taking into account the effects of anharmonicity, rotational correction and rotation-vibration coupling. At 30°C, their β factor for an isolated water molecule is 11.064, smaller than our result (12.516) by a factor of 0.884. By reproducing their calculation using the molecular constants provided in the paper, we find that this discrepancy is primarily due to the omission of the anharmonic correction to zero point energy (ZPE) in our calculation, which alone contributes a factor of 0.888. This term arises from the anharmonicity of various normal modes and their couplings at the ZPE level. Adding the rotational correction introduces a factor of 0.995. The anharmonic effect on excited vibrational states and the rotation-vibration coupling lead to factors of 1.00009 and 0.99998, respectively, and thus can be safely ignored. Note that the solvation effect for water is treated by multiplying the β factor for a gaseous molecule with the experimental liquid-gas fractionation factor, which is presumably free of systematic error. The overall uncertainty in the β factor of liquid water is therefore dominated by the omission of anharmonity at the ZPE level.

The significance of the above errors to the β factor for ketones can only be evaluated qualitatively, because the relevant molecular constants needed for quantitative calculations are unknown. The ketones studied here are large polyatomic molecules, and their moments of inertia are large enough that rotational corrections are negligible at or above room temperature (Bigeleisen and Mayer, 1947). The effect of rotation-vibration coupling is difficult to evaluate but unlikely to be orders of magnitude larger for the ketone than for water molecules.

Errors associated with use of the PCM solvation model can be assessed as follows. The measured vapor pressure isotope effect (VPIE) for hydrocarbons is small (~4‰) at 24°C (Wang and Huang, 2001). We also calculated VPIE over 0–100°C for the ketones used in our calibration, with the results generally between 0 and 10‰. Thus correction for the solvation effect is at most ~10‰, and systematic errors associated with the specific PCM model are likely to be smaller than that. We also tested the effects of using explicit hydration with three, four, and five water molecules in our calculations. The resulting fractionation factors for the six linear ketones were then regressed against the experimental results, which give regression slopes around 1.1 and intercepts of 10–40‰ (summarized in Appendix Table 1-A5), with even larger temperature variability than that using implicit solvation model. Although explicit H-bonding was shown to have significant effect on hydrogen equilibrium fractionation factors in the H_4SiO_4-H_2O system (Felipe et al., 2003), it is apparently much less important for C-bound H that interacts weakly with water, compared to O-bound H.

The size of anharmonic effects on the value of β factors for ketones can be qualitatively evaluated by examining the "frequency scaling factor". For a specific ab initio method, the scaling factor is obtained by calibrating the calculated vibrational frequencies against corresponding experimental frequencies to correct the former for anharmonic effects. The precision and accuracy of the scaling factor thus depend on the size and diversity of the calibration dataset. However, applying scaled ab initio frequencies to calculate β factors using the Bigeleisen-Mayer-Urey equation (Eq. 1-6), which adopts the Harmonic Oscillator approximation, will overestimate the anharmonic correction to ZPE (Scott and Radom, 1996; Otake et al., 2008) and will not correctly account for the anharmonic effect on

excited vibrational states. Thus applying these scaling factors alone cannot produce accurate β factors (see Table 1-A5). Nevertheless, they can be used to evaluate the relative significance of anharmonicity between various species. (Mathematical demonstration about the effect of scaling factor on β factor is provided in Appendix 2.) We therefore applied the recommended scaling factor for B3LYP/6-311G** (0.967, Computational Chemistry Comparison and Benchmark DataBase (CCCBDB), NIST) and recalculated β factors based on the scaled frequencies. Results are plotted in Fig. 1-9 as the ratio of β factors calculated using scaled (β_s) and unscaled (β_u) frequencies.

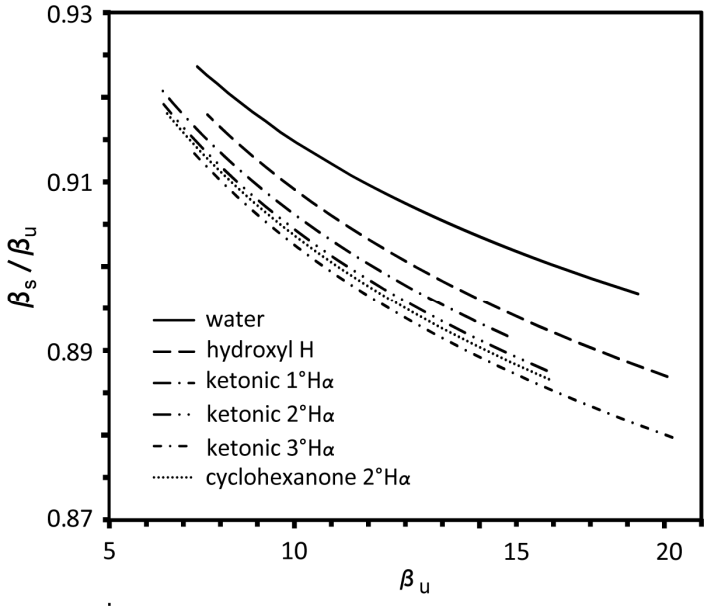

Figure 1-9. The ratio between β factors calculated using scaled frequencies (β_s) and those using unscaled frequencies (β_u) over 0–100°C for various organic H positions.

Fig. 1-9 shows that anharmonicity uniformly lowers the value of β factor to similar extents (β_s/β_u ~0.9) for both water and ketones, which implies that errors due to the omission of anharmonicity will largely cancel when β_u is used to calculate α_{eq}, consistent with the excellent agreement between experiment and theory for linear ketones. The β_s/β_u ratios for the ketones are slightly below that for water. Therefore, accounting for anharmonicity will lower the β factor for ketones more than that for water, and thereby decrease the fractionation factor. This is consistent with the fact that the experimentally determined fractionation factors are generally more negative than the calculated

fractionation factors (calibration intercepts < 0). Moreover, the β_s/β_u ratio progressively decreases from primary to secondary and tertiary H_α, such that accounting for anharmonicity will lower the β factor for tertiary H_α (with positive ε_{eq} values) more than that for primary H_α (with the most negative ε_{eq} values), leading to calibration slopes < 1.

Anharmonicity is also likely responsible for the temperature dependence of our calibration curve, because its effect gradually increases with temperature while the harmonic term rapidly decreases. Otake et al. (2008) showed that the relative decrease in β factors due to anharmonicity is larger at higher temperature and for molecules of larger size. Therefore the cancellation of errors between ketone and water will vary slightly with temperature, and potentially give rise to the temperature dependence of the experimental-theoretical calibration. As shown in Fig. 1-7, lowering of the regression slope is primarily due to the fast decrease in ε_{eq} values of tertiary H_α, for which the mechanism is currently unclear.

Another mechanism possibly underlying the temperature variability is conformational changes with temperature. The ketones are large floppy molecules for which long-range internal torsion along the carbon chain can exist at ambient temperatures. Therefore, a single stable conformation might be inadequate to describe the real molecule, especially at higher temperatures. Using 2,4-dimethyl-3-pentanone (the ketone showing the largest temperature variation in ε_{eq} values) as an example, we calculated its entire torsional potential around the O=C−C−C dihedral. The value of ε_{eq} was then calculated for the optimized geometry at each local minimum and weighted according to the Boltzmann distribution to generate a conformation-averaged fractionation factor. The result is indistinguishable from that based on a single geometry at the global minimum across the range of 0–100°C. This observation is consistent with the "cutoff" effect found in previous studies (Stern and Wolfsberg 1966a,b; Hartshorn and Shiner, 1972), wherein structures beyond the γ position from the substituted atom can be largely ignored in the calculation of isotopic fractionation. It is also buttressed by the frequency data, which show that the value of the β factor is mainly controlled by the isotopic frequency shifts in the stretching and bending modes that directly involve the substituted C−H bond, whereas frequency shifts for the torsional modes are more than 100 times smaller.

In conclusion, uncertainties in the ab initio calculation are likely dominated by anharmonic effects, based on their capacity to explain most discrepancies between theory and experiment. Variation in the size of anharmonic effects with changing temperature and H position probably leads to the observed temperature-dependence of the calibration curve, which cannot be corrected by simply applying the scaling factor (see Table 1-A5). Quantitative calculation of anharmonicity requires computing a wide range of the entire potential surface (Young, 2001; Otake et al., 2008) which would be prohibitively time-consuming for the large organic molecules we deal with.

4.4.3. Limitations in applying the calibration to other molecules

To estimate the error that might arise from applying our calibration to molecules other than ketones, we first analyzed variations in the value of the scaling factor. To do so, we calculated the scaling factor using frequency data from the CCCBDB database for individual compound classes, including linear alkanes, alkenes, ketones, aldehydes, esters, ethers, and alcohols (Details in Appendix 2.2). Their scaling factors are very consistent at 0.967 ± 0.002 (see Appendix Fig. 1-A2). Then we applied this scaling factor to calculate the β_s/β_u ratio for C-bound H in these compounds. The results are virtually identical to those in ketones for analogous positions (primary, secondary, tertiary; Fig. 1-9), indicating that the relative size of anharmonicity is consistent for the three types of H positions in linear molecules. Therefore our calibration curve based on ketones should be widely applicable to other n-alkyl compounds. When the ±0.002 uncertainty in scaling factor is propagated into the calculation of ε_{eq}, the results vary by ±4–8‰ (1σ). We take this range as a conservative estimate of systematic biases arising from the application of our calibration curve to other linear molecules. It is only about one-third as large as uncertainties in the experimental calibration dataset.

We further note that the β_s/β_u ratios for hydroxyl H in alcohols and carboxylic acids are slightly higher than those for C-bound H (Fig. 1-9). As a result, applying the same calibration tends to systematically underestimate ε_{eq} for hydroxyl H by 6–10‰. Also, β_s/β_u ratios for H_α in cyclohexanone are virtually the same as those for linear ketones (Fig. 1-9), implying that the significant offsets between experiment and theory for cyclohexanone are

unlikely due to the anharmonic effect on ZPE. A possible explanation is that the ring structure of cyclohexanone can introduce stronger couplings among the normal modes and between the vibration and rotation motions, as compared to the linear structures. Until the underlying mechanisms for this discrepancy are understood, the calibration presented here should be applied only to simple straight and branched carbon chains.

In addition, when applying this calibration to molecules with functional groups other than ketones, one might expect that systematic errors could arise since electrostatic interactions with water molecules change substantially from hydrocarbons (dispersion forces) to alcohols and carboxylic acids (hydrogen bonding). Nevertheless, our calibration curve is derived from ketones that are more polar than alkanes but less polar than alcohols and carboxylic acids, which should help to mitigate such problems. Also, most sedimentary organic molecules of interest are long aliphatic chains with at most one or two functional groups. For such molecules, even large uncertainties for the few H atoms surrounding the functional group would have only a slight impact on overall δ^2H values.

Finally, deviations from our calibration are likely to arise with decreasing molecular size, because other systematic errors, e.g., rotational correction and rotation-vibration coupling, cannot be safely ignored for small molecules. Hence we suggest the use of the calibration be restricted to molecules with five or more carbon atoms. Also, because the effect of anharmonicity, as well as many other systematic errors, changes systematically with temperature, use of this calibration for temperatures outside the calibration range (0-100°C) should be approached with caution.

5. CONCLUSIONS

Equilibrium ^{2}H/^{1}H fractionations between H_α in linear ketones and water were measured at 25, 50, and 70°C via isotope exchange experiments with uncertainties typically between 10–20‰. Results are in the ranges of −170‰ to −150‰, −130‰ to −110‰, and +30‰ to −30‰ for primary, secondary, and tertiary H_α, respectively. Primary and secondary H_α exhibit a positive temperature dependence, while tertiary H_α exhibit a

negative temperature dependence. Fractionations were also calculated using vibrational frequencies from ab initio calculations (B3LYP/6-311G**), with a standard deviation of 4–8‰ for structurally similar H_α in different molecules. Systematic errors in the calculations are likely dominated by the omission of anharmonicity, and largely cancel in the value of α_{eq} by taking the ratio of β factors. Consequently, experimental and theoretical α_{eq} values match very well in both magnitude and temperature dependence, yielding a linear but temperature-dependent calibration curve with slope = 1.081 − 0.00376T and intercept = 8.404 − 0.387T, where T is temperature in degrees Celsius. Since the effect of anharmonicity is of the same size for C-bound H in most linear compounds other than ketones, we propose that this calibration can be applied to analogous theoretical calculations for a wide variety of organic molecules with linear carbon skeletons containing five or more C atoms, and for temperatures in the range of 0–100°C. Considering all sources of uncertainty, we estimate that this approach should yield results that are accurate to within 10–20‰.

ACKNOWLEDGEMENTS

The authors thank Arndt Schimmelmann for the analysis of ^{2}H-enriched water standards employed here. We also acknowledge Adri van Duin, Edwin A. Schauble and Weifu Guo for helpful discussion on ab initio calculations. This work was supported by the Petroleum Research Fund (PRF) of the American Chemical Society (ACS), #43746-G2, and National Science Foundation (NSF) grant #EAR-0645502.

REFERENCES

Alexander R., Kagi R. I. and Larcher A. V. (1982) Clay catalysis of aromatic hydrogen-exchange reactions. *Geochim. Cosmochim. Acta* **46**, 219–222.

Amyes T. L. and Richard J. P. (1996) Determination of the pK(a) of ethyl acetate: Bronsted correlation for deprotonation of a simple oxygen ester in aqueous solution. *J. Am. Chem. Soc*. **118**, 3129–3141.

Andersen N., Paul H. A., Bernasconi S. M., McKenzie J. A., Behrens A., Schaeffer P. and Albrecht P. (2001) Large and rapid climate variability during the Messinian salinity crisis: Evidence from deuterium concentrations of individual biomarkers. *Geology* **29**, 799–802.

Becke A. D. (1993) Density-functional thermochemistry. 3. The role of exact exchange. *J. Chem. Phys.* **98**, 5648–5652.

Bigeleisen J. and Mayer M. G. (1947) Calculation of equilibrium constants for isotopic exchange reactions. *J. Chem. Phys.* **15**, 261–267.

Chikaraishi Y. and Naraoka H. (2003) Compound-specific delta D-delta C-13 analyses of n-alkanes extracted from terrestrial and aquatic plants. *Phytochemistry* **63**, 361–371.

Chikaraishi Y., Naraoka H. and Poulson S. R. (2004) Carbon and hydrogen isotopic fractionation during lipid biosynthesis in a higher plant (Cryptomeria japonica). *Phytochemistry* **65**, 323–330.

Chikaraishi, Y., Naraoka, H. and Poulson, S. R. (2004) Hydrogen and carbon isotopic fractionations of lipid biosynthesis among terrestrial (C3, C4 and CAM) and aquatic plants. *Phytochemistry* **65**, 1369–1381.

Coplen T. B. (1988) Normalization of oxygen and hydrogen isotope data. *Chem. Geo.* **72**, 293–297.

Criss R. E. (1999) *Principles of stable isotope distribution*. Oxford University Press, New York, pp. 71–76.

Dawson D., Grice K. and Alexander R. (2005) Effect of maturation on the indigenous δD signatures of individual hydrocarbons in sediments and crude oils from the Perth Basin (Western Australia). *Org. Geochem.* **36**, 95–104.

Dawson, D., Grice, K., Wang, S.X., Alexander, R. and Radke, J. (2004) Stable hydrogen isotopic composition of hydrocarbons in torbanites (Late Carboniferous to Late Permian) deposited under various climatic conditions. *Org. Geochem.* **35**, 189–197.

Estep M. F. and Hoering T. C. (1981) Stable hydrogen isotope fractionations during autotrophic and mixotrophic growth of microalgae. *Plant Physiology* **67**, 474–477.

Felipe M. A., Kubicki J. D. and Rye D. M. (2003) Hydrogen isotope exchange kinetics between H_2O and H_4SiO_4 from ab initio calculations. *Geochim. Cosmochim. Acta* **67**, 1259–1276.

Feng X. H. and Epstein S. (1994) Climatic implications of an 8000-year hydrogen isotope time-series from bristlecone-pine trees. *Science* **265**, 1079–1081.

Galimov E. M. (1971) Relation between isotope separation factor and equilibrium constants for carbon isotope exchange reactions in hydrocarbon systems. *Russ. J. Phys. Chem*. **45**, 665–667.

Gourier D., Robert F., Delpoux O., Binet L., Vezin H., Moissette A. and Derenne S. (2008) Extreme deuterium enrichment of organic radicals in the Orgueil meteorite: Revisiting the interstellar interpretation? *Geochim. Cosmochim. Acta* **72**, 1914–1923.

Greeley B. H., Russo T. V., Mainz D. T., Friesner R. A., Langlois J. M., Goddard W. A., Donnelly R. E. and Ringnalda M. N. (1994) New pseudospectral algorithms for electronic-structure calculations — length scale separation and analytical 2-electron integral corrections. *J. Chem. Phys.* **101**, 4028–4041.

Hartshorn Sr. and Shiner V. J. (1972) Calculation of h/d, c-12/c-13, and c-12/c-14 fractionation factors from valence force fields derived for a series of simple organic-molecules. *J. Am. Chem. Soc*. **94**, 9002–9012.

Hill P. S. and Schauble E. A. (2008) Modeling the effects of bond environment on equilibrium iron isotope fractionation in ferric aquo-chloro complexes. *Geochim. Cosmochim. Acta* **72**, 1939–1958.

Horita J. and Wesolowski D. J. (1994) Liquid-vapor fractionation of oxygen and hydrogen isotopes of water from the freezing to the critical-temperature. *Geochim. Cosmochim. Acta* **58**, 3425–3437.

Huang Y. S., Wang Y., Alexandre M. R., Lee T., Rose-Petruck C., Fuller M. and Pizzarello S. (2005) Molecular and compound-specific isotopic characterization of monocarboxylic acids in carbonaceous meteorites. *Geochim. Cosmochim. Acta* **69**, 1073–1084.

Jancso G. and Van Hook W. A. (1974) Condensed phase isotope-effects (especially vapor-pressure isotope-effects). *Chem. Rev.* **74**, 689–750.

Knyazev D. A., Myasoedov N. F. and Bochkarev A. V. (1992) The theory of the equilibrium isotope effects of hydrogen. *Russ. Chem. Rev.* **61**, 204–220.

Koepp M. (1978) D/H isotope exchange reaction between petroleum and water: A contributory determinant for D/H-isotope ratios in crude oils? In *The Fourth International Conference, Geochronology, Cosmochronology, Isotope Geology USGS Open-File Report 78–701* (R.E. Zartman, ed.). U.S. Geological Survey. pp. 221–222.

Krull E., Sachse D., Mugler I., Thiele A. and Gleixner G. (2006) Compound-specific delta C-13 and delta H-2 analyses of plant and soil organic matter: A preliminary assessment of the effects of vegetation change on ecosystem hydrology. *Soil Biol. Biochem.* **38**, 3211–3221.

Langley C. H., Lii J. H. and Allinger N. L. (2001) Molecular mechanics calculations on carbonyl compounds. II. Open-chain ketones. *J. Comput. Chem.* **22**, 1426–1450.

Larcher A. V., Alexander R., Rowland S. J. and Kagi R. I. (1986) Acid catalysis of alkyl hydrogen-exchange and configurational isomerization-reactions — acyclic isoprenoid acids. *Org. Geochem.* **10**, 1015–1021.

Lee C. T., Yang W. T. and Parr R. G. (1988) Development of the colle-salvetti correlation-energy formula into a functional of the electron-density. *Phy. Rev. B*, **37**, 785–789.

Li C., Sessions A. L., Kinnaman F. S. and Valentine D. L. (2009) Hydrogen-isotopic variability in lipids from Santa Barbara Basin sediments. *Geochim. Cosmochim. Acta* **73**, 4803–4823.

Liu Y. and Tossell J. A. (2005) Ab initio molecular orbital calculations for boron isotope fractionations on boric acids and borates. *Geochim. Cosmochim. Acta* **69**, 3995–4006.

Lis G., Wassenaar L. I. and Hendry M. J. (2007) High-precision laser spectroscopy D/H and 18O/16O measurements of microliter natural water samples. *Anal. Chem.* **80**, 287–293.

Meloche H. P., Monti C. T. and Cleland W. W. (1977) Magnitude of the equilibrium isotope effect on carbontritium bond synthesis. *Biochim. Biophy. Acta — Enzymology* **480**, 517–519.

O'Neil J. R. (1986) Theoretical and experimental aspects of isotopic fractionation. In *Stable isotopes in high temperature geological processes* 16 (J.W. Valley, H.P. Taylor, Jr., J.R. O'Neil, eds.). Am. Mineral., pp. 1–40.

Otake T., Lasaga A. C. and Ohmoto H. (2008) Ab initio calculations for equilibrium fractionations in multiple sulfur isotope systems. *Chem. Geo.* **249**, 357–376.

Pagani M., Pedentchouk N., Huber M., Sluijs A., Schouten S., Brinkhuis H., Damste J. S. S. and Dickens G. R. (2006) Arctic hydrology during global warming at the Palaeocene/Eocene thermal maximum. *Nature* **442**, 671–675.

Pedentchouk N., Freeman K. H. and Harris N. B. (2006) Different response of delta D values of n-alkanes, isoprenoids, and kerogen during thermal maturation. *Geochim. Cosmochim. Acta* **70**, 2063-2072.

Richard J. P., Williams G., O'Donoghue A. C. and Amyes T. L. (2002) Formation and stability of enolates of acetamide and acetate anion: An eigen plot for proton transfer at alpha-carbonyl carbon. *J. Am. Chem. Soc*. **124**, 2957–2968.

Richet P., Bottinga Y. and Javoy M. (1977) Review of hydrogen, carbon, nitrogen, oxygen, sulfur, and chlorine stable isotope fractionation among gaseous molecules. *Ann. Rev. Earth Planet. Sci.* **5**, 65–110.

Roberts I. and Urey H. C. (1939) Kinetics of the exchange of oxygen between benzoic acid and water. *J. Am. Chem. Soc*. **61**, 2580–2584.

Sachs J. P., Sachse D., Smittenberg R. H., Zhang Z., Battisti D. S. and Golubic S. (2009) Southward movement of the Pacific intertropical convergence zone AD 1400–1850. *Nature Geosci.* **2**, 519–525.

Sauer P.E., Schimmelmann A., Sessions A.L. and Topalov K. (2009) Simplified batch equilibration for D/H determination of non-exchangeable hydrogen in solid organic material. *Rapid Comm. Mass Spec.* **23**, 949–956.

Schimmelmann A. (1991) Determination of the concentration and stable isotopic composition of nonexchangeable hydrogen in organic-matter. *Anal. Chem.* **63**, 2456–2459

Schimmelmann A. and Deniro M. J. (1993) Preparation of organic and water hydrogen for stable isotope analysis — effects due to reaction vessels and zinc reagent. *Anal. Chem.* **65**, 789–792.

Schimmelmann A., Lewan M. D. and Wintsch R. P. (1999) D/H isotope ratios of kerogen, bitumen, oil, and water in hydrous pyrolysis of source rocks containing kerogen types I, II, IIS, and III. *Geochim. Cosmochim. Acta* **63**, 3751–3766.

Schimmelmann A., Sessions A. L., Boreham C. J., Edwards D. S., Logan G. A. and Summons R. E. (2004) D/H ratios in terrestrially sourced petroleum systems. *Org. Geochem.* **35**, 1169–1195.

Schimmelmann A., Sessions A. L. and Mastalerz M. (2006) Hydrogen isotopic composition (D/H) of organic matter during diagenesis and thermal maturation. *Ann. Rev. Earth Planet. Sci.* **34**, 501–533.

Schoell M. and Whiticar M. J. (1982) Isotope geochemistry of natural gases in Central-Europe. *J. Petrol. Geol.* **5**, 209–210.

Scott A. P. and Radom L. (1996) Harmonic vibrational frequencies: An evaluation of Hartree-Fock, Moller-Plesset, quadratic configuration interaction, density functional theory, and semiempirical scale factors. *J. Chem. Phys.* **100**, 16502–16513

Sessions A. L. and Hayes J. M. (2005) Calculation of hydrogen isotopic fractionations in biogeochemical systems. *Geochim. Cosmochim. Acta* **69**, 593–597.

Sessions A. L., Burgoyne T. W., Schimmelmann A. and Hayes J. M. (1999) Fractionation of hydrogen isotopes in lipid biosynthesis. *Org. Geochem.* **30**, 1193–1200.

Sessions A. L., Sylva S. P., Summons R. E. and Hayes J. M. (2004) Isotopic exchange of carbon-bound hydrogen over geologic timescales. *Geochim. Cosmochim. Acta* **68**, 1545–1559.

Stern M. J. and Wolfsberg M. (1966a) On absence of isotope effects in absence of force constant changes. *J. Chem. Phys.* **45**, 2618.

Stern M. J. and Wolfsberg M. (1966) Simplified Procedure for Theoretical Calculation of Isotope Effects Involving Large Molecules. *J. Chem. Phys.* **45**, 4105.

Sternberg L., Deniro M. J. and Ajie H. (1984) Stable hydrogen isotope ratios of saponifiable lipids and cellulose nitrate from cam, C-3 and C-4 plants. *Phytochemistry* **23**, 2475–2477.

Tannor D. J., Marten B., Murphy R., Friesner R. A., Sitkoff D., Nicholls A., Ringnalda M., Goddard W. A. and Honig B. (1994) Accurate first principles calculation of molecular charge-distributions and solvation energies from ab-initio quantum-mechanics and continuum dielectric theory. *J. Am. Chem. Soc*. **116**, 11875–11882.

Thomson J. F. (1960) Fumarase activity in D2O. *Arch. Biochem. Biophys.* **90**, 1–6.

Urey H. C. (1947) The thermodynamic properties of isotopic substances. *J. Chem. Soc*. MAY, 562–581.

Urey H. C. and Rittenberg D. (1933) Some thermodynamic properties of the (HH2)-H-1, (HH2)-H-2 molecules and compounds containing the H-2 atom. *J. Chem. Phys.* **1**, 137–143.

Urey H. C., Brickwedde F. G. and Murphy G. M. (1932) A hydrogen isotope of mass 2. *Phys. Rev*. **39**, 164–165.

Van Hook W. A. (1968) Vapor pressures of isotopic waters and ices. *J. Phys. Chem.* **72**, 1234

Wang Y. and Huang Y. S. (2001) Hydrogen isotope fractionation of low molecular weight n-alkanes during progressive vaporization. *Org. Geochem.* **32**, 991–998.

Wang Y. and Sessions A. L. (2008) Memory effects in compound-specific D/H analysis by gas chromatography/pyrolysis/isotope-ratio mass spectrometry. *Anal. Chem.* **80**, 9162–9170

Wang Y., Sessions A. L., Nielsen R. J. and Goddard W. A. (2009) Equilibrium 2H/1H fractionations in organic molecules. Part II: Linear alkanes, alkenes, ketones, carboxylic acids, esters, alcohols and ethers. *Geochim. Cosmochim. Acta* (in press).

Wedeking K. W. and Hayes J. M. (1983) Exchange of oxygen isotopes between water and organic material. *Isotope Geosci.* **1**, 357–370.

Whiticar M. J., Faber E. and Schoell M. (1985) Hydrogen and carbon isotopes of c-1 to c-5 alkanes in natural gases. *AAPG Bull.* **69**, 316.

Xu X. J., Xiao H. M., Gong X. D., Ju X. H. and Chen Z. X. (2005) Theoretical studies on the vibrational spectra, thermodynamic properties, detonation properties, and pyrolysis mechanisms for polynitroadamantanes. *J. Phys. Chem. A* **109**, 11268–11274.

Yang H. and Huang Y. S. (2003) Preservation of lipid hydrogen isotope ratios in Miocene lacustrine sediments and plant fossils at Clarkia, northern Idaho, USA. *Org. Geochem.* **34**, 413–423.

Young D. C. (2001) *Computational chemistry: a practical guide for applying techniques to real world problems.* Wiley-Interscience, New York, pp. 92–98.

Zhang Z. and Sachs J. P. (2007) Hydrogen isotope fractionation in freshwater algae: I. Variations among lipids and species. *Org. Geochem.* **38**, 582–608.

Zhang X., Gillespie A. L. and Sessions A. L. (2009) Large D/H variations in bacterial lipids reflect central metabolic pathways. *Proc. Nat. Acad. Sci. USA* **106**, 12580–12586.

APPENDIX

1. Mechanism of H_α Substitution

H_α substitution in carbonyl compounds, including ketones, carboxylic acids, and the derivatives (R(C=O)X, X = OH/O^-/OR/SR/NH_2…), takes place via keto-enol tautomerism that can be catalyzed by both base and acid. In basic environment, H_α is abstracted by a base moiety to leave an enolate ion that is resonance-stabilized with the negative charge spread over the carbon and oxygen atoms (Fig. 1-A1-a). Reprotonation by water molecules can occur either on C_α to regenerate the keto form or on the oxygen to produce the enol form. For simple ketones and aldehydes, the keto form predominates (99.99%). The rate-limiting step is deprotonation by hydroxide ion. Therefore the pseudo-first-order rate constant can be expressed as $k = k_{OH}[OH^-]$, where k_{OH} is the second-order rate constant. Acid-catalyzed exchange is initiated by protonating the oxygen, which further acidifies the H_α and thus allows water to abstract the proton (Fig. 1-A1-b).

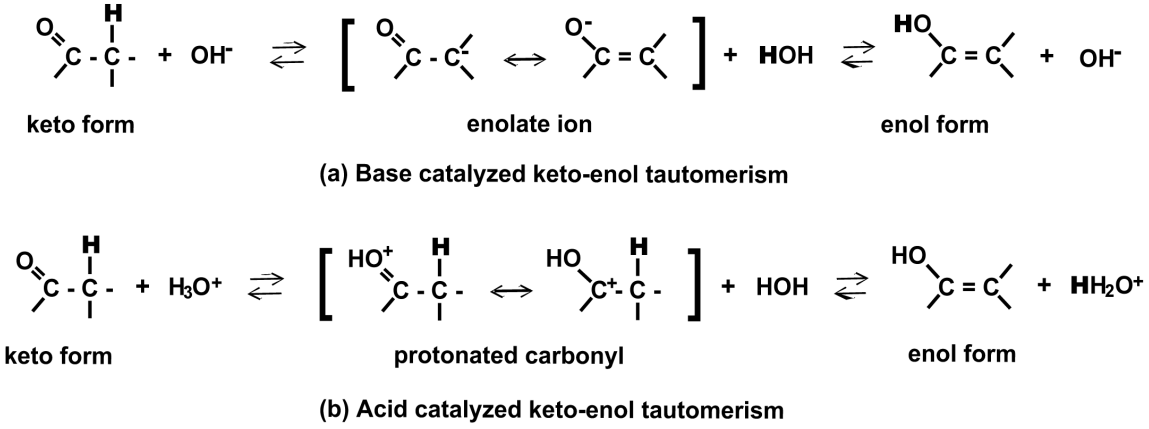

Figure 1-A1. Mechanisms of (a) base- and (b) acid-catalyzed H_α substitution. H undergoing exchange is in bold.

2. Evaluation of anharmonic effects using the frequency scaling factor.

Anharmonic effects arise because the potential energy variation for molecular vibrations is not a simple quadratic function of the coordinate changes, i.e., the Simple Harmonic Oscillator (SHO) approximation widely adopted in ab initio methods to calculate vibrational frequencies and in the equation of reduced partition function ratio (1-5) to calculate isotopic fractionation factors. For a polyatomic molecule, adopting the SHO potential gives the vibrational energy as:

$$E_n^{SHO} = hc\sum_i \omega_i^{SHO}(n_i + \frac{1}{2}) \tag{1-A1}$$

where ω_i^{SHO} is the harmonic frequency (in cm^{-1}) for the *i*th normal mode, c is the speed of light, h is Plank's constant, and n_i is the integer quantum number for the *i*th normal mode. The summation goes over the 3N-6 degrees of freedom, where N is the number of atoms in the molecule. Adding the second-order anharmonic correction to the potential surface gives the vibration energy as:

$$E_n = hc[G_0 + \sum_i \omega_i\,(n_i + \frac{1}{2}) + \sum_{j\geq i} x_{ij}(n_i + \frac{1}{2})(n_j + \frac{1}{2})] \tag{1-A2}$$

where G_0 (cm^{-1}) is a constant, ω_i is the harmonic frequency, and x_{ij} (cm^{-1}) is the anharmonic coefficient. The anharmonicity of individual normal mode *i* is depicted by x_{ii}, while x_{ij} ($i \neq j$) represent the anharmonic coupling between normal mode *i* and *j*. Note that the value of ω_i is usually close but not equal to that of ω_i^{SHO}. At room temperature, the most important contribution to the vibrational partition function comes from the zero potential energy (ZPE) which, in corresponding to (1-A1) and (1-A2), respectively, is

$$E_0^{SHO} = \frac{1}{2}hc\sum_i \omega_i^{SHO} \tag{1-A3}$$

and

$$E_0 = hc[G_0 + \frac{1}{2}\sum_i \omega_i + \frac{1}{4}\sum_{j\geq i} x_{ij}] \tag{1-A4}$$

Due to the omission of anharmonic effects, the value of ω_i^{SHO} calculated by ab initio methods is about 10% higher than the fundamental frequency (ω_i^{fund}) measured by spectroscopy which results from the energy transition from level E_1 to E_0. Using (1-A2), ω_i^{fund} can be calculated as:

$$\omega_i^{fund} = \frac{E_1(n_i = 1, n_{j\neq i} = 0) - E_0}{hc} = \omega_i + 2x_{ii} + \frac{1}{2}\sum_{j\neq i} x_{ij} \qquad \text{(1-A5)}$$

Note the change in the summation index, and that $x_{ij} = x_{ji}$.

2.1. The effect of scaling factor on ZPE and β factor

The scaling factor *s* is used to scale the calculated value of ω_i^{SHO} to match that of ω_i^{fund} , so we have:

$$\omega_i^{fund} = s\omega_i^{SHO} \qquad \text{(1-A6)}$$

If the scaled ab initio frequencies are used in (1-5) to calculate the reduced partition function ratio (the β factor), the ZPE would be calculated according to the SHO approximation (1-A3):

$$\begin{aligned} E_0^{scaled} &= \frac{1}{2}hc\sum_i s\omega_i^{SHO} = \frac{1}{2}hc\sum_i (\omega_i + 2x_{ii} + \frac{1}{2}\sum_{j\neq i} x_{ij}) \\ &= \frac{1}{2}hc\sum_i \omega_i + hc\sum_i x_{ii} + \frac{1}{2}hc\sum_{j>i} x_{ij} \end{aligned} \qquad \text{(1-A7)}$$

Compared to the real ZPE as given by (A2-4), E_0^{scaled} overestimates the anharmonic contribution to ZPE by $\frac{3}{4}hc\sum_i x_{ii} + \frac{1}{4}hc\sum_{j>i} x_{ij}$.

Similarly, the partition function ratio corresponding to E_0^{scaled} can be calculated as:

$$\beta_{ZPE}^{scaled} = \prod_i \frac{\exp(-\frac{1}{2}\frac{hc}{kT} s\omega_{2i}^{SHO})}{\exp(-\frac{1}{2}\frac{hc}{kT} s\omega_{1i}^{SHO})} \cdot \quad \text{(1-A8)}$$

where the subscript 1 and 2 denote the isotopologues that contain the common and rare isotope, respectively. (1-A8) can be rearranged into:

$$\beta_{ZPE}^{scaled} = \exp[-\frac{1}{2}\frac{hc}{kT}\sum_i(\omega_{2i}^{SHO} - \omega_{1i}^{SHO})]\exp[\frac{1}{2}\frac{hc}{kT}(1-s)\sum_i(\omega_{2i}^{SHO} - \omega_{1i}^{SHO})]$$

Note that the first term of the right-hand side (RHS) is the partition function ratio of ZPE calculated using unscaled ab initio frequencies ($\beta_{ZPE}^{unscaled}$). The second RHS term thus is equal to the ratio of $\beta_{ZPE}^{scaled} / \beta_{ZPE}^{unscaled}$ (defined as R):

$$R = \beta_{ZPE}^{scaled} / \beta_{ZPE}^{unscaled} = \exp[\frac{1}{2}\frac{hc}{kT}(1-s)\sum_i(\omega_{2i}^{SHO} - \omega_{1i}^{SHO})] \quad \text{(1-A9)}$$

Since the partition function ratio of ZPE is by far the largest contributor to the total partition function ratio (the β factor), R is approximately equal to $\beta^{scaled} / \beta^{unscaled}$ and thus can be used to evaluate the effect of scaling factor on the value of β factors. R is an exponential function of both (1-s) and $\sum_i(\omega_{2i}^{SHO} - \omega_{1i}^{SHO})$. The second term is the total isotopic frequency shift which is characteristic for specific bonding environments, while the first term reflects the ratio between the anharmonic coefficients and the harmonic frequencies. Therefore the value of R manifests the intrinsic significance of anharmonicity for individual molecules to an extent tuned by the value of *s*.

2.2. The uncertainty in scaling factor for relevant molecules.

The scaling factor is typially derived for a specific ab initio method using available experimental frequencies for all kinds of molecules, including small organic molecules containing O, N, S, P, Si, B, X, etc. As a result, it gives rise to relatively large uncertainties

(for example, 0.967±0.021 for BLY3P/6-311G**), which, if propagated into the value of β^{scaled}, would result in errors of ±60‰ in the fractionation factor for C-bound H corresponding to a change of ±0.02 in the scaling factor. Since we are only interested in hydrocarbons with or without a few function groups that are relevant to sedimentary organic matter, we examined the variation in scaling factor among these compounds. Specifically, the scaling factor was derived, respectively, for water, alkanes (C_3–C_6), alkenes (C_4–C_5), ketone and aldehydes (C_3), ester (C_3), and ether and alcohol (C_2) by regression between experimental and calculated frequencies (Fig. A2-1). The frequency data were obtained from the complete list of molecular frequencies used to derive the recommended scaling factor for the BLY3P/6-311G** method on the NIST website (http://cccbdb.nist.gov/). The results (see the legend of Fig. A2-1) are very consistent at 0.967±0.002.

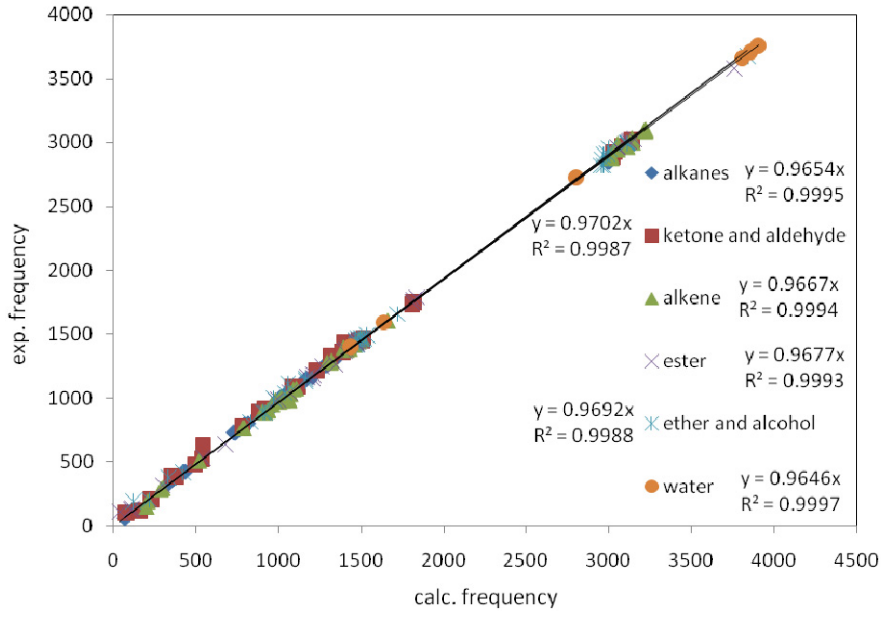

Figure 1-A2. Regression between experimental and calculated frequencies for water, alkanes, alkenes, ketone and aldehydes, ester, and ether and alcohol

Table 1-A1. Measured hydrogen isotopic compositions of each incubated ketone substrate (δ^2H_K) and the corresponding water (δ^2H_W) at equilibrium[a]

ketone	δ^2H (‰)	0	1	2	3	4	5	6	7	8
4-Heptanone	δ^2H_W	475.7 (0.2)	373.9 (0.2)	224.2 (0.2)	98.0 (0.4)	-35.2 (0.2)	-150.7 (0.2)	-281.2 (0.3)		
	25°C δ^2H_K	31.5 (1.8)	6.9 (4.0)	-35.1 (3.3)	-56.4 (2.6)	-92.8 (2.9)	-120.5 (1.4)	-161.0 (2.5)		
	50°C δ^2H_K	45.6 (4.9)	13.4 (1.7)	-20.8 (3.4)	-50.7 (0.1)	-85.6 (0.1)	-112.6 (0.5)	N/A		
	70°C δ^2H_K	33.4 (1.8)	0.6 (1.0)	-27.5 (0.8)	-60.4 (0.2)	-99.0 (1.8)	-123.6 (1.1)	-162.9 (0.5)		
5-Nonanone	δ^2H_W	475.4 (0.1)	345.7 (0.1)	244.1 (0.1)	107.8 (0.5)	-33.0 (0.2)	-175.7 (0.3)	-280.8 (0.2)		
	25°C δ^2H_K	7.6 (2.1)	-18.6 (N/A)	-36.5 (1.0)	-61.1 (2.5)	-93.5 (4.7)	-120.0 (3.4)	-138.8 (5.0)		
	50°C δ^2H_K	11.3 (1.1)	-13.8 (0.1)	-39.9 (3.5)	-64.6 (1.5)	-87.3 (2.1)	-118.1 (2.5)	-139.8 (3.3)		
	70°C δ^2H_K	0.9 (0.8)	N/A	-41.8 (1.8)	-72.7 (2.3)	-96.3 (1.6)	N/A	N/A		
2-Methyl-3-hexanone	δ^2H_W	476.5 (0.1)	352.4 (0.6)	229.0 (0.4)	100.1 (0.2)	-26.3 (0.2)	-143.2 (0.3)	-278.8 (0.4)		
	25°C δ^2H_K	-10.5 (4.9)	-35.6 (2.0)	-59.3 (2.6)	-85.1 (3.9)	-108.6 (4.9)	-132.0 (0.4)	-160.5 (0.6)		
	50°C δ^2H_K	-4.1 (4.2)	-26.6 (3.3)	-53.1 (3.6)	-79.6 (0.6)	-104.1 (1.6)	-128.6 (5.1)	-153.6 (5.8)		
	70°C δ^2H_K	-15.6 (1.1)	-33.9 (4.2)	-58.4 (4.9)	-83.4 (1.8)	-112.2 (4.9)	-133.9 (3.9)	-159.4 (4.2)		
2-heptanone	δ^2H_W	476.1 (0.2)	348.3 (0.4)	230.3 (0.2)	100.8 (0.2)	-34.7 (0.2)	-135.9 (0.2)	-280.5 (0.2)		
	25°C δ^2H_K	58.3 (4.6)	15.2 (N/A)	-26.9 (N/A)	-64.8 (N/A)	-104.9 (N/A)	-140.2 (N/A)	-166.1 (0.1)		
	50°C δ^2H_K	62.2 (6.1)	37.7 (2.5)	-13.2 (1.1)	-48.4 (3.9)	-91.2 (0.7)	-124.2 (0.3)	-160.7 (3.9)		
	70°C δ^2H_K	69.8 (2.0)	34.4 (1.5)	-6.0 (0.1)	-43.9 (4.3)	-81.4 (0.7)	-124.6 (3.2)	-158.3 (3.8)		
2,4-Dimethyl-3-pentanone	δ^2H_W	475.4 (0.2)	365.3 (0.3)	226.3 (0.5)	98. 0 (0.3)	-29.2 (0.3)	-150.4 (0.3)	-279.8 (0.4)		
	25°C δ^2H_K	-3.6 (0.1)	-21.3 (N/A)	-42.2 (0.2)	-60.5 (1.6)	-78.3 (1.4)	-97.8 (0.9)	-114.4 (1.5)		
	50°C δ^2H_K	-6.3 (3.0)	-24.3 (5.7)	-45.0 (3.5)	-61.9 (1.5)	-81.1 (0.7)	-96.9 (2.7)	-115.7 (2.6)		
	70°C δ^2H_K	-10.5 (4.5)	-23.8 (2.3)	-46.9 (3.5)	-63.6 (2.5)	-83.3 (2.0)	-98.4 (1.8)	-113.4 (1.0)		
3,5-Dimethyl-4-heptanone	δ^2H_W	476.1 (0.1)	351.8 (0.1)	227.7 (0.5)	85.1 (0.2)	-42.0 (0.3)	-172.2 (0.3)	-279.5 (0.4)		
	25°C δ^2H_K	7.3 (1.2)	-7.4 (1.1)	-21.8 (0.8)	-31.7 (0.8)	-53.6 (0.3)	-66.1 (3.2)	-76.7 (1.2)		
	δ^2H_W	477.1	391.5	298.9	109.9	-52.0	-179.6	-281.5		
	50°C δ^2H_K	11.5 (2.7)	-1.5 (1.3)	-8.3 (0.4)	-31.9 (3.2)	-47.4 (0.8)	-62.1 (3.0)	-72.1 (0.8)		
	70°C δ^2H_K	19.1 (2.6)	13.9 (1.3)	1.2 (2.3)	-18.1 (4.7)	-35.7 (0.7)	-49.4 (4.4)	-61.5 (1.5)		
Cyclohexanone	δ^2H_W	459.0 (0.4)	337.2 (0.4)	219.4 (0.5)	98.1 (0.1)	-29.4 (0.2)	-153.2 (0.2)	-279.4 (0.3)		
	25°C δ^2H_K	-14.2 (0.9)	-53.8 (0.1)	-93.1 (0.6)	-134.3 (2.9)	-179.2 (1.6)	-213.5 (0.9)	-264.0 (4.0)		
	δ^2H_W	464.9 (1.0)	373.0 (3.2)	285.3 (1.4)	186.8 (2.1)	97.5 (3.6)	-3.7 (1.0)	-89.1 (2.0)	-187.9 (1.7)	-277.2 (4.8)
	50°C δ^2H_K	-17.6 (1.6)	-45.9 (2.2)	-71.5 (1.7)	-105.6 (0.9)	-139.1 (3.8)	-170.4 (0.3)	-205.2 (1.8)	-232.6 (3.7)	-266.8 (2.5)
	70°C δ^2H_K	-9.2 (3.8)	-48.1 (3.7)	-76.7 (1.8)	-112.9 (1.8)	-139.2 (2.2)	-173.5 (5.2)	-207.6 (3.5)	-237.1 (1.4)	-268.7 (3.0)

(a) The standard deviations from 2–3 replicates of each ketone sample and from 3–4 replicates of each water sample are shown in brackets.

Table 1-A2. Optimized geometries and experimental geometries in gas phase for the ketones[a]

ketones	O=C bond length (Å)	C-C_α bond length (Å)	O=C-C_α angle (°)	O=C-C_α-C_β dihedral (°)	O=C-C_α-H_α dihedral (°)
Calculated in this study (B3LYP/6-311G)**					
4-heptanone	1.211	1.525	121.8	7.4	131.8, -115.3
5-nonanone	1.211	1.525	121.9	7.2	131.6, -115.5
2-heptanone	1.210	1.524 (2° C_α) 1.519 (1° C_α)	122.0 (2° C_α) 121.6 (1° C_α)	6.3	130.7, -116.5 (2° H_α) 7.8, (1° H_α)
2-Methyl-3-hexanone	1.211	1.522 (2° C_α) 1.534 (3° C_α)	121.9 (2° C_α) 121.3 (3° C_α)	8.7 (2° C_β) 36.9, -85.9 (1° C_β)	157.3 (3° H_α) 133.6, -113.9 (2° H_α)
3,5-Dimethyl-4-heptanone	1.212	1.532	121.4	92.4 (2° C_β) -31.9 (1° C_β)	-151.6
2,4-Dimethyl-3-pentanone	1.212	1.532	121.4	30, -93	-151.2
Cyclohexanone	1.210	1.523	122.4	131.2	6.9 (equatorial) -109.2 (axial)
Experimental data					
Acetone[b]	1.215	1.515	121.8		
2-Butanone[c]	1.218	1.512 (2° C_α) 1.507 (1° C_α)	122.9 (2° C_α)	0	0 (1° H_α)
3-Methyl-2-butanone[d]	1.217	1.525 (1° C_α)	120.8 (1° C_α)		140 (3° H_α)
Cyclohexanone[e]	1.229	1.503		128.3	

(a) Experimental geometry data for ketones with more than five C atoms are unavailable except for cyclohexanone. Thus, smaller ketone molecules (C_3–C_5) are instead listed for comparison. H and C atoms are labeled according to relative distance from the carbonyl group (subscript Greek letters) and configuration of the bound C atom (1° = primary, 2° = secondary, 3° = tertiary).

(b) Sverdlov, L. M.; Kovner, M. A.; Krainov, E. P. *Vibrational Spectra of Polyatomic Molecules*; Wiley: New York, 1974.

(c) Durig, J. R.; Feng, F. S.; Wang, A.; Phan, H. V. *Can. J. of Chem.* 1991, *69*, 1845–1856.

(d) Landolt-Bornstein *Group II: Atomic and Molecular Physics.* Springer-Verlag: Berlin, 1992.

(e) Dillen, J.; Geise, H. J. *J. Mol. Struct.* 1980, *69*, 137–144.

Table 1-A3. Calculated β factors from 0°C to 100°C for water[a]

T(°C)	T(K)	β_{gas}(this study)	β_{liquid} (this study)	β_{gas} (Richet et al., 1977)	β_{gas} (Urey, 1947)
0	273.15	17.351	**19.291**	15.131	16.467
5	278.15	16.351	**18.053**		
10	283.15	15.441	**16.939**	13.531	
15	288.15	14.611	**15.932**		
20	293.15	13.852	**15.020**	12.193	
25	298.15	13.156	**14.192**		12.518
30	303.15	12.516	**13.436**	11.064	
35	308.15	11.927	**12.747**		
40	313.15	11.383	**12.114**	10.101	
45	318.15	10.880	**11.533**		
50	323.15	10.413	**10.998**	9.275	
55	328.15	9.980	**10.504**		
60	333.15	9.578	**10.048**		
65	338.15	9.203	**9.625**		
70	343.15	8.852	**9.232**		
75	348.15	8.525	**8.867**	7.657	
80	353.15	8.219	**8.527**		
85	358.15	7.932	**8.209**		
90	363.15	7.662	**7.912**		
95	368.15	7.409	**7.634**		
100	373.15	7.171	**7.374**	6.487	

(a) β factors of liquid water are calculated based on that of gasous water and the liquid-vapor fractionation factor from Wesolowski and Horita (1994, GCA):

$$1000\ln\alpha_{liquid-gas} = \frac{1158.8}{10^9}T^3 - \frac{1620.1}{10^6}T^2 + \frac{794.84}{10^3}T - 161.04 + \frac{2.9992}{T^3}10^9$$

Table 1-A4. Calculated β factors from 0°C to 100°C for H_α in ketones

T	2,4-dimethyl-3-petanone	3,5-dimethyl-4-heptanone	2-methyl-3-hexanone		4-heptanone	5-nonanone	2-heptanone		cyclohexanone	
(°C)	3° H_α	3° H_α	3° H_α	2° H_α	2° H_α	2° H_α	1° H_α	2° H_α	2° H_{eql}	2° H_{axi}
0	20.215	19.655	20.292	16.812	16.817	16.671	15.753	16.819	18.215	16.881
5	18.851	18.339	18.921	15.754	15.759	15.625	14.799	15.761	17.038	15.816
10	17.625	17.154	17.689	14.797	14.803	14.680	13.934	14.805	15.976	14.853
15	16.518	16.086	16.577	13.931	13.936	13.823	13.148	13.938	15.016	13.980
20	15.517	15.118	15.571	13.143	13.149	13.043	12.432	13.150	14.144	13.188
25	14.608	14.239	14.658	12.425	12.431	12.333	11.777	12.431	13.351	12.465
30	13.782	13.440	13.828	11.769	11.775	11.684	11.178	11.775	12.627	11.805
35	13.028	12.710	13.070	11.168	11.174	11.090	10.628	11.174	11.966	11.201
40	12.338	12.043	12.378	10.617	10.623	10.544	10.122	10.623	11.359	10.647
45	11.706	11.431	11.743	10.109	10.115	10.042	9.656	10.115	10.802	10.137
50	11.126	10.868	11.160	9.642	9.647	9.579	9.225	9.647	10.289	9.667
55	10.592	10.350	10.623	9.210	9.215	9.151	8.826	9.215	9.815	9.233
60	10.099	9.872	10.128	8.810	8.815	8.755	8.456	8.815	9.378	8.831
65	9.643	9.431	9.671	8.439	8.444	8.387	8.112	8.444	8.973	8.459
70	9.221	9.021	9.247	8.094	8.100	8.046	7.792	8.100	8.597	8.113
75	8.830	8.642	8.854	7.774	7.779	7.728	7.494	7.779	8.247	7.791
80	8.467	8.289	8.489	7.475	7.480	7.432	7.216	7.480	7.922	7.491
85	8.128	7.960	8.150	7.196	7.201	7.156	6.955	7.201	7.618	7.211
90	7.813	7.654	7.833	6.935	6.940	6.897	6.712	6.940	7.335	6.949
95	7.518	7.367	7.537	6.691	6.696	6.655	6.483	6.696	7.070	6.704
100	7.243	7.100	7.261	6.462	6.467	6.428	6.268	6.467	6.821	6.474

(a) Listed β factors are the average value for H atoms bound to the same C atom.

(c) H position is indicated by the subscript Greek letter as relative to the carbonyl group.

(d) 1° = primary, 2° = secondary, 3° = tertiary

(d) Superscript "eql" or "axl" denotes the equatorial or axial Hα in cyclohexnaone.

Table 1-A5. Regression between experimental and calculated fractionation factors for the six ketones at 25, 50, and 70°C. Calculation conditions are denoted using capital letters: **K =** ketones; **W =** water; **IS** = the solvation effect is modeled by implicit solvation model; **EHn =** the solvation effect is modeled by explicit hydration method, where **n = 3, 4, or 5** water molecules; **LV** = the solvation effect for water is modeled by multiplying the experimental liquid-vapor fractionation factor; **U** = using unscaled frequency; **S** = using scaled frequency (scaling factor = 0.967[c]).

Calculation method			**25°C**		**50°C**		**70°C**		**Δslope[b]**
#	**ketone**	**water**	**slope**	**intercept**	**slope**	**intercept**	**slope**	**intercept**	
1[a]	IS+U	LV+U	**0.982**±0.035	**-3.1**±3.6	**0.904**±0.072	**-6.8**±7.1	**0.811**±0.038	**-21.0**±3.7	**0.171**
2	IS+S	LV+S	**1.069**±0.044	**15.8**±4.6	**0.987**±0.074	**9.579**±7.7	**0.883**±0.049	**7.3**±5.1	**0.186**
3	IS+U	IS+U	**0.921**±0.037	**-79.7**±2.8	**0.856**±0.064	**-72.0**±4.1	**0.769**±0.042	**-76.3**±2.5	**0.152**
4	IS+S	IS+S	**0.972**±0.040	**-80.9**±2.8	**0.918**±0.069	**-59.2**±4.6	**0.833**±0.046	**-57.6**±3.0	**0.140**
5	EH3+ U	EH3+ U	**1.140**±0.034	**33.5**±3.8	**1.052**±0.094	**29.8**±10.8	**0.949**±0.056	**13.0**±6.4	**0.191**
6	EH3+ S	EH3+ S	**1.211**±0.035	**43.8**±4.0	**1.120**±0.100	**39.4**±11.6	**1.01**±0.061	**21.5**±7.1	**0.202**
7	EH4+ U	EH4+ U	**1.119**±0.033	**32.3**±3.7	**1.023**±0.106	**25.9**±12.1	**0.921**±0.063	**8.2**±7.3	**0.198**
8	EH4+ S	EH4+ S	**1.186**±0.035	**41.3**±4.0	**1.085**±0.113	**34.1**±12.9	**0.978**±0.069	**15.6**±7.9	**0.208**
9	EH5+ U	EH5+ U	**1.102**±0.046	**19.3**±4.8	**1.011**±0.102	**15.2**±10.8	**0.917**±0.032	**-0.3**±3.5	**0.186**
10	EH5+ S	EH5+ S	**1.168**±0.048	**28.0**±5.1	**1.073**±0.109	**23.2**±11.6	**0.974**±0.035	**6.9**±3.8	**0.195**

(a) The calculation methods applied in this paper

(b) The difference between regression slope at 25°C and 70°C, indicating the temperature variation of the regression curve

(c) A scaling factor of 0.967±0.021 for B3LYP/6-311G** method is recommended by Computational Chemistry Comparison and Benchmark DataBase (CCCBDB), NIST.

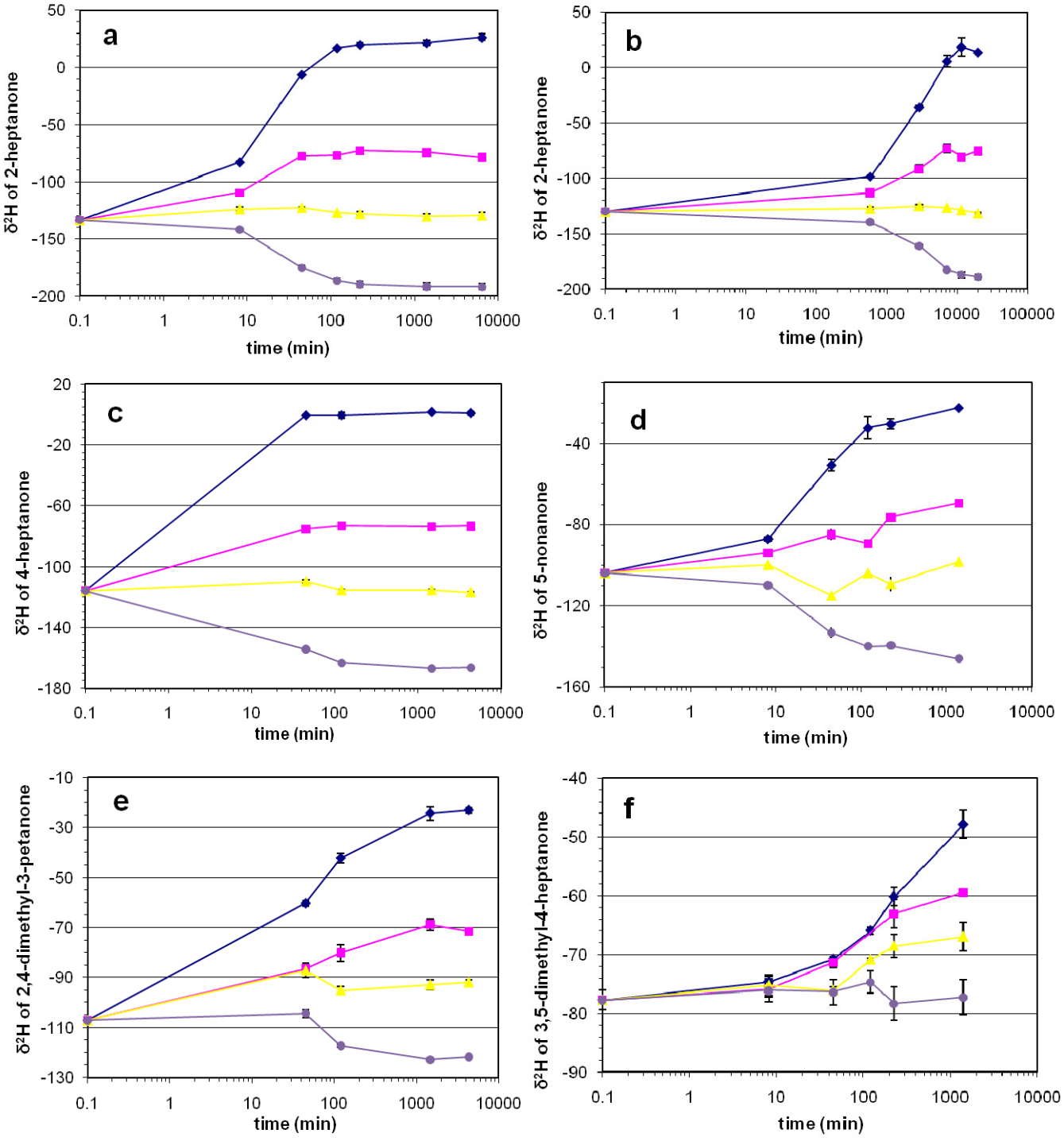

Figure 1-A3. δ^2H values of the ketone substrates over time during incubations with waters of varying δ^2H values (diamond = 457.2‰, square = 121.2‰, triangle = -64.2‰, circle = -271.7 ‰). (a) 2-heptanone at 70°C, pH 12.00; (b) 2-heptanone at 70°C, pH 1.20; (c) 4-heptanone at 70°C, pH 12.40; (d) 5-nonanone at 70°C, pH 12.00; (e) 2,4-dimethyl-3-pentanone at 70°C, pH 12.40; (f) 2,4-dimethyl-3-pentanone at 70°C, pH 12.00

C h a p t e r 2

EQUILIBRIUM $^{2}H/^{1}H$ FRACTIONATIONS IN ORGANIC MOLECULES

II. LINEAR ALKANES, ALKENES, KETONES, CARBOXYLIC ACIDS, ESTERS, ALCOHOLS AND ETHERS

Ying Wang[1], Alex L. Sessions[1], Robert J. Nielsen[2], and William A. Goddard III[2]

[1]Division of Geological and Planetary Sciences,
[2]Materials and Process Simulation Center,
California Institute of Technology, Pasadena, CA, USA

(*Geochimica et Cosmochimica Acta*, 2009, *in press*)

ABSTRACT

Equilibrium $^{2}H/^{1}H$ fractionation factors (α_{eq}) for various H positions in alkanes, alkenes, ketones, carboxylic acids, esters, alcohols, and ethers were calculated between 0 and 100˚C using vibrational frequencies from ab initio QM calculations (B3LYP/6-311G**). Results were then corrected using a temperature-dependent linear calibration curve based on experimental data for H_{α} in ketones (Chapter 1). The total uncertainty in reported α_{eq} values is estimated at 10–20‰. The effects of functional groups were found to increase the value of α_{eq} for H next to electron-donating groups, e.g., −OR, −OH, or −O(C=O)R, and to decrease the value of α_{eq} for H next to electron-withdrawing groups, e.g., −(C=O)R or −(C=O)OR. Smaller but significant functional group effects are also observed for H_{β} and sometimes H_{γ}. By summing over individual H positions, we estimate the equilibrium fractionation relative to water to be −90‰ to −70‰ for n-alkanes and around −100‰ for pristane and phytane. The temperature dependence of these fractionations is very weak between 0 and 100°C. Our estimates of α_{eq} agree well with field data for thermally mature hydrocarbons ($\delta^{2}H$ values between -80‰ and -110‰ relative to water). Therefore the observed $\delta^{2}H$ increase of individual hydrocarbons and the disappearance of the biosynthetic $\delta^{2}H$ offset between *n*-alkyl and linear isoprenoid lipids during maturation of organic matter can be confidently attributed to H exchange towards an equilibrium state. Our results also indicate that many *n*-alkyl lipids are biosynthesized with $\delta^{2}H$ values that are close to equilibrium with water. In these cases, constant down-core $\delta^{2}H$ values for *n*-alkyl lipids cannot be reliably used to infer a lack of isotopic exchange.

1. INTRODUCTION

Compound-specific hydrogen isotope analysis has become widespread over the past decade and has led to a variety of studies using the H isotopic composition (δ^2H value) of sedimentary organic matter (SOM) and oils as paleoenvironmental proxies (Xie et al., 2000; Huang et al., 2002; Dawson, 2004; Sachse et al., 2006). However, such applications implicitly assume the preservation of biosynthetic isotopic compositions over geological timescales, and therefore must address the exchangeability of C-bound H (Sessions et al., 2004). A recent review of field data (Schimmelmann et al., 2006) shows that, as thermal maturity increases, δ^2H values of individual hydrocarbons steadily increase while the typical 100‰ biosynthetic offsets between linear and isoprenoid structures (Sessions et al., 1999) steadily disappear. Furthermore, this systematic change in δ^2H values is negligible where the hydrocarbons are ^{2}H-depleted relative to water by 80–110‰ (typically associated with very high maturity) and is more apparent where the depletion is smaller or larger (dos Santos Neto and Hayes, 1999; Lis et al., 2006). These observations can potentially be explained by H exchange between hydrocarbons and sediment porewater and imply that the endpoint of exchange results in fractionations between hydrocarbons and water in the range of −80 to −110‰ (Schimmelmann et al., 2006). Testing this hypothesis requires quantitative knowledge of the equilibrium ^{2}H/^{1}H fractionation factors (α_{eq}).

Currently, accurate values of α_{eq} are not known for fractionations involving organic molecules larger than methane. This primarily reflects the difficulties involved in measuring equilibrium fractionations in organic materials: experimental studies suffer from very slow exchange rates of C-bound H (Koepp, 1978; Sessions et al., 2004), while theoretical calculations incorporate potential systematic errors that are particularly limiting for the H-isotope system (Richet et al., 1977). Knyazev et al. (1992) systematically calculated β factors for various H positions in major organic compounds. The results were later modified by Sessions et al. (2004) who incorporated the vapor pressure isotope effect to give α_{eq} values in aqueous phase at 27°C, but the estimated systematic errors amount to ±100‰, far too large to be useful for studies of natural-abundance isotopic variations.

To address these issues, we developed a calibration based on α_{eq} values measured via isotope exchange experiments to correct theoretical estimates using frequencies calculated by the B3LYP/6-311G** method. Details of that calibration are provided in Chapter 1, where we show that α_{eq} values for H_α in various linear ketone molecules can be calculated with uncertainties < 8‰ for temperatures of 0–100°C. Here we apply the same computational methods and calibration to systematically estimate α_{eq} values for H positions in other common organic compounds, including alkanes, alkenes, carboxylic acids, esters, alcohols, and ethers. In doing so, our goal is to provide a modular dataset for equilibrium $^2H/^1H$ fractionations in organic moieties common to sedimentary organic matter, in a form that can be used to piece together estimated fractionation factors for any complete molecule without resorting to further molecular modeling. As a demonstration of this approach, we calculate α_{eq} values for *n*-alkane and linear isoprenoid molecules and discuss the implications of those values to paleo-environment and petroleum studies.

2. METHODS AND NOMENCLATURE

Methods for ab initio calculations are described fully in Chapter 1 and only briefly here. Complete vibrational frequencies for selected organic molecules were calculated for the optimized geometries using the hybrid Hartree-Fock and Density Functional Theory (DFT), B3LYP/6-311G** method (Lee et al., 1988; Becke, 1993), with solvation effect treated by the Poisson-Boltzmann continuum solvation model (Tannor et al.1994). Values of the reduced partition function ratio (β factor) for ^2H-substitution at individual organic H positions were then calculated from vibrational frequencies based on the theoretical method of Urey (1947) and Bigeleisen and Mayer (1947). The β factor for liquid water was obtained by first calculating the β factor for gaseous molecules using the same method, which was then multiplied by the experimental liquid-gas fractionation factor measured by Horita and Wesolowski (1994). The complete dataset of calculated β factor values are provided as the Appendix.

Equilibrium $^{2}H/^{1}H$ fractionation factors (α_{eq}) were then calculated as the ratio of β factors between the organic molecule in aqueous phase and liquid water:

$$\alpha_{eq} = \frac{\beta(CH)_{aqueous}}{\beta(H_2O)_{liquid}}$$

The value of α_{eq} was then corrected using a linear calibration curve based on experimental data for ketones (see Chapter 1) with slope = 1.081 – 0.00376T and intercept = 8.404 – 0.387T, where T is the temperature in degrees Celsius. Application of the ketone-derived calibration curve assumes the same calculation error for other organic compounds as that for ketones. We have shown that the dominant error in the calculation of β factors is the omission of anharmonicity, which is of similar size for C-bound H in most other linear compounds as in ketones (Chapter 1). Therefore errors resulting from the application of ketone-derived calibration are generally expected to be small (4–8‰).

Fractionation factors were calculated over the temperature range of 0–100°C for molecules in several major classes, including alkanes, alkenes, acids, esters, alcohols, and ethers. In each compound class, the value of α_{eq} was calculated for every H position in 4–10 different molecules with carbon numbers between C_5 and C_{11}. In order to compactly summarize data for a large number of compounds, we average data for analogous positions (i.e., methyl, methylene group, etc.) in different molecules to report a single α_{eq} value. Reported uncertainties for that value then combine the uncertainty of the calibration curve with true variations in α_{eq} for analogous H positions in different molecules (typically 1–7‰). This approach gives a total uncertainty in the estimated α_{eq} values to be 10–20‰.

It is important to realize that the calculated values of β and thus α_{eq} presented here are specific to individual atomic positions within a molecule, rather than to the whole molecule. When equilibrium has been established with respect to non-equivalent groups in the same molecule, the molecular β factor can be estimated based on the individual β factors for each group, using the method derived by Galimov (1971). It takes on the form of the arithmetic mean of individual β factors weighted by the number of equivalent atoms

in each group. In the text and figures, fractionation factors are often presented in terms of the isotopic enrichment factor ε_{eq}:

$$\varepsilon_{eq} = (\alpha_{eq} - 1)$$

which is reported in permil (‰) units for easier comparison with the standard δ^2H (‰) notation.

Finally, we remind the reader that we have followed the convention (Chapter 1) of using Greek letters in subscripts to denote molecular positions of specific H atoms, i.e., H_α is the H atom on the first carbon (C_α) that attaches to a functional group, H_β is on the second carbon (C_β), etc. In addition, a saturated C atom is classified as primary, secondary, or tertiary depending on how many other C atoms are attached to it, a descriptor which is also used to denote the H atoms attached to this C atom.

3. RESULTS AND DISCUSSION

3.1. Calculated fractionation factors

A complete list of α_{eq} values for all organic H positions calculated in this study is provided in Table 2-1 in the form of temperature-dependent functions over the range of 0–100°C. We first note two general features of the results: (*i*) The value of α_{eq} for C-bound H is primarily determined by the atoms or functional groups attached to the same carbon center, i.e., the "cutoff effect" that has been observed in this (Chapter 1) and many other studies (Stern and Wolfsberg, 1966a,b; Hartshorn and Shiner, 1972). We therefore define each H position by specifying all surrounding groups within two bonds, or further when necessary. (*ii*) H atoms attached to the same C atom are often sterically symmetric and thus have virtually identical α_{eq} values. However in some cases, e.g., the methlene H atoms on the C next to a double bond can show α_{eq} offsets up to 50‰ depending on their orientations relative to the double bond. Considering the rotation around C−C bonds, equivalent H atoms on the same C atom should be indistinguishable in nature. We therefore report α_{eq} as

the average value of all H atoms on that C atom. Below, the results are summarized by compound class, accompanied by brief discussions of the underlying chemistry.

Table 2-1. Equilibrium $^2H/^1H$ fractionation factors (α_{eq}, between organic H and water) from 0°C to 100°C in the form of $1000\ ln\alpha_{eq} = A + 10^3B/T + 10^6C/T^2$ (T is temperature in Kelvins; standard deviations for α_{eq} are between 0.010–0.020). Also listed is the value of ε_{eq} at 25°C.

H position	*A*	*B*	*C*	ε_{eq} (‰)	H position	*A*	*B*	*C*	ε_{eq} (‰)
H in alkanes					*H in carboxylic acids and esters*				
-C**H**$_3$	-216.7	85.19	-19.66	-141	-CH_2CH_2COO**H**	-435.4	222.7	-22.84	56
-CH_2C**H**$_2$$CH_2$-	-242.3	75.23	-7.822	-75	-CH_2C**H**$_2$COOR[a]	-205.5	59.62	-9.613	-107
-CH_2C**H**$_2$$CH_3$	-255.7	83.03	-8.085	-66	-CH_2C**H**$_2$$CH_2$COOR[a]	-275.4	93.53	-7.900	-49
-CH_2C**H**(CH_3)CH_2-	-291.0	85.13	-0.239	-8	-CH_2COOC**H**$_3$	-323.6	140.1	-18.16	-56
-CH_2C**H**(CH_3)$_2$	-310.3	96.26	-0.640	5	-CH_2COOC**H**$_2$$CH_3$	-369.3	145.0	-8.419	22
H in alkenes					-CH_2COOC**H**$_2$$CH_2$-	-358.9	138.6	-8.074	15
C**H**$_2$=	-122.4	37.41	-20.46	-203	-CH_2COOCH_2C**H**$_2$$CH_2$-	-260.0	84.96	-7.771	-61
CH_2=C**H**- and (E)-C**H**=C**H**-	-158.2	42.44	-13.63	-156	*H in alcohols*				
					-CH_2O**H**[a]	-477.8	270.3	-35.20	33
(Z)-C**H**=C**H**-	-155.2	32.63	-8.973	-136	-CH_2CHO**H**CH_3	-469.3	257.0	-30.69	49
=CH(C**H**$_2$)CH_2-	-238.2	73.33	-7.897	-78	-CH_2CHO**H**CH_2-	-468.8	258.8	-31.77	43
=CHC**H**(CH_3)CH_2-	-273.8	111.8	-8.042	11	-C**H**$_2$OH	-330.8	122.4	-8.060	-11
=CHC**H**$_2$CH=	-232.5	84.70	-10.76	-67	-CH_2C**H**OHCH_2-	-432.4	165.3	-2.670	96
-CH=C**H**C**H**=CH-	-158.3	36.83	-10.53	-142	-C**H**$_2$$CH_2$OH	-248.2	78.43	-7.669	-69
-CH=C**H**C(CH_3)=C**H**-	-162.0	34.80	-8.284	-129	-CH_2C**H**$_2$CHOH-	-228.0	67.36	-7.603	-84
H in ketones					-CH_2C**H**$_2$$CH_2$CHOH-	-269.3	89.85	-7.717	-53
-COC**H**$_3$	-189.3	74.67	-21.81	-168	*H in ethers*				
-COC**H**$_2$$CH_2$-	-188.0	51.18	-10.31	-124	-CH_2OC**H**$_3$	-283.2	116.8	-17.89	-89
-COC**H**(CH_3)$_2$	-336.9	111.5	-0.8047	28	-CH_2OC**H**$_2$$CH_3$	-315.3	112.6	-7.324	-20
-COC**H**(CH_3)CH_2-	-309.6	95.75	-0.2783	8	-CH_2OC**H**$_2$$CH_2$-	-307.9	108.9	-7.591	-28
-$COCH_2$C**H**$_2$$CH_2$-	-268.4	90.03	-7.998	-55	-CH_2OCH_2C**H**$_2$$CH_2$-	-253.1	81.41	-7.847	-66

(a) R represents either H (in carboxylic acids) or an alkyl moiety (in esters)

3.1.1. H in alkanes

We calculated ε_{eq} values for C_5, C_6, C_7, C_9, and C_{11} *n*-alkanes, and for 2-methyl, 3-methyl, and 4-methyl heptanes. These molecules contain no functional groups. The primary, secondary, and tertiary Hs are each characterized by distinct ε_{eq} values and temperature dependences (Fig. 2-1). At room temperature the values of ε_{eq} are near −140‰, −70‰ and 0‰ for primary, secondary, and tertiary H, respectively. Results from the calculations by Knyazev et al. (1992) and Sessions et al. (2004), −163 ± 78‰ for primary H and −56 ± 102‰ for secondary H at 27°C, are consistent with these new estimates. Replacing an ethyl or longer alkyl branch with a methyl group increases the value of ε_{eq} for H located on the branching carbon. For example, in *n*-alkane molecules, ε_{eq} for the secondary H atoms on the C next to the methyl groups is ~10‰ higher than for the other secondary H atoms. Similarly, ε_{eq} for the tertiary H in 2-methylheptane is ~10‰ higher than the tertiary H in 3-methylheptane.

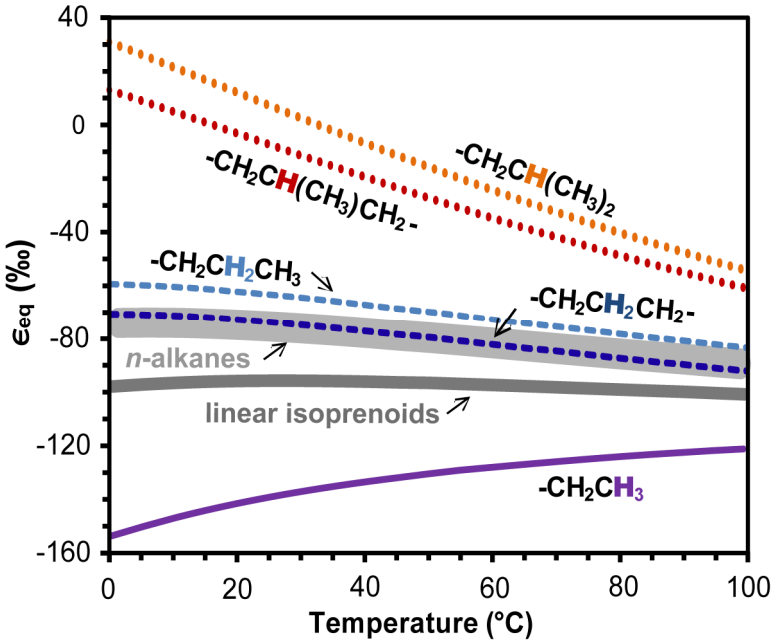

Figure 2-1. Equilibrium $^2H/^1H$ isotopic enrichment factors (ε_{eq}) between organic H and water for five distinct H positions in linear alkanes (curves). Also shown (gray areas) are the ranges of ε_{eq} values for C_{14} – C_{33} *n*-alkanes and for phytane and pristane.

Consequently, five H positions with distinct ε_{eq} values can be used to summarize all relevant structures in natural linear (straight and branched) alkanes, specifically (target H position in bold), $-C\mathbf{H_3}$, $-CH_2C\mathbf{H_2}CH_3$, $-CH_2C\mathbf{H_2}CH_2-$, $-CH_2C\mathbf{H}(CH_3)CH_2-$, and $-CH_2C\mathbf{H}(CH_3)_2$. The average values of ε_{eq} for each analogous position in all modeled alkane molecules are plotted against temperature in Fig. 2-1. To check for potential effects on ε_{eq} from distant functional groups, we also calculated ε_{eq} for the same five analogous H positions in 10 linear ketones. The effects of the carbonyl group on ε_{eq} are found to reach as far as H_β, but no farther. Thus when H_α and H_β in the ketone are excluded, then ε_{eq} values for equivalent H positions in linear alkanes and ketones are virtually identical (data not shown). We conclude that our results for linear alkanes are also suitable for estimating fractionations in the aliphatic chains of functionalized molecules.

The increase of ε_{eq} for H bonded to C with increasing alkyl substitution is likely related to the inductive electron-donating effect (+I) of alkyl groups, with the methyl group being the strongest donor. It acts to increase the electron density of the neighboring C−H bond, which gives rise to a stiffer bond and thus higher ε_{eq} values (Bigeleisen and Mayer, 1947; Hartshorn and Shiner, 1972). This effect is superimposed on the influence of functional groups, for example as seen in the similar patterns of ε_{eq} for primary, secondary, and tertiary H in alkanes and adjacent to carbonyl groups in ketones (Chapter 1). Therefore, in the following sections, ε_{eq} values for H near functional groups are compared to alkane H at analogous positions (i.e., primary, secondary, or tertiary H) to highlight the effect of that functional group.

Values of ε_{eq} for linear aliphatic hydrocarbon molecules can be calculated as the weighted average of ε_{eq} for all individual hydrogen positions (Galimov, 1971). Results are between −70 to −90‰ for *n*-alkanes (C_{14}–C_{33}) and around -100‰ for pristane and phytane (Fig. 2-1). They agree well with the predicted range of −80 to −110‰ based on field data (Schimmelmann et al., 2006). The value of ε_{eq} for C_{14}–C_{34} *n*-alkanes increases with chain-length by 7–11‰ between 0–100˚C, due to the slightly higher proportion of secondary H in longer molecules. It has been shown that artificial thermal maturation of natural oils can produce ^{2}H-enrichments with increasing chain-length by 4–17‰ due to kinetic fractionation (Tang et al., 2005). Therefore in some highly mature natural samples, the

observed 10–30‰ increase with chain-length (Schimmelmann et al., 2004; Pedentchouk et al., 2006) could result at least partially from equilibrium isotope effects. Another noteworthy feature is that the value of ε_{eq} for these hydrocarbons varies only slightly with temperature over the range 0–100°C. For *n*-alkanes, this reflects the fact that secondary H has little temperature dependence, whereas for isoprenoids the temperature dependences of primary and tertiary H are opposite and very nearly cancel.

3.1.2. H in alkenes

Values of ε_{eq} were first calculated for five monounsaturated alkene molecules, including 1-hexene, 3-methyl-1-hexene, 5-methyl-1-hexene, trans-5-decene, and cis-5-decene. Results for specific H positions that are affected by the double bond are plotted in Fig. 2-2. At room temperature, ε_{eq} values for H atoms in C**H**$_2$= are ~60‰ more negative than primary H in alkanes. A similar offset is observed between H in cis −C**H**= and secondary H in alkanes. H on a *trans* double bond is further depleted relative to the cis isomer by ~20‰. The decrease of ε_{eq} values with lower coordination number of the C atom in the C−H bond was also observed by Hartshorn and Shiner (1972) and Knyazev et al. (1992).

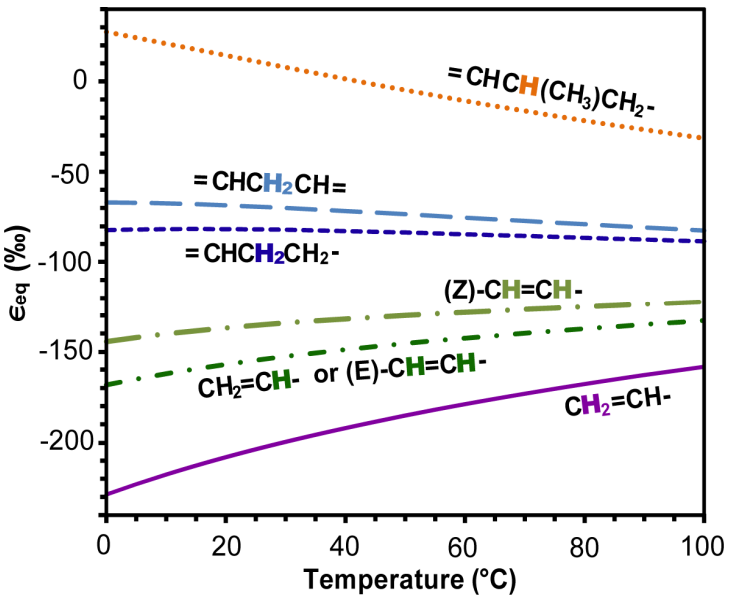

Figure 2-2. Equilibrium $^2H/^1H$ isotopic enrichment factors (ε_{eq}) between various linear alkene positions and water

For H bonded to a C atom adjacent to a double bond (either *cis* or *trans*), one of the C−H bonds is lying in the plane containing the double bond, while the other two bonds are at ~60° angles to the plane. H_α^{eql} (equatorial) and H_α^{axl} (axial) are used to denote these two positions, respectively (Fig. 2-3a). Compared to analogous position in alkanes, ε_{eq} for H_α^{axl} is ~30‰ more negative, while ε_{eq} for H_α^{eql} is ~15‰ more positive. The average ε_{eq} for secondary H next to a double bond is thus slightly lower than that for secondary H in alkanes (Fig. 2-2). The depletion of ε_{eq} for H_α^{axl} is likely associated with the σ-π hyperconjugation effect, in which the σ-electron pair of the C-H_α^{axl} bond interacts with the π-electrons on the double bond and reduces the electron density of the C-H_α^{axl} bond because of its +I effect. At positions further away from the double bond, ε_{eq} values are indistinguishable from those for alkane H.

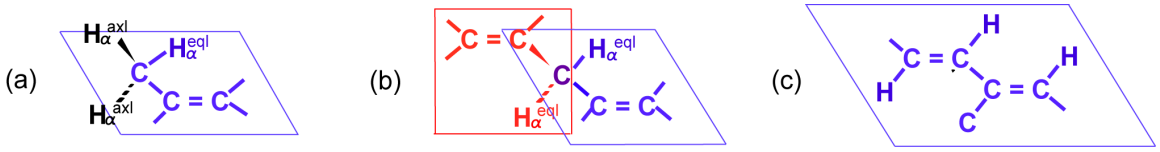

Figure 2-3. (a) Configuration of H_α atoms next to a single double bond; (b) Configuration of two "methylene interrupted" cis double bonds; (c) Configuration of two conjugated double bonds with or without a methyl branch. Each box depicts a plane containing the bonds and atoms of the same color.

We also calculated ε_{eq} values for two types of doubly-unsaturated alkenes. The first has two cis double bonds separated by a $-CH_2-$ group, a structure often seen in multiply unsaturated fatty acids, i.e., "methylene interrupted" unsaturations (Fig. 2-3b). The two double bonds are oriented in perpendicular planes, and the ε_{eq} value for H on either double bond is not appreciably affected by the other double bond. The secondary H atoms on the methylene group between the double bonds are each coplanar with one of the double bonds. They have ε_{eq} values that are slightly higher than secondary H in alkanes (Fig. 2-2). The other type of doubly-unsaturated alkenes contains two conjugated double bonds, either with or without a methyl group attached to the double bonds (Fig. 2-3c), a structure characterizing many carotenoid pigments. The conjugated double bonds are coplanar. At room temperature, the value of ε_{eq} is −160‰ for H on the two ends of the conjugated double bond and −140‰ for H in between, comparable to H on a single double bond. A

methyl group attached to either double bond raises the ε_{eq} value of the neighboring H atoms on the double bonds by 10–15‰, while H on that methyl group has the same ε_{eq} values as for primary H in alkanes.

3.1.3. H in ketones, carboxylic acids and esters

Values of ε_{eq} were calculated for differing H positions in 10 linear ketones. In addition to the six ketones described in Chapter 1, we also included 2-octanone, 5-methyl-2-hexanone, 6-methyl-2-heptanone, and 5-methyl-2-heptanone to obtain a larger dataset. Results for H positions affected by the carbonyl functional group are plotted in Fig. 2-4a. ε_{eq} values for primary and secondary H_α are lower by 30–55‰ compared to those in alkanes, consistent with the electron-withdrawing effect of the carbonyl group that acts to decrease the electron density of the C_α−H_α bond. In contrast, ε_{eq} values for tertiary H_α in ketones are 15–20‰ higher than for alkane tertiary H, a result for which the mechanism is currently unclear. It is possibly associated with the stable conformation of the O=C−C_α−C_β dihedral, where one alkyl branch on the tertiary C_α is at 30–37° to the carbonyl group, compared to ~0° on the secondary C_α in straight-chain ketones (Chapter 1). The effect of the carbonyl group is found to reach as far as H_β, where secondary H_β is 15–20‰ more enriched than secondary alkane H at equilibrium. The effect of a carbonyl group on H_β is in the opposite direction as that on H_α, which is also observed for esters and acids. It is possibly related to the field inductive effect from the functional group on H_β (see 3.2.).

Values of ε_{eq} were calculated for pentanoic acid, hexanoic acid and methyl-, ethyl-, propyl-, and *n*-butyl-esters of pentanoic acid. Results for selected H positions are plotted in Fig. 2-4b. Just as in ketones, the −(C=O)OR group (R = H or alkyl moiety) is electron-withdrawing and leads to lower ε_{eq} values. Thus for secondary H_α next to the carbonyl group, ε_{eq} values are ~30‰ lower than for secondary H in alkanes. However, the electron lone pairs on the singly-bonded O in the acid/ester are donated towards the electron-deficient π-orbital of the carbonyl C (Amyes and Richard, 1996; Richard, 2002), which reduces the polarity of the C=O bond and its subsequent effect on fractionation at H_α. Thus ε_{eq} values for H_α in acids/esters are ~20‰ higher (closer to that in alkanes) than for the same position in ketones. For esters, H on the C atom next to the singly-bonded O has ε_{eq}

values ~90‰ higher than alkane H at room temperature, which could also be attributed to the strong electron-donating effect of the electron lone pairs on the singly-bonded O atom. The hydroxyl H in carboxylic acids is enriched in ^{2}H relative to water by ~55‰ at room temperature (Section 3.1.4.).

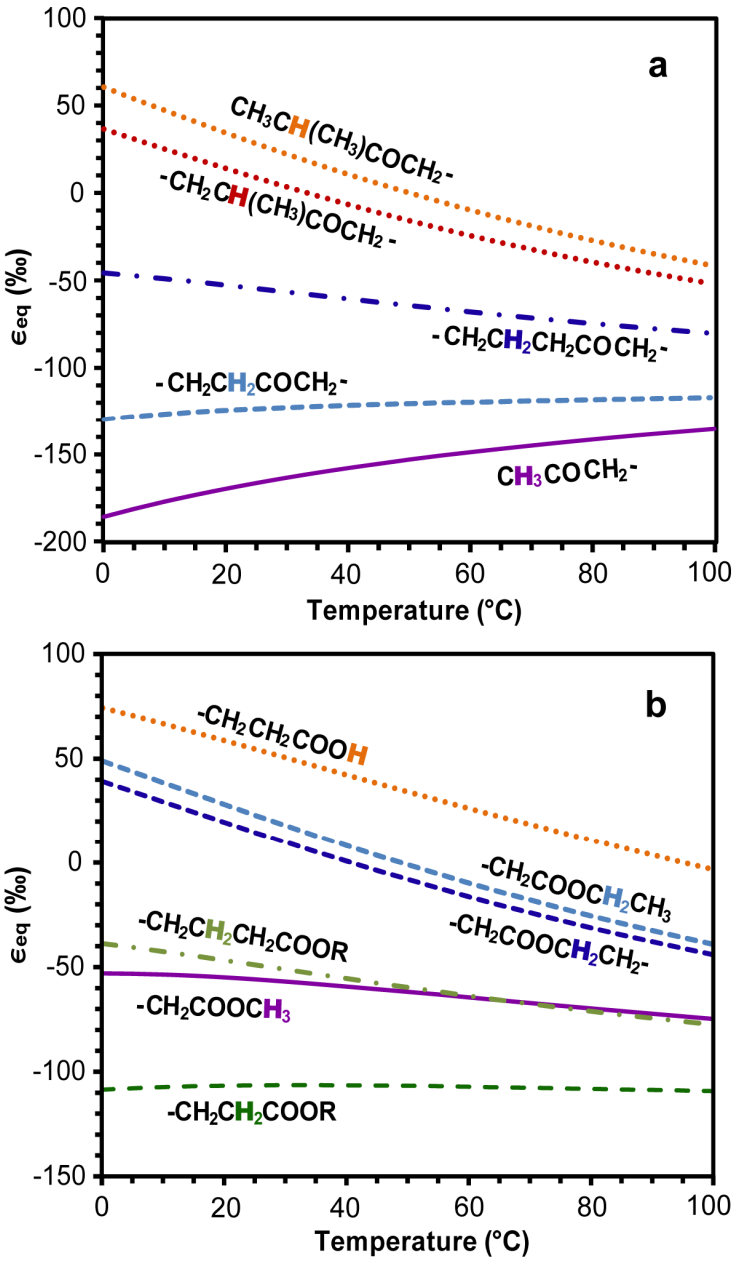

Figure 2-4. Equilibrium $^{2}H/^{1}H$ isotopic enrichment factors (ε_{eq}) between organic H and water in (a) linear ketones and (b) linear carboxylic acids and esters. In (b), the R group can represent either H (acids) or an alkyl moiety (esters).

3.1.4. H in alcohols and ethers

We calculated ε_{eq} for four *n*-heptanol isomers with the hydroxyl group on C-1 through C-4, and for pentyl-methyl ether, pentyl-ethyl ether, and pentyl-propyl ether (Fig. 2-5). The hydroxyl H is ^{2}H-enriched relative to water by 35–50‰ at room temperature, similar to the hydroxyl H in carboxylic acids. The values of ε_{eq} for secondary H_{α} (H on the same C as the hydroxyl group) are found to be as high as 100‰ at room temperature and quickly decline with temperature to ~0 at 100°C. In primary alcohols, positions beyond H_{α} are not appreciably affected by the hydroxyl group. In secondary alcohols, ε_{eq} for H_{β} is ~10‰ lower than analogous position in alkanes, while for H_{γ} (three carbon atoms away from the hydroxyl) ε_{eq} is higher by an average of ~25‰. For ethers, only H_{α} is significantly affected by the alkoxy group, with the ε_{eq} value ~50‰ higher than H at analogous positions in alkanes.

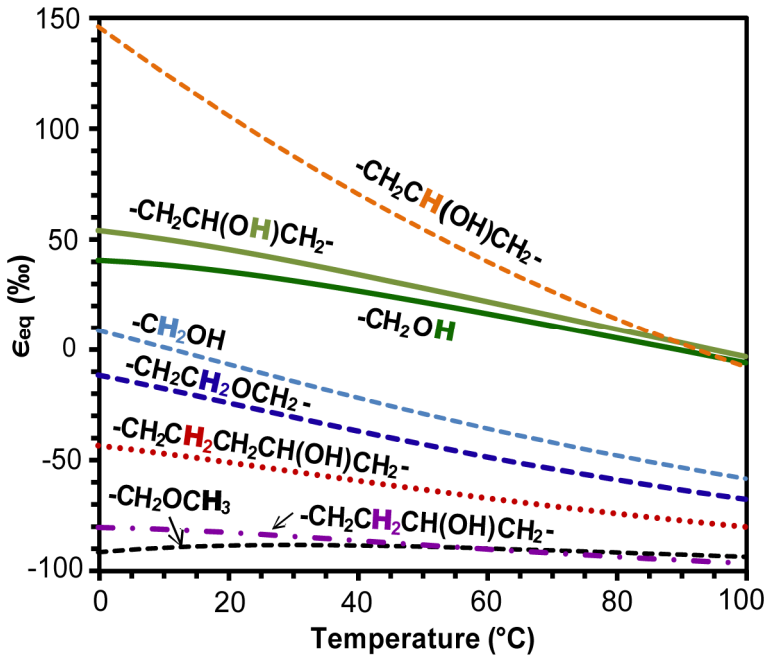

Figure 2-5. Equilibrium $^{2}H/^{1}H$ isotopic enrichment factors (ε_{eq}) between organic H and water in linear alcohols and ethers

The effects of the hydroxyl group are characterized by the negative inductive (−I) effect of the O atom and the electron-donating effect of the electron lone pairs on the O atom.

Hydroxyl H is primarily affected by the −I effect that attracts electrons towards O along the σ-bond and by the electrostatic interaction with water molecules, particularly hydrogen bonding. The combined effects seem to consistently result in positive ε_{eq} values of 30–50‰ at room temperature for hydroxyl H in either alcohols or carboxylic acids. Note that since calculation errors due to omission of anharmonicity are systematically smaller for hydroxyl H than for C-bound H (Chapter 1, Section 4.4.3.), applying the calibration curve based on ketones tends to overcorrect for hydroxyl H, i.e., underestimate the value of ε_{eq} for hydroxyl H by 6–10‰. Nevertheless, our estimates are still consistent with Bigeleisen (1965), who calculated the $^2H/^1H$ fractionation between hydroxyl H in small alcohol and carboxylic acid molecules (C_1-C_4) and water to be 30–90‰.

The electron lone pairs on O are diffusive and can transmit their influence over relatively large distances via the field inductive effect (see Section 3.2.). Consequently, the effect on nearby C−H bonds seems to depend heavily on the spatial orientation of the C−H bond relative to the hydroxyl group. For example, in secondary alcohols, where the hydroxyl group is on one side of the carbon chain, H_γ is more affected than H_β. This is probably because the C_γ−H_γ bonds are close and parallel to the hydroxyl group, which would facilitate σ-p hydroconjugation. In contrast, C_β−H_β bonds are pointing in the opposite direction due to the zig-zag structure of the aliphatic chain.

3.2. The effects of functional group on equilibrium fractionations of C-bound H.

The presence of functional groups changes the fractionation of nearby C-bound H to various degrees depending on the chemistry, geometry and spacial orientation of the functional group. The influence is generally not further than H_β, but sometimes can reach as far as H_γ, e.g., in secondary alcohols. To compare the effects of various functional groups on the value of ε_{eq} for nearby C-bound H, we take the aliphatic fragment $-CH_2C\mathbf{H_2}CH_2-$ (ideally in an infinitely long aliphatic chain) as the reference state, and calculate the equilibrium fractionation between secondary H in the vicinity of a certain

functional group and secondary H in the reference aliphatic fragment. Results are plotted versus temperature in Fig. 2-6.

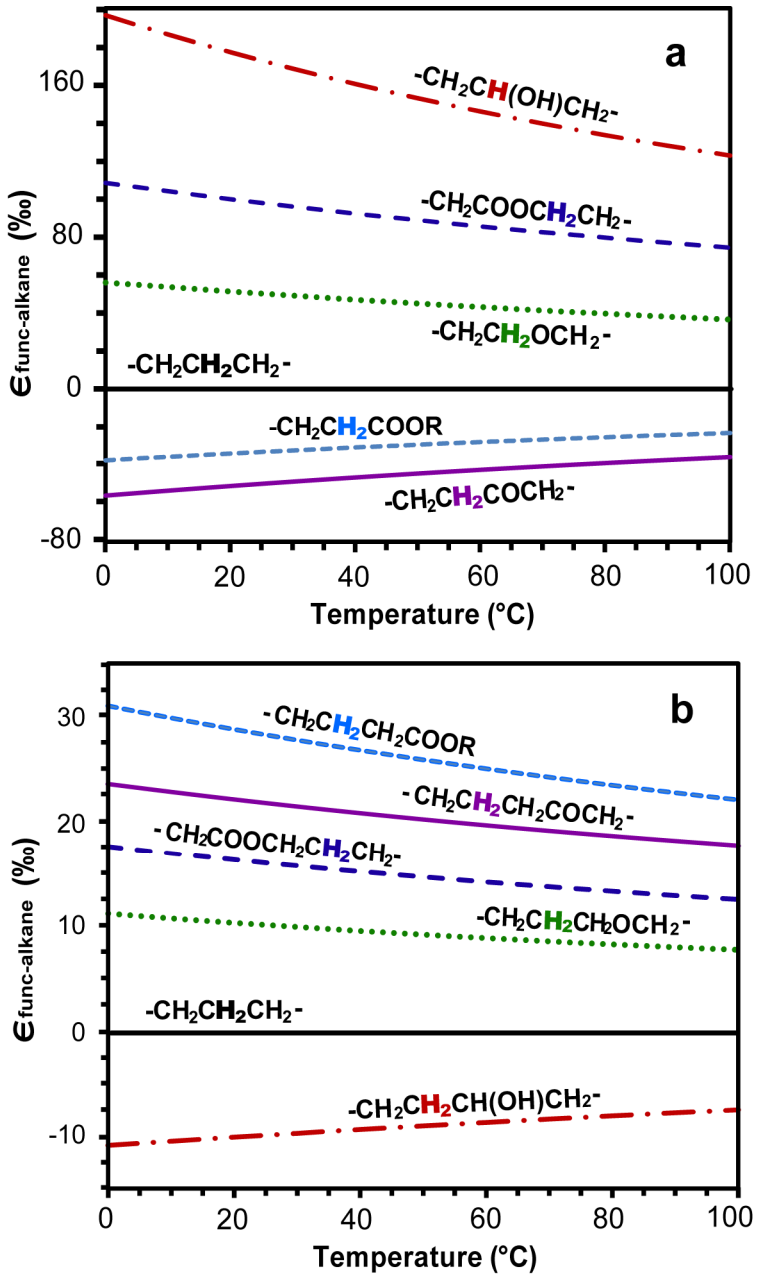

Figure 2-6. $^{2}H/^{1}H$ fractionations ($\varepsilon_{func\text{-}alkane}$) between secondary H near various functional groups and secondary H in the alkane fragment $-CH_2C\mathbf{H_2}CH_2-$ (the reference state). Panel (a) compares H positions, while panel (b) compares H_β positions. To facilitate comparison between (a) and (b), the same line pattern and color are assigned to the same fragment in both panels.

Fig. 2-6a demonstrates that H_α next to an electron-deficient atom in a π system, e.g., −(C=O)R and −(C=O)OR, has a lower ε_{eq} value relative to alkane H, while H_α next to an atom with electron lone pairs, e.g., −OH, −OR and −O(C=O)R, has more positive ε_{eq} values. This pattern is analogous to the well-known substituent effects on an aromatic ring, which result from a combination of resonance and inductive effects of the functional group. In that system, the lone-pair electrons on the O atom that is singly-bonded to the benzene ring are strongly donating towards the arene sytem through p-π conjugation, even though oxygen is more electronegative than carbon. In contrast, the π-π conjugation between the C=O double bond and the benzene ring results in electron-withdrawing from the arene sytem because of the high electronegativity of oxygen. Similarly, in the saturated system that we study the σ electrons in C−H bonds can interact with the π-electrons or lone pairs of the functional groups in an analogous way through σ-π or σ-p hyperconjugation, leading to enhanced or reduced electron density in the C−H bond and corresponding changes in the bond stiffness.

The effects of functional groups on H_β positions (Fig. 2-6b) or further are much smaller than those for H_α, but are nevertheless significant considering that δ^2H values can be measured with a precision of 2–5‰. Chemists have long recognized that there are two basic mechanisms by which a polar group conveys its influence on a remote probe in saturated systems, the σ- (through-bond) inductive effect and field (through-space) inductive effect (Robinson, 1932; Dewar and Grisdale, 1962; Reynolds, 1980). Since Kirkwood and Westheimer (1938) highlighted the electrostatic field model, the importance of the field inductive effect has been gradually established via numerous experimental and theoretical studies (Adcock and Trout, 1999; Nolan and Linck, 2000; Otto and Zdenek, 2007). In many cases it is difficult to accurately ascribe substituent effects to either mechanism. Nevertheless, a general consensus is that for probe groups beyond two bond-lengths the field effect is the dominant "inductive" mechanism (Bowden and Grubbs, 1996; Otto, 1999). We thus infer that functional group effects on fractionation at H and further are caused mainly by the through-space inductive effect.

The magnitude of field effects is a complex function of the geometry and dielectric properties of the molecule and the cavity it occupies in the solvent continuum (Ehrenson,

1977). In other words, there is no simple relationship between the electronic properties of a functional group and the shifts in ε_{eq} values that it induces either for H_β or H_γ. As a result, the effects of functional groups on fractionation at H_β are observed to be generally uncorrelated with those at H_α (Fig. 2-6).

3.3. Temperature dependence and the equilibrium vapor-aqueous fractionations.

The temperature dependence of ε_{eq} for C-bound H is observed to be generally positive for H positions with ε_{eq} < -100‰ and negative for H positions with ε_{eq} > -100‰. In other words, the ε_{eq} values for various C-bound H tend to converge from both sides towards a depletion of ~100‰ relative to water as temperature rises. Therefore the fractionations between various H positions will continuously decrease with increasing temperature. At higher temperatures, the calculated β factors for C-bound H display the expected linear decrease towards unity with increasing temperature squared (Bigeleisen and Mayer, 1947; data not shown). In addition, a cross-over effect (i.e., the sign of ε_{eq} changes) is observed between 0 and 100°C for tertiary H in alkanes, tertiary H next to a double bond or carbonyl group, and secondary H next to oxygen in esters.

We also calculated the equilibrium vapor-aqueous fractionation for selected linear hydrocarbon molecules. The results are generally from 0‰ to 10‰ for various C-bound H positions over 0–100°C, with the vapor phase being enriched in ^2H. Wang and Huang (2001) measured the vapor pressure isotope effect of low molecular weight *n*-alkanes (C_7-C_9) during progressive vaporization and found results around 4‰, consistent with our calculation. This inverse vapor pressure isotope effect (VPIE), as well as the cross-over effect, has been theoretically predicted and experimentally observed for many small hydrocarbon molecules (Jancso and Vanhook, 1974). It results from the effects of dispersion forces on the internal vibrational motions and a lack of intermolecular bonding effects, e.g., hydrogen bonding, which give rise to the normal VPIE for water (Bigeleisen, 1961; Jancso and Vanhook, 1974). The agreement between calculated and experimental

estimates of vapor pressure isotope effects lends further credence to the accuracy our calculations.

3.4. Application to organic geochemical studies

Here we review published δ^2H data for sedimentary organic matter (SOM) and oils with regard to the equilibrium $^2H/^1H$ fractionation factors that we have calculated. Discussion is focused on the potential mechanisms for δ^2H changes during maturation and on estimation of the extent of H exchange in natural systems.

3.4.1. δ^2H changes during maturation of organic matter in natural systems

Post-burial changes in the δ^2H values of organic matter have been documented by numerous field measurements and laboratory maturation experiments. Schimmelmann et al. (2006) recently reviewed the results of more than 20 field and 15 experimental studies. They paint a coherent picture in which δ^2H values increase both for bulk SOM and for individual molecular components during maturation and oil generation. At the same time, offsets in δ^2H between linear and isoprenoid lipids that are present in modern sediments steadily disappear.

Two potential mechanisms have been invoked to explain these changes. Peters et al. (1981) and Schoell (1983) attributed δ^2H increases in bulk SOM to a progressive loss of ^2H-depleted gaseous hydrocarbons, i.e., as a result of kinetic fractionations during hydrocarbon cracking. However, this process should produce equivalent ^2H enrichments in kerogens of similar type and thermal maturity regardless of their original δ^2H value or the δ^2H value of the formation water. This prediction is inconsistent with empirical data. Moreover, loss of ^2H-depleted gases cannot easily explain the convergence of δ^2H values between isoprenoid and *n*-alkyl molecules (Dawson et al., 2005; Pedentchouk et al., 2006).

The alternative explanation, previously proposed by Schimmelmann et al. (1999, 2001), involves H exchange between water and organic H during maturation reactions, e.g.,

isomerization, cracking, rearrangement, and dehydration. Several studies have lent further support to this mechanism (see Schimmelmann et al., 2006 for a recent review). Lis et al. (2006) compared two kerogen sequences of the same type with similar source rock and depositional environment. The primary difference between them was that the formation water associated with one kerogen had δ^2H values that were 40‰ higher than in the other. Within comparable ranges of maturity (R_o ~ 0.3–1.4%), the δ^2H value of the first kerogen was observed to increase twice as much as for the second, indicating that water does play a role in altering the isotopic compositions of kerogen. Santos Neto and Hayes (1999) measured δ^2H values of oils from lacustrine, marine-evaporitic, and transitional paleoenvironments across a maturity gradient in the Potiguar Basin, Brazil. At low thermal maturity, the three paleoenvironments were distinguished by their δ^2H values (lacustrine $\delta^2H \sim -90$‰; transitional $\delta^2H \sim -110$‰; marine-evaporitic $\delta^2H \sim -120$‰ to −135‰). But at higher maturity, oils from the three paleoenvironments converged from both sides toward δ^2H values of −110‰. Several other studies have documented cases in which there was no measureable change in δ^2H values with increasing thermal maturity, both for bulk organic matter (reviewed by Schimmelmann et al., 2006) or for individual *n*-alkanes (Pedentchouk et al., 2006). A common feature of these studies is that the organic compounds were depleted relative to water by 80–110‰.

Based on these data, Schimmelmann et al. (2006) predicted that the equilibrium fractionation between hydrocarbons and water must lie in the range of −80‰ to −110‰. While we do not yet have appropriate data for cyclic and aromatic compounds, this prediction is now confirmed for linear alkanes by our experimental and theoretical estimates of ε_{eq} (Fig. 2-1). Moreover, the disappearance of biosynthetic offsets in δ^2H values between *n*-alkyl and linear isoprenoid lipids can be fully explained by their similar equilibrium fractionations: −90 to −70‰ for *n*-alkanes and near -100‰ for linear isoprenoids, both over the range of 0–100°C. We are thus confident that the hypothesis of Schimmelmann et al. (1999, 2001), attributing changes in SOM δ^2H values to hydrogen exchange, is generally correct.

Our data provide two other conclusions about the interpretation of δ^2H values in thermally mature SOM and oils. First, the molecular equilibrium fractionation factors

change minimally with temperature. Once equilibrium is achieved, any further changes in δ^2H values are likely not attributable to exchange. Thus fractionations between hydrocarbons and water, or between different linear hydrocarbons, will not yield reliable geothermometers. Second, δ^2H enrichments up to 11‰ are possible as the chain length of *n*-alkanes increases. Similar patterns have been recognized in moderately to highly mature organic matter (Sessions et al., 2002; Schimmelmann et al., 2004; Pedentchouk et al., 2006), although to a larger extent (typically 10–30‰). These patterns likely reflect a combination of isotopic equilibrium and the effects of kinetic fractionations during hydrocarbon cracking (Tang et al., 2005).

3.4.2. Constraints on the use of organic δ^2H as a paleoenvironmental proxy

Many recent studies have sought to use the δ^2H values of sedimentary lipids as a proxy for paleoenvironmental conditions (Huang et al., 2002; Dawson, 2004; Sachse et al., 2006). Implicit in this approach are the assumptions that (*i*) biosynthetic fractionations between water and lipids are known, and (*ii*) the δ^2H values of lipids have not been significantly altered by isotopic exchange. Limitations to the former assumption have been discussed elsewhere (Sessions et al., 1999; Zhang and Sachs, 2007; Zhang et al., 2009). For the latter assumption, the ability to detect isotopic exchange in ancient lipids is obviously key.

A number of studies have attempted to rule out isotopic exchange in ancient lipids by showing that the δ^2H values of *n*-alkanes are very different from formation water, or that they do not change with increasing thermal maturity. For example, Yang and Huang (2003) studied leafwax lipids isolated from plant fossils in Miocene lacustrine deposits, and found δ^2H offsets between lipid H and sedimentary water of −103‰ to −108‰ for *n*-alkanes and −88‰ to −102‰ for *n*-acids. These offsets are similar to their modern relatives (−81 to −144‰), and the authors concluded that no isotopic exchange had occurred over the 15–20 Ma history of the sediments. Pedentchouk et al. (2006) studied a lacustrine sediment core from the Lower Cretaceous that spans ~20 Ma, and showed that there was no change in *n*-alkane δ^2H values over this range. They concluded that the *n*-alkanes had not been affected by isotopic exchange, and would thus make a suitable target for paleoenvironmental reconstruction. Our data now clearly shows that both approaches are problematic, because

in many cases the δ^2H values of sedimentary *n*-alkanes lie close to isotopic equilibrium with environmental water. In these cases we should expect that *n*-alkane δ^2H values will change little, even with extensive H exchange. Nor does the situation improve with increasing temperature, because the fractionations are insensitive to temperature. These "tests" for isotopic exchange are thus inconclusive, and do not have the ability to discern appreciable exchange in the *n*-alkyl lipids.

More convincing tests for isotopic exchange in *n*-alkanes would involve the preservation of δ^2H values that are far out of equilibrium with porewaters, such as might be found for high-latitude terrestrial leafwaxes deposited in marine sediments, or the preservation of differing δ^2H values between homologous compounds. For example, Dawson et al. (2004) studied *n*-alkanes from immature torbanites deposited over widely ranging paleolatitudes during Late Carboniferous to the Late Permian. They showed that *n*-alkanes in torbanites deposited under glacial conditions are depleted in deuterium by up to 70‰ relative to *n*-alkanes deposited under a tropical climate regime, and that there is a "saw-toothed" profile of δ^2H values for the alkanes with offsets up to 40‰. These data indicate that the original isotope ratio in some cases can be preserved for hundreds of millions of years.

A second approach to evaluating isotopic exchange in ancient lipids is to compare δ^2H values between hydrocarbons with *n*-alkyl and linear isoprenoid carbon skeletons (Andersen et al., 2001; Sessions et al., 2004). Extensive field and culture data shows that these lipids classes are biosynthesized with very different δ^2H values (Sessions et al., 1999; Zhang and Sachs, 2007; Li et al., 2009), whereas their equilibrium fractionations versus water are quite similar (Fig. 2-1). Thus isotopic exchange leads to a convergence of δ^2H values in linear isoprenoids and *n*-alkanes over time. Examples of such a pattern have now been conclusively shown for Cretaceous lacustrine sediments (Pedentchouk et al., 2006) and for Triassic shales (Dawson et al., 2005). Andersen et al. (2001) documented ~100‰ offsets between δ^2H values of 5α-cholestane and *n*-docosane in a Messinian sapropel, similar to that seen in fresh biomass. Accurate estimates for equilibrium $^2H/^1H$ fractionation between polycyclic and linear hydrocarbons are not yet available, although they seem unlikely to be as large as 100‰.

A significant advantage of this second type of test for isotopic exchange is that the δ^2H value of exchanging porewaters does not need to be known. However, we caution that such measurements are only able to resolve isotopic exchange in the isoprenoid structures (which usually lie far from isotopic equilibrium), and not the *n*-alkanes. It has been observed that H exchange near a tertiary carbon center proceeds much faster than in *n*-alkanes when catalyzed by clay minerals, presumably due to a catalytic mechanism involving carbocation-like intermediates (Larcher et al., 1986). Nevertheless, a pattern of changing isoprenoid δ^2H values with constant *n*-alkane δ^2H values could still be consistent with significant isotopic exchange of the *n*-alkanes. In particular we note that isoprenoid δ^2H values are never (to our knowledge) observed to increase above those of coexisting *n*-alkanes, which might be expected in certain cases if only the isoprenoids were undergoing appreciable exchange. In summary, we believe that the existing body of evidence supports the conclusion that sedimentary *n*-alkanes are largely resistant to isotopic exchange during diagenesis, and thus are generally suitable targets for paleoenvironmental reconstruction. However, explicitly testing this conclusion for specific samples remains problematic, and is likely to hamper our ability to push the use of organic δ^2H measurements deeper into geologic time.

5. CONCLUSIONS

We report equilibrium $^2H/^1H$ isotopic enrichment factors (ε_{eq}) between 0 and 100˚C for various H positions in alkanes, alkenes, ketones carboxylic acids, esters, alcohols, and ethers, with total uncertainties typically in the range of 10–20‰. The values are based on ab initio calculations of molecular vibrational frequencies and are calibrated to experimental ε_{eq} values for H_α in ketones. These data should be useful for applications seeking to predict ^2H abundance in numerous geochemical, chemical, and biologic reactions. The effects of functional groups are found to increase the value of ε_{eq} for H next to electron-donating groups, e.g., −OR, −OH or −O(C=O)R groups and to decrease the value of ε_{eq} for H next to electron-withdrawing groups, e.g., −(C=O)R or −(C=O)OR

groups. Smaller but significant effects are also observed for H_β and sometimes H_γ positions, probably due to the field inductive effect of the functional group.

Estimated values of ε_{eq} for *n*-alkanes and linear isoprenoids agree well with the range predicted by field data from sediments and oils (−80‰ to −110‰), and support the conclusion that changes in the δ^2H value of sedimentary organic matter during maturation are likely caused by H exchange towards an equilibrium state. The progressive convergence of δ^2H values for linear isoprenoid and *n*-alkyl lipids are also consistent with isotopic equilibration. Since in many cases *n*-alkyl lipids are biosynthesized with δ^2H values close to equilibrium with water, a lack of down-core variation in δ^2H values for *n*-alkyl lipids cannot be construed as evidence for no exchange.

ACKNOWLEDGEMENTS

We acknowledge Adri van Duin, Edwin A. Schauble, and Weifu Guo for helpful discussions of ab initio calculations. This work is supported by Petroleum Research Fund (PRF) of the American Chemical Society (ACS), #43746-G2, and by National Science Foundation (NSF) grant #EAR-0645502.

REFERENCES

Adcock W. and Trout N. A. (1999) Nature of the Electronic Factor Governing Diastereofacial Selectivity in Some Reactions of Rigid Saturated Model Substrates. *Chem. Rev*. **99**, 1415–1436.

Amyes T. L. and Richard J. P. (1996) Determination of the pK_a of ethyl acetate: Bronsted correlation for deprotonation of a simple oxygen ester in aqueous solution. *J. Am. Chem. Soc*. **118**, 3129–3141.

Andersen N., Paul H. A., Bernasconi S. M., McKenzie J. A., Behrens A., Schaeffer P. and Albrecht P. (2001) Large and rapid climate variability during the Messinian salinity crisis: Evidence from deuterium concentrations of individual biomarkers. *Geology* **29**, 799–802.

Becke A. D. (1993) Density-functional thermochemistry. 3. The role of exact exchange. *J. Chem. Phys.* **98**, 5648–5652.

Bigeleisen J. (1961) Statistical Mechanics of Isotope Effects on Thermodynamic Properties of Condensed Systems. *J. Chem. Phys.* **34**, 1485–1493.

Bigeleisen J. (1965) Chemistry of isotopes. *Science* **147**, 463–471.

Bigeleisen J. and Mayer M. G. (1947) Calculation of Equilibrium Constants for Isotopic Exchange Reactions. *J. Chem. Phys.* **15**, 261–267.

Bowden K. and Grubbs E. J. (1996) Through-bond and through-space models for interpreting chemical reactivity in organic reactions. *Chem. Soc. Rev*. **25**, 171–177.

Dawson D., Grice K., Wang S. X., Alexander R. and Radke J. (2004) Stable hydrogen isotopic composition of hydrocarbons in torbanites (Late Carboniferous to Late Permian) deposited under various climatic conditions. *Org. Geochem.* **35**, 189–197.

Dawson D., Grice K. and Alexander R. (2005) Effect of maturation on the indigenous delta D signatures of individual hydrocarbons in sediments and crude oils from the Perth Basin (Western Australia). *Org. Geochem.* **36**, 95–104.

Dewar M. J. S. and Grisdale P. J. (1962) Substituent effects.I. Introduction. *J. Am. Chem. Soc*. **84**, 3539–3548.

dos Santos Neto E. V. and Hayes J. M. (1999) Use of hydrogen and carbon stable isotopes characterizing oils from the Potiguar Basin (onshore) Northeastern Brazil. *AAPG Bulletin*. **83**, 496–518.

Ehrenson S. (1977) Solvent dielectric attenuation of substituent effects — field transmission in partially occluded cavities. *J. Chem. Phys.* **81**, 1520–1526.

Galimov E. M. (1971) Relation between isotope separation factor and equilibrium constants for carbon isotope exchange reactions in hydrocarbon systems. *Russ. J. Phys. Chem*. **45**, 665–667.

Hartshorn S. and Shiner V. J. (1972) Calculation of h/d, c-12/c-13, and c-12/c-14 fractionation factors from valence force fields derived for a series of simple organic-molecules. *J. Am. Chem. Soc*. **94**, 9002–9012.

Horita J. and Wesolowski D. J. (1994) Liquid-vapor fractionation of oxygen and hydrogen isotopes of water from the freezing to the critical-temperature. *Geochim. Cosmochim. Acta* **58**, 3425–3437.

Huang Y. S., Shuman B., Wang Y. and Webb T. (2002) Hydrogen isotope ratios of palmitic acid in lacustrine sediments record late Quaternary climate variations. *Geology* **30**, 1103–1106.

Jancso G. and Vanhook W. A. (1974) Condensed phase isotope-effects (especially vapor-pressure isotope-effects). *Chem. Rev.* **74,** 689–750.

Kirkwood J. G. and Westheimer F. H. (1938) The electrostatic influence of substituents on the dissociation constants of organic acids. *J. Chem. Phys.* **6**, 506–512.

Knyazev D. A., Myasoedov N. F. and Bochkarev A. V. (1992) The theory of the equilibrium isotope effects of hydrogen. *Russ. Chem. Rev.* **61**, 204–220.

Koepp M. (1978) D/H isotope exchange reaction between petroleum and water: A contributory determinant for D/H-isotope ratios in crude oils? In *The Fourth International Conference, Geochronology, Cosmochronology, Isotope Geology USGS Open-File Report 78-701* (R.E. Zartman, ed.). U.S. Geological Survey, pp. 221–222.

Larcher A. V., Alexander R., Rowland S. J. and Kagi R. I. (1986) Acid catalysis of alkyl hydrogen-exchange and configurational isomerization-reactions — acyclic isoprenoid acids. *Org. Geochem.* **10**, 1015–1021

Lee C. T., Yang W. T. and Parr R. G. (1988) Development of the colle-salvetti correlation-energy formula into a functional of the electron-density. *Phy. Rev. B*, **37**, 785–789.

Li C., Sessions A. L., Kinnaman F. S., and Valentine D. L. (2009) Hydrogen-isotopic variability in lipids from Santa Barbara Basin sediments. *Geochim. Cosmochim. Acta* **73**, 4803–4823.

Lis G. P., Schimmelmann A. and Mastalerz M. (2006) D/H ratios and hydrogen exchangeability of type-II kerogens with increasing thermal maturity. *Org. Geochem.* **37**, 342–353.

Nolan E. M. and Linck R. G. (2000) Charge Variations in Substituted Alkanes: Evidence for a Through-Space Effect. *J. Am. Chem. Soc.* **122**, 11497–11506.

Otto E. (1999) The inductive effect: theory and quantitative assessment. *J. Phys.* Org. *Chem.* **12**, 265–274.

Otto E. and Zdenék F. (2007) Transmission of Substituent Effects: The Through-Space and Through-Bond Models and their Experimental Verification. In *Progress in Physical Organic Chemistry* (W.T. Robert, ed.). Wiley-Interscience, pp. 259–294.

Pedentchouk N., Freeman K. H. and Harris N. B. (2006) Different response of delta D values of n-alkanes, isoprenoids, and kerogen during thermal maturation. *Geochim. Cosmochim. Acta* **70**, 2063–2072.

Peters K. E., Rohrback B. G. and Kaplan I. R. (1981) Carbon and hydrogen stable isotope variations in kerogen during laboratory-simulated thermal maturation. *AAPG Bull.* **65**, 501–508.

Reynolds W. F. (1980) An approach for assessing the relative importance of field and sigma-inductive contributions to polar substituent effects based on the non-proportionality of field and sigma-inductive substituent constants. *J. Chem. Soc., Perkin Trans.* **2**, 985–992.

Richard J. (2002) Formation and stability of enolates of acetamide and acetate anion: An eigen plot for proton transfer at alpha-carbonyl carbon. *J. Am. Chem. Soc*. **124**, 2957–2968.

Richet P., Bottinga Y. and Javoy M. (1977) Review of hydrogen, carbon, nitrogen, oxygen, sulfur, and chlorine stable isotope fractionation among gaseous molecules. *Ann. Rev. Earth Planet. Sci.* **5**, 65–110.

Robinson R. (1932) *Outline of an Electrochemical (Electronic) Theory of the Course of Organic Reactions*. Institute of Chemistry of Gr. Britain & Ireland, London.

Sachse D., Radke J. and Gleixner G. (2006) Delta D values of individual n-alkanes from terrestrial plants along a climatic gradient — Implications for the sedimentary biomarker record. *Org. Geochem.* **37**, 469–483.

Schimmelmann A., Lewan M. D. and Wintsch R. P. (1999) D/H isotope ratios of kerogen, bitumen, oil, and water in hydrous pyrolysis of source rocks containing kerogen types I, II, IIS, and III. *Geochim. Cosmochim. Acta* **63**, 3751–3766.

Schimmelmann A., Boudou J. P., Lewan M. D. and Wintsch R. P. (2001) Experimental controls on D/H and C-13/C-12 ratios of kerogen, bitumen and oil during hydrous pyrolysis. *Org. Geochem.* **32**, 1009–1018.

Schimmelmann A., Sessions A. L., Boreham, C. J., Edwards D. S., Logan G. A. and Summons R. E. (2004) D/H ratios in terrestrially sourced petroleum systems. *Org. Geochem.* **35**, 1169–1195.

Schimmelmann A., Sessions A. L. and Mastalerz M. (2006) Hydrogen isotopic composition (D/H) of organic matter during diagenesis and thermal maturation. *Ann. Rev. Earth Planet. Sci.* **34**, 501–533.

Schoell M. (1983) Genetic-characterization of natural gases. *AAPG Bull.* **67**, 2225–2238.

Sessions A. L., Burgoyne T. W., Schimmelmann A. and Hayes J. M. (1999) Fractionation of hydrogen isotopes in lipid biosynthesis. *Org. Geochem.* **30**, 1193–1200.

Sessions A., Schimmelmann A., Summons R. E., Boreham C. J., Logan G. A., Hope J. M. and Hayes J. M. (2002) Hydrogen isotopic compositions of petroleum hydrocarbons. *Geochim. Cosmochim. Acta* **66,** A697

Sessions A. L., Sylva S. P., Summons R. E. and Hayes J. M. (2004) Isotopic exchange of carbon-bound hydrogen over geologic timescales. *Geochim. Cosmochim. Acta* **68**, 1545–1559.

Stern M. J. and Wolfsberg M. (1966a) On absence of isotope effects in absence of force constant changes. *J. Chem. Phys.* **45**, 2618.

Stern, M. J. and Wolfsberg, M. (1966b) Simplified Procedure for Theoretical Calculation of Isotope Effects Involving Large Molecules. *J. Chem. Phys.* **45**, 4105–4124.

Tang Y. C., Huang Y. S., Ellis G. S., Wang Y., Kralert P. G., Gillaizeau B., Ma Q. S. and Hwang R. (2005) A kinetic model for thermally induced hydrogen and carbon isotope fractionation of individual n-alkanes in crude oil. *Geochim. Cosmochim. Acta* **69**, 4505–4520.

Tannor D. J., Marten B., Murphy R., Friesner R. A., Sitkoff D., Nicholls A., Ringnalda M., Goddard W. A. and Honig B. (1994) Accurate first principles calculation of molecular charge-distributions and solvation energies from ab-initio quantum-mechanics and continuum dielectric theory. *J. Am. Chem. Soc*. **116**, 11875–11882.

Urey H. C. (1947) The thermodynamic properties of isotopic substances. *J. Chem. Soc*. MAY, 562–581.

Wang Y. and Huang Y. S. (2001) Hydrogen isotope fractionation of low molecular weight n-alkanes during progressive vaporization. *Org. Geochem.* **32**, 991–998.

Wang Y., Sessions A. L., Nielsen R. J. and Goddard W. A. (2009) Equilibrium 2H/1H fractionations in organic molecules. Part I: Experimental calibration of ab initio calculations. *Geochim. Cosmochim. Acta* (in press)

Xie S., Nott C. J., Avsejs L. A., Volders F., Maddy D., Chambers F. M., Gledhill A., Carter J. F. and Evershed R. P. (2000) Palaeoclimate records in compound-specific delta D values of a lipid biomarker in ombrotrophic peat. *Org. Geochem.* **31**, 1053–1057.

Yang H. and Huang Y. S. (2003) Preservation of lipid hydrogen isotope ratios in Miocene lacustrine sediments and plant fossils at Clarkia, northern Idaho, USA. *Org. Geochem.* **34**, 413–423.

Zhang Z. and Sachs J. P. (2007) Hydrogen isotope fractionation in freshwater algae: I. Variations among lipids and species. *Org. Geochem.* **38**, 582–608

Zhang X., Gillespie A. L. and Sessions A. L. (2009) Large D/H variations in bacterial lipids reflect central metabolic pathways. *Proc. Nat. Acad. Sci. USA* **106**, 12580–12586.

APPENDIX

Table 2-A1. Calculated β factors from 0°C to 100°C for H in alkanes

T	pentane			hexane			heptane				2-methyl-heptane		
	$CH_3CH_2CH_2CH_2CH_3$			$CH_3CH_2CH_2CH_2CH_2CH_3$			$CH_3CH_2CH_2CH_2CH_2CH_2CH_3$				$CH_3CH(CH_3)CH_2CH_2CH_2CH_2CH_3$		
(°C)	**1° H_1**	**2° H_2**	**2° H_3**	**1° H_1**	**2° H_2**	**2° H_3**	**1° H_1**	**2° H_2**	**2° H_3**	**2° H_4**	**1° H_1**	**3° H_2**	**2° H_3**
0	16.393	18.090	17.891	16.382	18.119	17.896	16.365	18.087	17.935	17.867	16.244	19.737	17.878
5	15.385	16.924	16.740	15.375	16.951	16.745	15.359	16.921	16.781	16.719	15.246	18.414	16.727
10	14.472	15.871	15.702	14.463	15.896	15.706	14.448	15.868	15.739	15.682	14.343	17.224	15.689
15	13.644	14.919	14.763	13.635	14.941	14.766	13.621	14.916	14.797	14.744	13.523	16.149	14.750
20	12.889	14.054	13.910	12.881	14.075	13.913	12.869	14.051	13.941	13.892	12.776	15.177	13.897
25	12.200	13.267	13.133	12.193	13.287	13.136	12.181	13.265	13.162	13.117	12.095	14.293	13.120
30	11.570	12.549	12.425	11.563	12.567	12.427	11.552	12.547	12.451	12.409	11.471	13.490	12.412
35	10.992	11.893	11.776	10.986	11.910	11.779	10.976	11.890	11.801	11.762	10.899	12.756	11.764
40	10.461	11.291	11.182	10.455	11.306	11.184	10.445	11.289	11.205	11.169	10.373	12.085	11.170
45	9.971	10.737	10.636	9.966	10.752	10.638	9.957	10.735	10.657	10.623	9.888	11.470	10.624
50	9.520	10.228	10.133	9.514	10.242	10.135	9.506	10.226	10.153	10.121	9.441	10.905	10.121
55	9.101	9.758	9.669	9.096	9.771	9.671	9.089	9.756	9.687	9.657	9.027	10.384	9.657
60	8.714	9.323	9.239	8.709	9.336	9.241	8.702	9.322	9.257	9.229	8.644	9.904	9.228
65	8.354	8.921	8.842	8.350	8.932	8.843	8.343	8.919	8.858	8.832	8.288	9.460	8.831
70	8.020	8.547	8.473	8.016	8.558	8.474	8.009	8.546	8.488	8.463	7.956	9.049	8.462
75	7.708	8.200	8.129	7.704	8.210	8.131	7.698	8.199	8.144	8.120	7.648	8.667	8.119
80	7.417	7.877	7.810	7.414	7.886	7.811	7.408	7.875	7.823	7.801	7.360	8.313	7.800
85	7.146	7.575	7.512	7.142	7.584	7.513	7.136	7.574	7.524	7.504	7.091	7.982	7.502
90	6.891	7.293	7.233	6.888	7.302	7.235	6.883	7.292	7.245	7.226	6.839	7.674	7.224
95	6.653	7.030	6.973	6.650	7.038	6.974	6.645	7.029	6.984	6.965	6.603	7.387	6.963
100	6.429	6.783	6.729	6.426	6.791	6.730	6.421	6.782	6.739	6.722	6.381	7.118	6.720

Table 2-A1 *(Continued)*

T	3-methyl-heptane				4-methyl-heptane			nonane					undecane					
	$CH_3CH_2CH(CH_3)CH_2CH_2CH_2CH_3$				$CH_3CH_2CH_2CH(CH_3)CH_2CH_2CH_3$			$CH_3CH_2CH_2CH_2CH_2CH_2CH_2CH_2CH_3$					$CH_3CH_2CH_2CH_2CH_2CH_2CH_2CH_2CH_2CH_2CH_3$					
(°C)	**2° H_2**	**3° H_3**	**1°H_{Me}**	**2° H_4**	**2° H_3**	**3° H_4**	**1° H_{Me}**	**1° H_1**	**2° H_2**	**2° H_3**	**2° H_4**	**2° H_5**	**1° H_1**	**2° H_2**	**2° H_3**	**2° H_4**	**2° H_5**	**2° H_6**
0	18.045	19.515	16.419	17.828	17.914	19.370	16.444	16.338	18.039	17.912	17.837	17.956	16.327	18.117	17.830	17.911	17.857	17.964
5	16.881	18.210	15.408	16.681	16.761	18.078	15.431	15.334	16.877	16.760	16.691	16.800	15.324	16.949	16.685	16.758	16.709	16.807
10	15.831	17.037	14.492	15.647	15.720	16.915	14.514	14.425	15.828	15.720	15.656	15.757	14.416	15.894	15.651	15.719	15.673	15.763
15	14.881	15.977	13.661	14.710	14.778	15.865	13.682	13.600	14.879	14.779	14.720	14.812	13.592	14.939	14.715	14.778	14.736	14.819
20	14.018	15.018	12.905	13.860	13.923	14.914	12.924	12.849	14.017	13.924	13.870	13.955	12.841	14.073	13.866	13.923	13.884	13.961
25	13.234	14.146	12.214	13.086	13.145	14.051	12.233	12.163	13.233	13.147	13.096	13.175	12.156	13.285	13.092	13.146	13.109	13.181
30	12.517	13.353	11.583	12.380	12.435	13.265	11.600	11.536	12.517	12.437	12.390	12.464	11.529	12.566	12.386	12.436	12.402	12.468
35	11.862	12.629	11.003	11.734	11.785	12.547	11.020	10.960	11.863	11.788	11.744	11.812	10.953	11.908	11.741	11.787	11.755	11.817
40	11.262	11.967	10.471	11.142	11.190	11.891	10.486	10.431	11.263	11.193	11.152	11.216	10.425	11.305	11.149	11.192	11.162	11.220
45	10.710	11.360	9.980	10.598	10.642	11.289	9.995	9.943	10.711	10.646	10.608	10.667	9.937	10.750	10.604	10.645	10.617	10.671
50	10.202	10.802	9.527	10.097	10.138	10.735	9.541	9.493	10.204	10.142	10.106	10.162	9.487	10.240	10.103	10.141	10.115	10.166
55	9.733	10.288	9.108	9.634	9.673	10.225	9.122	9.077	9.735	9.677	9.644	9.696	9.071	9.769	9.641	9.676	9.652	9.699
60	9.300	9.814	8.720	9.207	9.243	9.755	8.733	8.691	9.302	9.247	9.216	9.265	8.686	9.334	9.213	9.247	9.224	9.268
65	8.898	9.375	8.360	8.810	8.845	9.320	8.372	8.332	8.901	8.849	8.820	8.865	8.328	8.931	8.817	8.849	8.827	8.868
70	8.526	8.969	8.025	8.443	8.476	8.917	8.037	7.999	8.528	8.479	8.452	8.495	7.995	8.557	8.449	8.479	8.458	8.498
75	8.179	8.592	7.713	8.101	8.132	8.543	7.724	7.689	8.182	8.136	8.110	8.150	7.684	8.209	8.107	8.135	8.116	8.153
80	7.857	8.241	7.421	7.782	7.812	8.195	7.432	7.399	7.860	7.816	7.791	7.830	7.395	7.885	7.789	7.816	7.797	7.832
85	7.556	7.915	7.149	7.486	7.514	7.871	7.160	7.128	7.559	7.517	7.494	7.530	7.124	7.583	7.492	7.517	7.500	7.533
90	7.275	7.611	6.894	7.208	7.235	7.569	6.904	6.875	7.278	7.239	7.217	7.251	6.871	7.301	7.214	7.238	7.222	7.253
95	7.012	7.326	6.656	6.949	6.974	7.287	6.665	6.637	7.015	6.978	6.957	6.989	6.633	7.037	6.955	6.978	6.962	6.992
100	6.766	7.060	6.432	6.706	6.730	7.023	6.441	6.414	6.769	6.733	6.714	6.744	6.411	6.790	6.712	6.733	6.718	6.747

(a) Listed values of β factor are the average value for H atoms bound to the same C atom.

(b) H position is indicated by the subscript number starting from the end closer to the branch point.

(c) 1° = primary, 2° = secondary, 3° = tertiary

Table 2-A2. Calculated β factors from 0°C to 100°C for H in alkenes

T	1-hexene $CH_2=CHCH_2CH_2CH_2CH_3$						3-methyl-1-hexene $CH_2=CHCH(CH_3)CH_2CH_2CH_3$			5-methyl-1-hexene $CH_2=CHCH_2CH_2CH(CH_3)_2$					
(°C)	**2°$H_{1=}$**	**3°$H_{2=}$**	**2° H_3^{eql}**	**2° H_3^{axl}**	**2° H_4**	**2° H_5**	**2°$H_{1=}$**	**3° $H_{2=}$**	**3° H_3^{eql}**	**2°$H_{1=}$**	**3° $H_{2=}$**	**2° H_3^{eql}**	**2° H_3^{axl}**	**2° H_4**	**3° H_5**
0	15.136	16.271	18.263	17.458	18.140	18.257	15.144	16.118	19.819	14.884	16.017	18.419	17.340	17.850	19.673
5	14.226	15.262	17.082	16.343	16.969	17.076	14.233	15.121	18.490	13.997	15.032	17.227	16.237	16.705	18.358
10	13.401	14.350	16.017	15.336	15.912	16.011	13.408	14.220	17.293	13.192	14.141	16.152	15.240	15.671	17.174
15	12.651	13.523	15.052	14.425	14.956	15.048	12.657	13.402	16.214	12.461	13.332	15.179	14.338	14.735	16.105
20	11.968	12.770	14.177	13.597	14.088	14.173	11.974	12.658	15.236	11.794	12.595	14.296	13.518	13.886	15.137
25	11.344	12.083	13.381	12.843	13.298	13.378	11.349	11.979	14.349	11.184	11.923	13.493	12.771	13.112	14.258
30	10.773	11.455	12.655	12.155	12.578	12.652	10.777	11.358	13.541	10.625	11.308	12.760	12.089	12.406	13.458
35	10.248	10.880	11.991	11.526	11.919	11.988	10.252	10.788	12.804	10.112	10.744	12.090	11.465	11.760	12.728
40	9.765	10.351	11.382	10.948	11.315	11.379	9.769	10.265	12.130	9.640	10.225	11.476	10.892	11.168	12.060
45	9.320	9.864	10.823	10.417	10.760	10.820	9.323	9.784	11.512	9.204	9.748	10.911	10.366	10.623	11.447
50	8.909	9.415	10.308	9.928	10.249	10.305	8.911	9.339	10.945	8.801	9.307	10.392	9.881	10.122	10.884
55	8.528	8.999	9.833	9.477	9.777	9.830	8.530	8.928	10.422	8.428	8.899	9.912	9.433	9.659	10.366
60	8.175	8.615	9.393	9.059	9.341	9.391	8.177	8.548	9.939	8.081	8.522	9.469	9.018	9.231	9.887
65	7.847	8.258	8.987	8.672	8.938	8.985	7.848	8.195	9.494	7.759	8.171	9.058	8.634	8.834	9.445
70	7.541	7.926	8.609	8.313	8.563	8.607	7.543	7.866	9.080	7.460	7.845	8.678	8.278	8.466	9.035
75	7.256	7.617	8.258	7.979	8.215	8.257	7.258	7.560	8.697	7.180	7.541	8.324	7.946	8.124	8.655
80	6.990	7.329	7.932	7.667	7.890	7.930	6.992	7.275	8.341	6.919	7.257	7.994	7.637	7.805	8.301
85	6.742	7.060	7.627	7.377	7.588	7.626	6.743	7.009	8.009	6.674	6.993	7.687	7.349	7.507	7.972
90	6.509	6.808	7.343	7.106	7.305	7.341	6.510	6.759	7.700	6.446	6.745	7.400	7.079	7.230	7.665
95	6.290	6.572	7.077	6.852	7.041	7.075	6.291	6.526	7.411	6.231	6.513	7.131	6.827	6.970	7.378
100	6.085	6.350	6.828	6.614	6.794	6.826	6.086	6.307	7.141	6.029	6.295	6.880	6.590	6.726	7.110

Table 2-A2. *(Continued)*

T	(E)-5-decene $CH_3CH_2CH_2CH_2CH{=}CHCH_2CH_2CH_2CH_3$						(Z)-5-decene $CH_3CH_2CH_2CH_2CH{=}CHCH_2CH_2CH_2CH_3$						cis,cis-2,5-decadiene $CH_3CH{=}CHCH_2CH{=}CHCH_2CH_2CH_2CH_3$					
(°C)	1° H_1	2° H_2	2° H_3	2° H_4^{axl}	2° H_4^{eql}	3° $H_{5=}$	1° H_1	2° H_2	2° H_3	2° H_4^{axl}	2° H_4^{eql}	3° $H_{5=}$	1° H_1	3° $H_{2=}$	3° $H_{3=}$	2° H_4^{eql}	3° $H_{5=}$	3° $H_{6=}$
0	16.308	18.148	17.986	17.331	18.104	16.041	16.445	18.228	18.084	17.409	18.511	16.591	16.054	16.698	16.516	17.998	16.564	16.551
5	15.307	16.977	16.828	16.226	16.936	15.048	15.432	17.050	16.918	16.298	17.309	15.550	15.075	15.648	15.482	16.840	15.525	15.513
10	14.401	15.920	15.782	15.228	15.882	14.150	14.515	15.987	15.865	15.295	16.226	14.609	14.189	14.700	14.547	15.794	14.587	14.575
15	13.578	14.963	14.836	14.325	14.928	13.335	13.683	15.025	14.912	14.386	15.246	13.756	13.383	13.841	13.700	14.848	13.736	13.725
20	12.828	14.095	13.978	13.504	14.063	12.593	12.925	14.152	14.048	13.561	14.357	12.980	12.650	13.060	12.930	13.990	12.963	12.952
25	12.144	13.305	13.196	12.757	13.275	11.917	12.233	13.358	13.261	12.810	13.548	12.274	11.979	12.348	12.228	13.208	12.258	12.248
30	11.518	12.584	12.483	12.074	12.556	11.299	11.601	12.633	12.543	12.124	12.811	11.629	11.366	11.698	11.587	12.495	11.614	11.604
35	10.944	11.925	11.830	11.450	11.899	10.732	11.020	11.971	11.887	11.496	12.136	11.038	10.803	11.102	10.999	11.843	11.024	11.015
40	10.416	11.321	11.232	10.877	11.296	10.212	10.487	11.363	11.285	10.921	11.518	10.495	10.285	10.555	10.460	11.245	10.483	10.474
45	9.929	10.765	10.683	10.351	10.743	9.732	9.995	10.805	10.732	10.391	10.950	9.996	9.808	10.053	9.963	10.695	9.985	9.976
50	9.480	10.254	10.177	9.866	10.233	9.290	9.542	10.291	10.223	9.904	10.428	9.535	9.367	9.589	9.506	10.189	9.525	9.517
55	9.064	9.782	9.710	9.418	9.762	8.881	9.122	9.817	9.753	9.454	9.945	9.110	8.959	9.161	9.083	9.722	9.101	9.093
60	8.679	9.346	9.278	9.003	9.327	8.502	8.733	9.379	9.318	9.037	9.500	8.717	8.581	8.764	8.691	9.290	8.708	8.701
65	8.322	8.942	8.878	8.619	8.925	8.151	8.372	8.973	8.916	8.651	9.087	8.352	8.229	8.397	8.328	8.890	8.344	8.337
70	7.989	8.567	8.507	8.263	8.551	7.824	8.036	8.597	8.542	8.293	8.704	8.013	7.903	8.055	7.991	8.519	8.006	7.999
75	7.679	8.219	8.162	7.931	8.203	7.520	7.724	8.246	8.195	7.960	8.348	7.697	7.598	7.738	7.677	8.174	7.691	7.684
80	7.390	7.895	7.840	7.623	7.880	7.236	7.432	7.920	7.872	7.650	8.017	7.403	7.314	7.442	7.385	7.852	7.397	7.391
85	7.120	7.592	7.540	7.334	7.578	6.971	7.159	7.617	7.571	7.360	7.708	7.129	7.048	7.165	7.111	7.552	7.123	7.117
90	6.867	7.309	7.261	7.065	7.296	6.723	6.904	7.333	7.289	7.090	7.420	6.872	6.799	6.907	6.856	7.272	6.867	6.861
95	6.629	7.045	6.999	6.813	7.033	6.491	6.665	7.067	7.026	6.837	7.150	6.631	6.565	6.665	6.617	7.010	6.627	6.621
100	6.407	6.797	6.753	6.577	6.786	6.273	6.440	6.818	6.779	6.599	6.898	6.406	6.346	6.438	6.392	6.765	6.402	6.396

Table 2-A2. *(Continued)*

T	trans,trans-4,6-decadiene $CH_3CH_2CH_2CH{=}CHCH{=}CHCH_2CH_2CH_3$							5-methyl-trans,trans-4,6-decadiene $CH_3CH_2CH_2CH{=}CHC(CH_3){=}CHCH_2CH_2CH_3$					
(°C)	**2° H_2**	**2° H_3^{axl}**	**2° H_3^{eql}**	**3° $H_{4=}$**	**3° $H_{5=}$**	**3° $H_{6=}$**	**3° $H_{7=}$**	**2° H_3^{axl}**	**2° H_3^{eql}**	**3° $H_{4=}$**	**3° $H_{5=}$**	**1° H_{me}**	**3° $H_{6=}$**
0	18.239	17.331	18.290	16.072	16.478	16.372	16.136	17.346	18.264	16.371	16.703	16.295	16.725
5	17.060	16.226	17.106	15.077	15.448	15.352	15.135	16.239	17.083	15.352	15.653	15.295	15.670
10	15.997	15.228	16.038	14.176	14.517	14.429	14.230	15.240	16.016	14.430	14.704	14.390	14.718
15	15.034	14.325	15.072	13.360	13.673	13.592	13.410	14.336	15.052	13.595	13.844	13.568	13.855
20	14.161	13.504	14.195	12.617	12.905	12.831	12.663	13.514	14.176	12.835	13.063	12.820	13.071
25	13.366	12.757	13.398	11.940	12.206	12.137	11.982	12.766	13.380	12.142	12.351	12.137	12.357
30	12.641	12.075	12.670	11.320	11.566	11.503	11.359	12.083	12.653	11.508	11.700	11.511	11.704
35	11.978	11.450	12.005	10.752	10.980	10.921	10.788	11.458	11.989	10.928	11.105	10.938	11.107
40	11.371	10.877	11.395	10.231	10.443	10.388	10.264	10.884	11.380	10.395	10.558	10.410	10.559
45	10.812	10.351	10.834	9.750	9.948	9.897	9.782	10.357	10.821	9.904	10.054	9.924	10.055
50	10.298	9.866	10.318	9.307	9.491	9.444	9.336	9.872	10.305	9.452	9.591	9.476	9.590
55	9.824	9.418	9.843	8.898	9.069	9.025	8.925	9.423	9.830	9.034	9.162	9.061	9.161
60	9.385	9.003	9.403	8.518	8.679	8.637	8.544	9.009	9.391	8.646	8.765	8.676	8.763
65	8.979	8.619	8.995	8.166	8.316	8.278	8.190	8.624	8.984	8.287	8.398	8.319	8.395
70	8.602	8.263	8.617	7.839	7.980	7.944	7.861	8.267	8.607	7.953	8.056	7.986	8.053
75	8.252	7.931	8.266	7.534	7.667	7.632	7.555	7.936	8.256	7.642	7.738	7.677	7.735
80	7.926	7.623	7.939	7.250	7.375	7.342	7.270	7.626	7.929	7.352	7.442	7.388	7.438
85	7.622	7.334	7.634	6.984	7.102	7.072	7.003	7.338	7.625	7.082	7.165	7.118	7.161
90	7.338	7.065	7.349	6.736	6.847	6.818	6.754	7.069	7.340	6.828	6.906	6.865	6.902
95	7.072	6.813	7.082	6.503	6.608	6.581	6.520	6.816	7.074	6.591	6.664	6.628	6.660
100	6.823	6.577	6.833	6.285	6.384	6.358	6.301	6.580	6.825	6.369	6.437	6.406	6.433

(a) Listed β factors are the average value for H atoms bound to the same C atom, otherwise noted in (d).

(b) H position is indicated by the subscript number starting from the end closer to the double bond.

(c) 1° = primary, 2° = secondary, 3° = tertiary; Subscript "=" denotes H atoms directly attached to the double bond

(d) Superscript "eql" or "axl" denotes H atoms on the C next to the double bond which is either within (equatorial) or at an acute angle (axial) to the double bond plane

Table 2-A3. Calculated β factors from 0°C to 100°C for H in ketones

T	**2,4-dimethyl-3-petanone** $(CH_3)_2CHCOCH(CH_3)_2$		**3,5-dimethyl-4-heptanone** $CH_3CH_2(CH_3)CHCOCH(CH_3)CH_2CH_3$				**2-methyl-3-hexanone** $(CH_3)_2CHCOCH_2CH_2CH_3$					**4-heptanone** $CH_3CH_2CH_2COCH_2CH_2CH_3$		
(°C)	**3° H_α**	**1° H_β**	**3° H_α**	**2° H_β**	**1° H_β**	**1° H_γ**	**3° H_α**	**2° H_α**	**2° H_β**	**1° H_β**	**1° H_γ**	**2° H_α**	**2° H_β**	**1° H_γ**
0	20.215	16.581	19.655	18.457	16.611	16.440	20.292	16.812	18.542	16.571	16.478	16.817	18.528	16.432
5	18.851	15.557	18.339	17.260	15.585	15.428	18.921	15.754	17.339	15.548	15.463	15.759	17.325	15.420
10	17.625	14.630	17.154	16.179	14.656	14.512	17.689	14.797	16.253	14.621	14.544	14.803	16.241	14.504
15	16.518	13.788	16.086	15.202	13.812	13.680	16.577	13.931	15.272	13.781	13.710	13.936	15.259	13.673
20	15.517	13.023	15.118	14.316	13.045	12.923	15.571	13.143	14.381	13.015	12.951	13.149	14.369	12.916
25	14.608	12.324	14.239	13.509	12.344	12.232	14.658	12.425	13.570	12.317	12.258	12.431	13.559	12.225
30	13.782	11.685	13.440	12.774	11.704	11.600	13.828	11.769	12.831	11.678	11.624	11.775	12.821	11.593
35	13.028	11.098	12.710	12.101	11.116	11.020	13.070	11.168	12.155	11.092	11.042	11.174	12.145	11.013
40	12.338	10.560	12.043	11.485	10.576	10.487	12.378	10.617	11.536	10.554	10.507	10.623	11.526	10.480
45	11.706	10.064	11.431	10.919	10.079	9.996	11.743	10.109	10.967	10.058	10.015	10.115	10.958	9.989
50	11.126	9.606	10.868	10.397	9.620	9.542	11.160	9.642	10.443	9.600	9.560	9.647	10.434	9.536
55	10.592	9.182	10.350	9.917	9.196	9.123	10.623	9.210	9.960	9.177	9.140	9.215	9.952	9.117
60	10.099	8.790	9.872	9.472	8.802	8.734	10.128	8.810	9.514	8.785	8.750	8.815	9.506	8.728
65	9.643	8.425	9.431	9.061	8.437	8.373	9.671	8.439	9.100	8.421	8.388	8.444	9.092	8.367
70	9.221	8.087	9.021	8.679	8.098	8.038	9.247	8.094	8.717	8.082	8.052	8.100	8.709	8.032
75	8.830	7.771	8.642	8.324	7.782	7.725	8.854	7.774	8.360	7.767	7.738	7.779	8.353	7.719
80	8.467	7.477	8.289	7.994	7.487	7.433	8.489	7.475	8.028	7.473	7.446	7.480	8.021	7.428
85	8.128	7.202	7.960	7.686	7.211	7.161	8.150	7.196	7.719	7.198	7.173	7.201	7.712	7.155
90	7.813	6.944	7.654	7.399	6.953	6.906	7.833	6.935	7.430	6.941	6.917	6.940	7.423	6.900
95	7.518	6.703	7.367	7.130	6.712	6.667	7.537	6.691	7.160	6.700	6.677	6.696	7.153	6.661
100	7.243	6.477	7.100	6.878	6.485	6.442	7.261	6.462	6.906	6.473	6.452	6.467	6.900	6.437

Table 2-A3. *(Continued)*

T	5-nonanone $CH_3CH_2CH_2CH_2COCH_2CH_2CH_2CH_3$				2-heptanone $CH_3COCH_2CH_2CH_2CH_2CH_3$						2-octanone $CH_3COCH_2CH_2CH_2CH_2CH_2CH_3$						
(°C)	2° H_α	2° H_β	2° H_γ	1° H_δ	1° H_α	2° H_α	2° H_β	2° H_γ	2° H_δ	1° H_ε	1° H_α	2° H_α	2° H_β	2° H_γ	2° H_δ	2° H_ε	1° H_ζ
0	16.671	18.321	18.070	16.251	15.753	16.819	18.282	18.008	18.139	16.394	15.803	16.783	18.319	17.935	17.876	18.150	16.314
5	15.625	17.135	16.905	15.255	14.799	15.761	17.099	16.848	16.968	15.386	14.845	15.728	17.134	16.781	16.727	16.979	15.312
10	14.680	16.065	15.854	14.353	13.934	14.805	16.033	15.801	15.912	14.473	13.976	14.775	16.064	15.739	15.689	15.922	14.405
15	13.823	15.098	14.903	13.534	13.148	13.938	15.068	14.853	14.957	13.644	13.187	13.910	15.096	14.797	14.751	14.965	13.582
20	13.043	14.220	14.039	12.788	12.432	13.150	14.192	13.993	14.089	12.890	12.468	13.125	14.218	13.941	13.898	14.097	12.832
25	12.333	13.421	13.254	12.107	11.777	12.431	13.395	13.211	13.300	12.201	11.811	12.409	13.419	13.162	13.122	13.307	12.147
30	11.684	12.692	12.537	11.483	11.178	11.775	12.668	12.496	12.580	11.571	11.209	11.754	12.690	12.451	12.415	12.586	11.520
35	11.090	12.025	11.881	10.911	10.628	11.174	12.003	11.843	11.921	10.993	10.657	11.155	12.024	11.801	11.767	11.927	10.946
40	10.544	11.414	11.280	10.385	10.122	10.623	11.394	11.244	11.318	10.462	10.149	10.605	11.413	11.205	11.173	11.323	10.417
45	10.042	10.853	10.727	9.901	9.656	10.115	10.834	10.694	10.763	9.972	9.680	10.099	10.852	10.657	10.627	10.768	9.931
50	9.579	10.336	10.218	9.454	9.225	9.647	10.319	10.187	10.252	9.520	9.248	9.632	10.335	10.152	10.125	10.256	9.481
55	9.151	9.860	9.749	9.040	8.826	9.215	9.843	9.719	9.780	9.102	8.847	9.201	9.858	9.687	9.661	9.784	9.065
60	8.755	9.419	9.315	8.656	8.456	8.815	9.404	9.287	9.345	8.715	8.476	8.802	9.418	9.256	9.232	9.348	8.680
65	8.387	9.011	8.913	8.300	8.112	8.444	8.996	8.886	8.941	8.355	8.131	8.432	9.009	8.857	8.835	8.944	8.322
70	8.046	8.632	8.540	7.968	7.792	8.100	8.619	8.514	8.566	8.020	7.810	8.088	8.631	8.487	8.466	8.569	7.989
75	7.728	8.280	8.193	7.660	7.494	7.779	8.267	8.169	8.218	7.709	7.511	7.768	8.279	8.143	8.123	8.221	7.679
80	7.432	7.952	7.870	7.372	7.216	7.480	7.941	7.847	7.894	7.418	7.231	7.470	7.951	7.823	7.804	7.896	7.390
85	7.156	7.647	7.569	7.102	6.955	7.201	7.636	7.547	7.591	7.146	6.970	7.191	7.646	7.524	7.506	7.594	7.120
90	6.897	7.361	7.288	6.850	6.712	6.940	7.351	7.267	7.309	6.892	6.726	6.931	7.360	7.245	7.228	7.311	6.867
95	6.655	7.095	7.024	6.614	6.483	6.696	7.085	7.004	7.045	6.653	6.496	6.687	7.093	6.984	6.968	7.047	6.629
100	6.428	6.845	6.778	6.392	6.268	6.467	6.835	6.759	6.797	6.430	6.281	6.458	6.843	6.739	6.724	6.799	6.407

Table 2-A3. *(Continued)*

T	5-methyl-2-hexanone $CH_3COCH_2CH_2CH(CH_3)_2$					5-methyl-2-heptanone $CH_3COCH_2CH_2CH(CH_3)CH_2CH_3$							6-methyl-2-heptanone $CH_3COCH_2CH_2CH_2CH(CH_3)_2$					
(°C)	**1° H_α**	**2° H_α**	**2° H_β**	**3° H_γ**	**1° H_δ**	**1° H_α**	**2° H_α**	**2° H_β**	**3° H_γ**	**2° H_δ**	**1° H_δ**	**1° H_ε**	**1° H_α**	**2° H_α**	**2° H_β**	**2° H_γ**	**3° H_δ**	**1° H_ε**
0	15.802	16.921	18.266	19.845	16.303	15.742	16.970	18.150	19.526	18.051	16.430	16.357	15.792	16.762	18.394	17.943	19.609	16.248
5	14.844	15.854	17.084	18.513	15.301	14.789	15.900	16.977	18.221	16.886	15.418	15.352	14.834	15.709	17.202	16.787	18.297	15.251
10	13.975	14.890	16.017	17.314	14.393	13.924	14.932	15.919	17.046	15.836	14.501	14.443	13.966	14.757	16.127	15.743	17.117	14.347
15	13.186	14.017	15.052	16.232	13.569	13.139	14.056	14.962	15.985	14.885	13.669	13.617	13.178	13.893	15.155	14.799	16.051	13.527
20	12.467	13.223	14.177	15.253	12.819	12.423	13.259	14.093	15.025	14.022	12.912	12.865	12.459	13.109	14.272	13.942	15.086	12.780
25	11.810	12.500	13.380	14.364	12.134	11.769	12.533	13.303	14.153	13.237	12.221	12.178	11.803	12.394	13.469	13.162	14.210	12.099
30	11.208	11.839	12.654	13.555	11.508	11.171	11.870	12.582	13.360	12.520	11.589	11.550	11.202	11.740	12.737	12.451	13.413	11.475
35	10.656	11.234	11.989	12.817	10.933	10.621	11.262	11.923	12.635	11.865	11.009	10.973	10.650	11.142	12.068	11.800	12.685	10.903
40	10.148	10.678	11.380	12.142	10.405	10.115	10.705	11.318	11.973	11.264	10.475	10.443	10.142	10.592	11.454	11.203	12.019	10.377
45	9.680	10.167	10.821	11.523	9.918	9.649	10.192	10.763	11.365	10.712	9.984	9.955	9.675	10.087	10.890	10.655	11.409	9.892
50	9.247	9.696	10.306	10.954	9.469	9.218	9.719	10.251	10.807	10.204	9.531	9.504	9.242	9.621	10.371	10.150	10.847	9.444
55	8.847	9.261	9.830	10.430	9.054	8.820	9.283	9.779	10.292	9.735	9.112	9.087	8.842	9.190	9.892	9.684	10.331	9.031
60	8.475	8.858	9.391	9.947	8.668	8.450	8.879	9.343	9.818	9.302	8.723	8.701	8.471	8.792	9.450	9.253	9.854	8.647
65	8.130	8.484	8.984	9.500	8.311	8.106	8.504	8.939	9.379	8.900	8.363	8.342	8.127	8.422	9.040	8.854	9.413	8.291
70	7.809	8.138	8.607	9.087	7.978	7.787	8.156	8.565	8.972	8.527	8.027	8.009	7.806	8.079	8.659	8.484	9.005	7.959
75	7.510	7.815	8.256	8.703	7.669	7.489	7.832	8.216	8.595	8.181	7.715	7.698	7.507	7.759	8.306	8.140	8.626	7.651
80	7.231	7.514	7.929	8.346	7.380	7.211	7.530	7.892	8.244	7.858	7.424	7.407	7.228	7.461	7.977	7.819	8.274	7.363
85	6.970	7.233	7.625	8.014	7.109	6.951	7.249	7.589	7.918	7.558	7.151	7.136	6.967	7.183	7.670	7.520	7.946	7.094
90	6.725	6.970	7.340	7.704	6.857	6.707	6.985	7.307	7.613	7.277	6.896	6.883	6.722	6.923	7.384	7.241	7.640	6.842
95	6.496	6.725	7.074	7.415	6.620	6.479	6.739	7.042	7.329	7.014	6.657	6.645	6.493	6.680	7.116	6.980	7.354	6.606
100	6.280	6.494	6.825	7.145	6.397	6.264	6.507	6.795	7.063	6.767	6.433	6.421	6.278	6.451	6.865	6.735	7.087	6.384

(a) Listed β factors are the average value for H atoms bound to the same C atom.

(b) H position is indicated by the subscript Greek letter as relative to the functional group.

(c) 1° = primary, 2° = secondary, 3° = tertiary

Table 2-A4. Calculated β factors from 0°C to 100°C for H in carboxylic acids and esters

T	pentanoic acid $CH_3CH_2CH_2CH_2COOH$					hexanoic acid $CH_3CH_2CH_2CH_2CH_2COOH$				pentanoic acid, methyl ester $CH_3CH_2CH_2CH_2COOCH_3$				
(°C)	H_{OH}	2° H_α	2° H_β	2° H_γ	1° H_δ	H_{OH}	2° H_α	2° H_β	2° H_γ	1°$H_{me\text{-}\alpha}$	2° H_α	2° H_β	2° H_γ	1° H_δ
0	20.540	17.238	18.476	18.153	16.264	20.464	17.265	18.521	17.912	18.194	17.145	18.480	18.139	16.335
5	19.210	16.145	17.277	16.981	15.267	19.140	16.170	17.319	16.759	17.039	16.059	17.280	16.969	15.331
10	18.011	15.157	16.196	15.924	14.364	17.945	15.180	16.234	15.719	15.995	15.079	16.199	15.912	14.423
15	16.926	14.263	15.218	14.967	13.545	16.865	14.284	15.253	14.778	15.049	14.190	15.220	14.956	13.597
20	15.942	13.450	14.330	14.099	12.798	15.885	13.470	14.363	13.924	14.189	13.383	14.333	14.089	12.846
25	15.046	12.710	13.523	13.308	12.116	14.993	12.728	13.553	13.146	13.405	12.648	13.525	13.299	12.160
30	14.230	12.034	12.786	12.588	11.493	14.180	12.051	12.815	12.437	12.690	11.976	12.789	12.579	11.533
35	13.483	11.415	12.113	11.928	10.920	13.436	11.431	12.140	11.788	12.034	11.361	12.115	11.920	10.957
40	12.799	10.847	11.496	11.324	10.394	12.754	10.862	11.521	11.192	11.433	10.797	11.498	11.316	10.428
45	12.170	10.325	10.929	10.768	9.909	12.128	10.339	10.953	10.645	10.879	10.278	10.931	10.761	9.940
50	11.591	9.844	10.407	10.257	9.461	11.551	9.856	10.429	10.142	10.369	9.800	10.409	10.250	9.490
55	11.057	9.399	9.926	9.785	9.047	11.019	9.411	9.947	9.677	9.898	9.358	9.928	9.779	9.074
60	10.563	8.988	9.481	9.349	8.663	10.528	8.999	9.501	9.247	9.462	8.949	9.483	9.343	8.688
65	10.106	8.607	9.069	8.945	8.307	10.072	8.617	9.088	8.849	9.058	8.570	9.071	8.939	8.329
70	9.682	8.253	8.687	8.570	7.975	9.650	8.263	8.704	8.479	8.683	8.218	8.688	8.565	7.996
75	9.287	7.923	8.332	8.221	7.666	9.257	7.933	8.348	8.136	8.333	7.891	8.333	8.216	7.686
80	8.920	7.616	8.001	7.897	7.378	8.891	7.625	8.017	7.816	8.008	7.586	8.002	7.892	7.396
85	8.577	7.330	7.693	7.594	7.108	8.550	7.338	7.708	7.518	7.704	7.301	7.694	7.590	7.125
90	8.257	7.062	7.405	7.311	6.856	8.231	7.070	7.419	7.239	7.420	7.035	7.406	7.307	6.872
95	7.958	6.812	7.136	7.047	6.620	7.933	6.819	7.149	6.978	7.154	6.786	7.137	7.043	6.634
100	7.678	6.577	6.883	6.799	6.398	7.653	6.584	6.896	6.734	6.905	6.552	6.885	6.795	6.411

Table 2-A4. *(Continued)*

T	pentanoic acid, ethyl ester $CH_3CH_2CH_2CH_2COOCH_2CH_3$				pentanoic acid, propyl ester $CH_3CH_2CH_2CH_2COOCH_2CH_2CH_3$					pentanoic acid, butyl ester $CH_3CH_2CH_2CH_2COOCH_2CH_2CH_2CH_3$					
(°C)	$2°H_{me-\alpha}$	$1°H_{me-\beta}$	$2°\ H_{\alpha}$	$2°\ H_{\beta}$	$2°H_{me-\alpha}$	$2°H_{me-\beta}$	$1°H_{me-\gamma}$	$2°\ H_{\alpha}$	$2°\ H_{\beta}$	$2°H_{me-\alpha}$	$2°H_{me-\beta}$	$2°H_{me-\gamma}$	$1°H_{me-\delta}$	$2°\ H_{\alpha}$	$2°\ H_{\beta}$
0	20.018	16.520	17.168	18.456	19.875	18.445	16.481	17.155	18.389	19.855	18.208	18.278	16.395	17.087	18.385
5	18.688	15.501	16.080	17.258	18.557	17.249	15.465	16.068	17.198	18.538	17.031	17.096	15.386	16.006	17.194
10	17.491	14.579	15.098	16.178	17.370	16.170	14.546	15.087	16.123	17.353	15.970	16.030	14.474	15.030	16.119
15	16.409	13.741	14.208	15.201	16.297	15.194	13.712	14.198	15.150	16.282	15.009	15.065	13.645	14.145	15.147
20	15.429	12.979	13.400	14.315	15.325	14.309	12.952	13.390	14.268	15.311	14.137	14.189	12.890	13.342	14.265
25	14.538	12.283	12.663	13.509	14.442	13.503	12.259	12.654	13.465	14.430	13.344	13.392	12.202	12.609	13.462
30	13.727	11.647	11.990	12.773	13.637	12.768	11.625	11.982	12.733	13.626	12.621	12.665	11.571	11.941	12.730
35	12.987	11.064	11.374	12.101	12.903	12.096	11.043	11.366	12.063	12.893	11.959	12.000	10.993	11.328	12.061
40	12.309	10.527	10.809	11.484	12.230	11.481	10.508	10.802	11.449	12.221	11.352	11.391	10.462	10.766	11.447
45	11.687	10.033	10.289	10.918	11.613	10.915	10.015	10.282	10.886	11.605	10.795	10.831	9.972	10.249	10.884
50	11.115	9.577	9.810	10.397	11.046	10.394	9.561	9.804	10.367	11.038	10.282	10.316	9.520	9.773	10.365
55	10.588	9.155	9.368	9.916	10.523	9.914	9.140	9.361	9.888	10.516	9.808	9.840	9.102	9.333	9.886
60	10.102	8.765	8.959	9.472	10.041	9.470	8.750	8.952	9.445	10.034	9.370	9.400	8.715	8.926	9.444
65	9.652	8.402	8.579	9.060	9.594	9.059	8.388	8.573	9.035	9.588	8.965	8.993	8.355	8.548	9.034
70	9.235	8.064	8.227	8.679	9.180	8.677	8.052	8.221	8.655	9.175	8.589	8.616	8.020	8.197	8.654
75	8.847	7.750	7.899	8.324	8.796	8.323	7.738	7.893	8.302	8.791	8.239	8.264	7.709	7.871	8.301
80	8.487	7.457	7.593	7.994	8.439	7.993	7.446	7.588	7.973	8.434	7.914	7.938	7.418	7.567	7.972
85	8.152	7.183	7.308	7.686	8.106	7.685	7.173	7.303	7.666	8.101	7.610	7.633	7.146	7.283	7.665
90	7.839	6.927	7.041	7.398	7.795	7.398	6.917	7.037	7.380	7.791	7.327	7.348	6.892	7.018	7.379
95	7.547	6.687	6.792	7.129	7.505	7.129	6.677	6.787	7.112	7.501	7.061	7.082	6.653	6.770	7.111
100	7.273	6.461	6.558	6.877	7.233	6.877	6.452	6.554	6.861	7.230	6.813	6.832	6.429	6.537	6.860

(a) Listed β factors are the average value for H atoms bound to the same C atom.

(b) H position is indicated by the subscript Greek letter as relative to the functional group.

(c) 1° = primary, 2° = secondary, 3° = tertiary

Table 2-A5. Calculated β factors from 0°C to 100°C for H in alcohols and ethers

T	1-heptanol			2-heptanol						3-heptanol					
	$CH_3CH_2CH_2CH_2CH_2CH_2CH_2OH$			$CH_3CH_2CH_2CH_2CH_2CH(OH)CH_3$						$CH_3CH_2CH_2CH_2CH(OH)CH_2CH_3$					
(°C)	H_{OH}	2° H_1	2° H_2	1°H_1	H_{OH}	3° H_2	2° H_3	2° H_4	2° H_5	1°H_1	2° H_2	H_{OH}	3° H_3	2° H_4	2° H_5
0	19.866	19.296	18.028	16.215	20.246	21.810	17.725	18.278	17.972	16.412	17.901	20.136	21.804	17.673	18.347
5	18.619	18.027	16.866	15.220	18.959	20.307	16.588	17.095	16.815	15.403	16.750	18.860	20.301	16.540	17.158
10	17.492	16.883	15.818	14.320	17.795	18.958	15.562	16.028	15.770	14.489	15.712	17.707	18.951	15.518	16.086
15	16.470	15.849	14.869	13.503	16.742	17.742	14.633	15.062	14.825	13.660	14.772	16.662	17.735	14.592	15.116
20	15.540	14.911	14.008	12.758	15.784	16.642	13.789	14.186	13.967	12.905	13.918	15.712	16.636	13.752	14.235
25	14.693	14.059	13.224	12.079	14.912	15.646	13.022	13.389	13.186	12.216	13.141	14.847	15.639	12.987	13.435
30	13.918	13.282	12.509	11.457	14.116	14.741	12.321	12.662	12.473	11.585	12.432	14.056	14.734	12.289	12.704
35	13.208	12.572	11.855	10.886	13.387	13.916	11.680	11.997	11.821	11.006	11.784	13.333	13.909	11.650	12.036
40	12.555	11.922	11.255	10.362	12.718	13.163	11.092	11.388	11.224	10.475	11.189	12.668	13.156	11.064	11.424
45	11.955	11.326	10.704	9.878	12.102	12.473	10.552	10.828	10.675	9.984	10.643	12.057	12.466	10.526	10.861
50	11.401	10.777	10.197	9.432	11.535	11.841	10.054	10.312	10.169	9.532	10.140	11.494	11.834	10.030	10.344
55	10.890	10.271	9.729	9.019	11.011	11.259	9.595	9.837	9.702	9.114	9.675	10.974	11.252	9.572	9.866
60	10.416	9.803	9.296	8.637	10.527	10.722	9.170	9.397	9.271	8.726	9.246	10.492	10.716	9.149	9.424
65	9.976	9.370	8.895	8.281	10.077	10.227	8.777	8.990	8.871	8.366	8.848	10.045	10.221	8.757	9.016
70	9.567	8.969	8.523	7.951	9.660	9.769	8.411	8.612	8.500	8.031	8.479	9.631	9.763	8.393	8.636
75	9.187	8.597	8.177	7.643	9.271	9.345	8.072	8.261	8.155	7.719	8.136	9.244	9.338	8.054	8.284
80	8.832	8.250	7.855	7.356	8.910	8.951	7.755	7.934	7.834	7.428	7.816	8.885	8.944	7.739	7.956
85	8.501	7.927	7.554	7.087	8.572	8.584	7.460	7.630	7.535	7.156	7.518	8.549	8.578	7.445	7.649
90	8.191	7.626	7.274	6.836	8.256	8.243	7.185	7.345	7.255	6.901	7.239	8.235	8.237	7.170	7.364
95	7.900	7.344	7.011	6.600	7.960	7.924	6.927	7.079	6.993	6.662	6.979	7.941	7.918	6.913	7.096
100	7.628	7.080	6.766	6.379	7.683	7.627	6.685	6.829	6.748	6.438	6.735	7.665	7.621	6.672	6.846

Table 2-A5. *(Continued)*

4-heptanol					**pentyl methyl ether**				**pentyl ethyl ether**					**pentyl propyl ether**					
$CH_3CH_2CH_2CH(OH)CH_2CH_2CH_3$					$CH_3CH_2CH_2CH_2CH_2OCH_3$				$CH_3CH_2CH_2CH_2CH_2OCH_2CH_3$					$CH_3CH_2CH_2CH_2CH_2OCH_2CH_2CH_3$					
1°H_1	**2° H_2**	**2° H_3**	**H_{OH}**	**3° H_4**	**1°H_1**	**2° H_2**	**2° H_3**	**2° H_4**	**1°H_1**	**2°H_2**	**2° H_3**	**2° H_4**	**2° H_5**	**1°H_1**	**2°H_2**	**2°H_3**	**2° H_4**	**2° H_5**	**2° H_6**
16.330	18.473	17.719	20.076	21.631	17.507	19.009	17.944	18.132	16.449	19.109	18.975	18.091	18.027	16.419	18.415	18.899	18.926	18.229	17.988
15.327	17.274	16.583	18.805	20.143	16.407	17.771	16.789	16.961	15.437	17.855	17.756	16.924	16.865	15.409	17.221	17.662	17.671	17.050	16.829
14.419	16.193	15.557	17.656	18.806	15.411	16.647	15.748	15.905	14.520	16.724	16.633	15.871	15.817	14.494	16.145	16.547	16.555	15.987	15.784
13.594	15.215	14.628	16.615	17.602	14.509	15.631	14.805	14.950	13.687	15.701	15.618	14.919	14.868	13.664	15.170	15.538	15.546	15.025	14.838
12.843	14.328	13.785	15.669	16.513	13.688	14.710	13.949	14.083	12.930	14.774	14.698	14.054	14.007	12.908	14.286	14.624	14.631	14.152	13.979
12.157	13.521	13.018	14.807	15.526	12.940	13.872	13.170	13.293	12.238	13.931	13.861	13.267	13.224	12.218	13.482	13.792	13.800	13.358	13.198
11.530	12.785	12.317	14.020	14.629	12.256	13.108	12.459	12.573	11.605	13.163	13.098	12.549	12.509	11.586	12.749	13.034	13.041	12.633	12.484
10.954	12.111	11.676	13.299	13.812	11.629	12.410	11.808	11.915	11.025	12.461	12.401	11.892	11.854	11.007	12.078	12.341	12.348	11.970	11.832
10.425	11.495	11.089	12.637	13.066	11.054	11.771	11.212	11.311	10.491	11.818	11.762	11.290	11.255	10.475	11.463	11.706	11.713	11.363	11.234
9.938	10.928	10.548	12.028	12.382	10.524	11.184	10.664	10.756	10.000	11.228	11.176	10.737	10.704	9.985	10.899	11.123	11.130	10.805	10.684
9.488	10.406	10.051	11.466	11.755	10.036	10.643	10.160	10.245	9.546	10.685	10.636	10.228	10.196	9.532	10.379	10.587	10.593	10.291	10.178
9.072	9.925	9.592	10.948	11.178	9.585	10.145	9.694	9.774	9.127	10.184	10.138	9.758	9.728	9.113	9.899	10.092	10.099	9.817	9.711
8.686	9.480	9.167	10.468	10.647	9.167	9.685	9.263	9.338	8.738	9.722	9.679	9.323	9.295	8.725	9.456	9.636	9.642	9.378	9.279
8.328	9.068	8.774	10.023	10.156	8.779	9.259	8.864	8.935	8.377	9.294	9.253	8.921	8.894	8.365	9.045	9.213	9.219	8.972	8.879
7.995	8.686	8.409	9.609	9.702	8.419	8.865	8.494	8.560	8.041	8.897	8.859	8.547	8.522	8.030	8.665	8.820	8.826	8.596	8.508
7.684	8.331	8.069	9.224	9.281	8.084	8.498	8.150	8.212	7.728	8.528	8.492	8.200	8.176	7.717	8.311	8.456	8.462	8.246	8.163
7.395	8.000	7.753	8.866	8.891	7.771	8.156	7.830	7.888	7.437	8.185	8.151	7.877	7.854	7.426	7.981	8.117	8.122	7.920	7.841
7.124	7.692	7.458	8.531	8.527	7.479	7.838	7.531	7.586	7.164	7.865	7.834	7.575	7.554	7.154	7.674	7.801	7.806	7.616	7.542
6.871	7.404	7.183	8.218	8.189	7.207	7.541	7.252	7.303	6.909	7.567	7.537	7.294	7.273	6.899	7.387	7.506	7.511	7.332	7.262
6.633	7.135	6.925	7.924	7.873	6.951	7.264	6.990	7.039	6.669	7.288	7.260	7.030	7.010	6.660	7.119	7.230	7.235	7.066	7.000
6.410	6.883	6.683	7.649	7.578	6.711	7.004	6.746	6.792	6.445	7.027	7.000	6.783	6.765	6.436	6.868	6.972	6.977	6.818	6.754

(a) Listed β factors are the average value for H atoms bound to the same C atom.

(b) H position is indicated by the subscript Greek letter as relative to the functional group.

(c) 1° = primary, 2° = secondary, 3° = tertiary

C h a p t e r 3

EQUILIBRIUM $^{2}H/^{1}H$ FRACTIONATIONS IN ORGANIC MOLECULES

III. CYCLIC MOLECULES

Ying Wang and Alex L. Sessions

Division of Geological and Planetary Sciences,
California Institute of Technology, Pasadena, CA, USA

ABSTRACT

Cyclic lipids are important components of sedimentary organic matter and oils. Similar to *n*-alkyl lipids, it is necessary to know their equilibrium $^2H/^1H$ fractionations so as to quantitatively interpret the δ^2H data of natural samples. In Chapter 1, the calibration curve for ab initio calculations based on acyclic ketones was shown to be inapplicable to cyclohexanone. To systematically investigate the ring system, we performed similar experimental and theoretical studies on five more monocyclic ketones. The measured ε_{eq} values for secondary and tertiary H_α are in the ranges of −130 to −150‰ and 10 to −40‰ respectively, with experimental uncertainties between 5–15‰. Calculation of the same cyclic ketones was performed for both the chair and twist-boat conformations, using vibrational frequencies from ab initio calculations (B3LYP/6-311G**). By averaging over the equatorial and axial positions, the calculated ε_{eq} values for secondary H_α are higher than the experimental results by ~60‰; whereas the experiment-theory discrepancy for tertiary H_α is only ~10‰. Based on stereochemistry and the mechanism of base-catalyzed H_α substitution, we propose that the measured equilibrium fractionation is the value for axial H_α, rather than the average of axial and equatorial H_α, because reprotonation on C_α in the enolate ion always takes place along the axial direction and subsequently forms the axial C_α–H_α bond. According to this mechanism, regression between experimental and theoretical ε_{eq} values produces a calibration curve with slope of 1.44±0.05 and intercept of 32.8±5.1. Applying this calibration, the molecular fractionation for cyclic biomarkers was calculated to be in the range of −75 to −100‰ for steroids and hopanoids between 0 to 100°C, similar to *n*-alkyl lipids and acyclic isoprenoids. Thus post-burial H exchange will generally remove the ~50–100‰ biosynthetic fractionations between cyclic and *n*-alkyl lipid molecules, which can be used to evaluate the extent of H exchange in sedimentary organic matter and oils.

1. INTRODUCTION

Cyclic hydrocarbon molecules are ubiquitous components of biomarkers in sediments and petroleum of all geological eras (Brocks and Summons, 2003). Most of the useful cyclic biomarkers belong to the isoprenoid family and display a great diversity of structures. The most abundant of them are the tetracyclic steroids and pentacyclic hopanoids, primarily derived from eukaryotes and bacteria respectively (Farrimond et al., 1998; Rohmer et al., 1984; Volkman, 2003). Isoprenoids are constructed by repeating the C_5 isoprene units via the mevalonate (Qureshi and Porter, 1981) and deoxyxylulose (Eisenreich et al., 1998) pathways, which give rise to biosynthetic fractionations between −150‰ and −350‰ relative to growth water (Sessions et al., 1999; Chikaraishi and Naraoka, 2003; Zhang and Sachs, 2007). In general, the cyclic isoprenoids are depleted in ^{2}H relative to *n*-alkyl lipids by 50–100‰ but more enriched by ~50‰ than the acyclic isoprenoids, e.g., phytane and pristane that are derived from phytol. Sauer et al. (2001) showed that δ^2H values of steroids from modern marine and lake sediments closely track the δ^2H values of water by a constant fractionation around −200‰. Similar to the aliphatic lipids we discussed in Chapter 1 and 2, applying this proxy to geological samples must address the isotopic exchange processes that may change δ^2H values of the steroids during diagenesis and catagenesis, which in turn requires quantitative knowledge of the equilibrium ^{2}H/^{1}H fractionation factor (α_{eq}).

It has been shown in Chapter 1 that, using frequencies from ab initio QM calculations (B3LYP/6-311G**) and averaging all H_α positions, the theoretical α_{eq} values for H_α in cyclohexanone are systematically higher than the experimental fractionation by ~60‰, unlike the acyclic ketones where the theoretical and experimental results agree well. By applying the scaling factor, we demonstrated that the dominant error (omission of anharmonicity) in the calculated β factors is virtually of the same size for H_α in cyclohexanone and acyclic ketones (Fig. 1-9). It indicates that the large experiment-theory discrepancy for cyclohexanone is probably due to factors other than the omission of anharmonicity in theoretical calculations.

The most apparent difference between cyclic and acyclic hydrocarbon molecules resides in their conformations. Naturally occurring cyclic hydrocarbons primarily consist of six-membered rings. The angles between C-C bonds in the relaxed ring are 109.5°, the same as the angles in acyclic hydrocarbons, but these C-C bonds cannot rotate freely. Instead the ring can only adopt a few conformations that convert via distorted angles. The most stable conformation for a six-membered ring is the chair form which is free of ring strain. Other conformations it can adopt include the boat, twist-boat, and half-chair forms, but only the twist boat is a true local minimum (Fig. 3-1). In contrast, in acyclic molecules long-range tortional movements occur at continuous angles and do not significantly affect the local bonding environment. Moreover, in the six-membered ring system, the two C−H(R) bonds on the same C atom adopt either an equatorial or axial position, giving rise to distinctive stereochemistry that might affect the value of equilibrium fractionation factor. At room temperature, the equatorial and axial bonds on the same C atom are constantly interconverting through the chair-chair interconversion, also called a "ring flip", where the twist-boat conformations serve as intermediates (Fig. 3-1). During this dynamic conformational equilibrium, the equatorial position is generally preferred by substituent groups to avoid steric interference with other axial bonds.

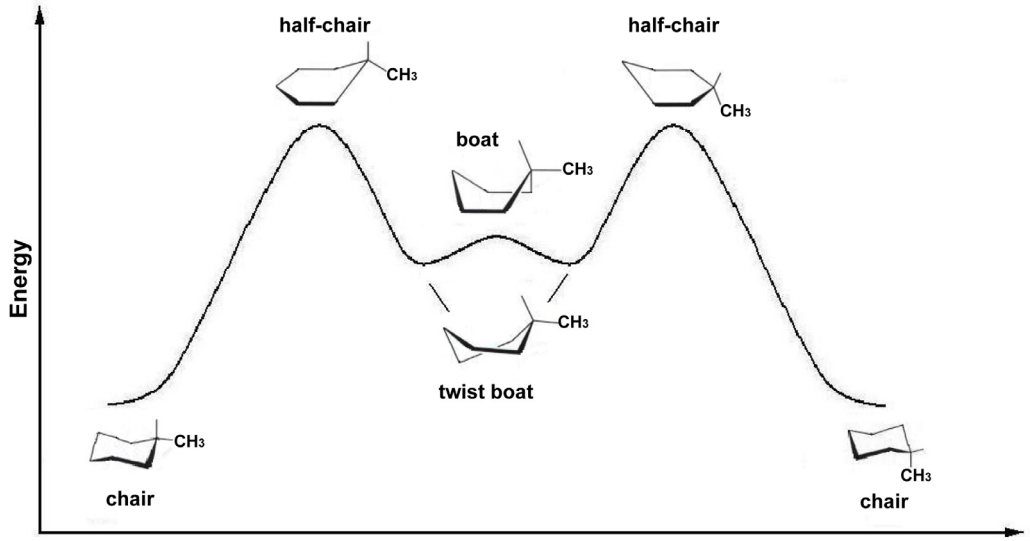

Figure 3-1. Conformational changes of a six-membered ring. The chair conformation is the most stable, followed by the twist boat. It also demonstrates the pathway of chair-chair interconversion (ring flip), where the methyl group is equatorial in one chair and axial in the other.

To systematically investigate equilibrium $^{2}H/^{1}H$ fractionation for cyclic hydrocarbons, we applied the same experimental and theoretical methods as in Chapter 1 to measure the value of α_{eq} for H_{α} in cyclohexanone and five methylated monocyclic ketones. In this chapter, we report the experimental and theoretical values of α_{eq} between 0–100°C for the six cyclic ketones. A mechanism based on stereochemistry and base-catalyzed H_{α} substitution is proposed to explain the experiment-theory discrepancies. In the end, we use the calibration dataset to estimate α_{eq} values for common cyclic biomarker molecules and discuss their implications in paleo-environment studies. Please note that in this chapter we follow the notations and nomenclatures that have been outlined in Chapter 1, Section 2.

2. METHODS

2.1. Experimental methods

Methods to measure equilibrium fractionation for H_{α} in ketones are described fully in Chapter 1 and only briefly below.

2.1.1. Materials

Five methylated cyclohexanones were chosen as the exchange substrates, including 2-methylcyclohexanone (98%), 3-methylcyclohexanone (97%), 4-methylcyclohexanone (98%), 2,6-dimethylcyclohexanone (99%), 2,2,6-trimethylcyclohexanone (98.5+%). All were obtained from Acros Organics. Cyclohexanone (99%) from Sigma-Aldrich which has been previously tested (Chapter1) was also included in the substrates to check the consistency of our methods. In particular, 2,6-dimethylcyclohexanone is a mixture of the cis- and trans-isomers (Fig. 3-1), with an abundance ratio of 4:1. In our isotope analysis (Chapter 1, Section 3.1.3.), the major component — *cis*-2,6-dimethylcyclohexanone — elutes about 10 s earlier than the trans-isomer and is the only component investigated in this study. The six substrates contain secondary and/or tertiary H_{α} in six-membered cyclic ketones. Fig. 3-2 gives ball-and-stick depictions of the optimized structures in the chair conformation from ab initio modeling (see Section 3.2.1).

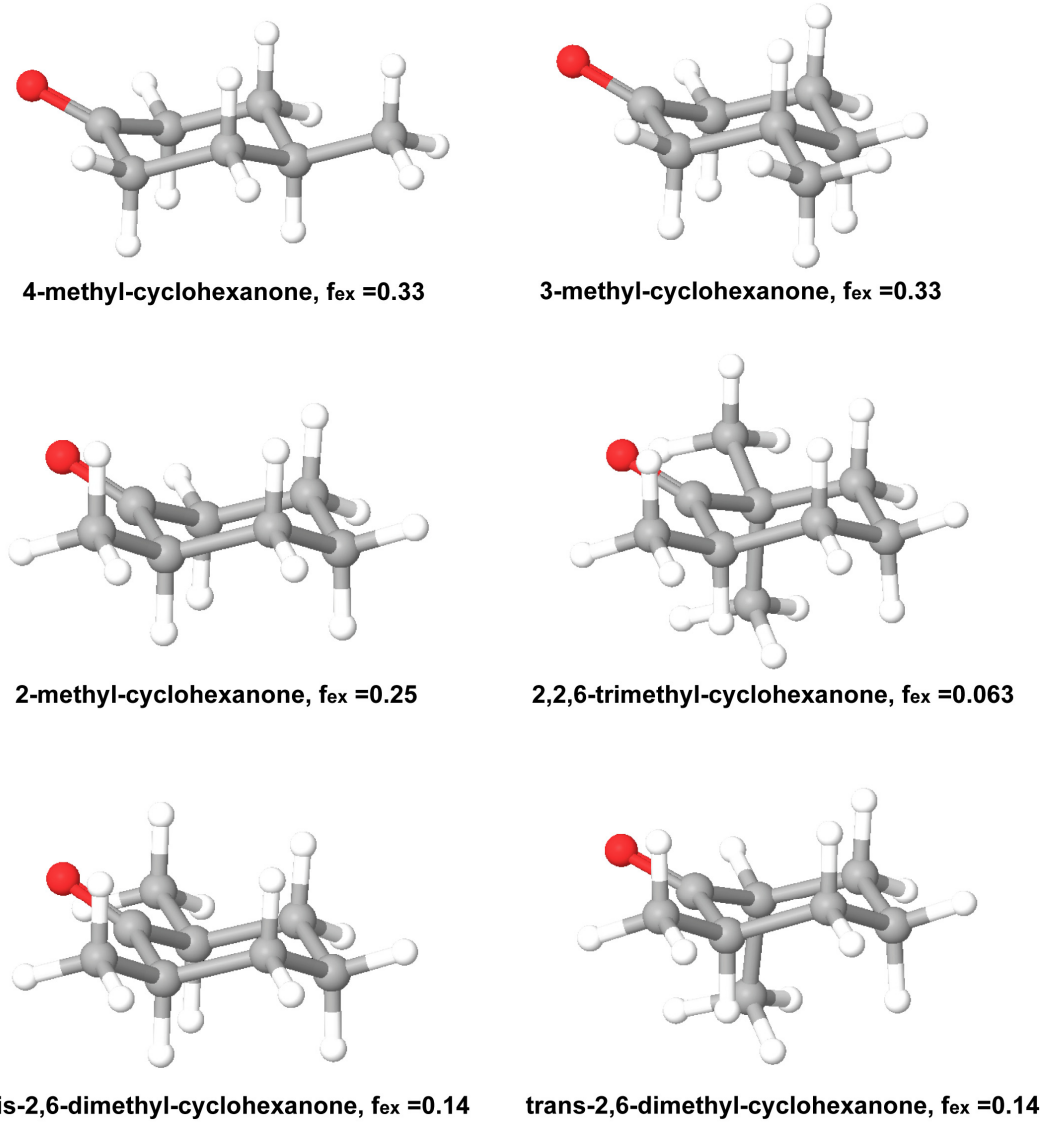

Figure 3-2. Optimized geometries of the substrate cyclic ketone molecules (● = O, ● = C, ○ = H) in the chair conformation. Cyclohexanone has been shown in Fig. 1-1, thus not presented here. f_{ex} is the fraction of exchangeable H in each molecule, assumed to be exclusively H_{α} (see Chapter 1, Section 3.1.5.). Note that 2,6-dimethylcyclohexanone is a mixture of the cis- and trans-isomers, but only the cis-isomer is investigated in this study.

Water for isotopic exchange was prepared by mixing ^{2}H-enriched (prepared by adding $^{2}H_2O$ to DI water) and ^{2}H-depleted water (obtained from a melted Antarctic ice core) at

varying volume ratios to produce a series of 8 waters with evenly spaced δ^2H values between −280‰ and +469‰. This range brackets the δ^2H values of the unexchanged cyclic ketones (−256.2 to +25.5‰) so that equilibrium can be approached from both directions for each ketone.

2.1.2. Isotope exchange experiments

Ketones were individually dissolved in each of the 8 waters, sealed in closed vessels with minimal headspace and incubated at constant temperature. At selected time points, samples were removed and the ketone extracted into hexane. The δ^2H values of both ketone and water were then analyzed as described in Chapter 1, Section 3.1.3. and 3.1.4.

In the first stage of experiments, incubated solutions were successively sampled and analyzed until equilibrium was confirmed. Based on the temporal evolution of substrate δ^2H values, exchange rate constants were estimated according to the mechanism of base-catalyzed keto-enol tautomerism (Chapter 1, Appendix 1) and the kinetics of second-order reactions (Chapter 1, Section 3.1.6.).

In the second stage of experiments, solutions were flame-sealed in glass ampoules so as to exclude any possible evaporation or exchange of water vapor. They were incubated at pH 12.0 in the water bath at 25, 50, or 70 °C, respectively. The length of incubation was determined according to rate constants from the first set of experiments. Similar to acyclic ketones, the value of α_{eq} between exchangeable H (H_α) and water at equilibrium were derived from the slope of a regression between δ^2H values of the ketone and the corresponding waters (Sessions and Hayes, 2005).

2.2. Computational methods

Complete vibrational frequencies for organic molecules were calculated for the optimized geometries using the hybrid Hartree-Fock and Density Functional Theory (DFT), B3LYP/6-311G** method (Lee et al., 1988; Becke, 1993), with solvation effect

treated by the Poisson-Boltzmann continuum solvation model (Tannor et al.1994). Using the frequency values, the reduced partition function ratio (β factor) for ^{2}H-substitution at individual organic H positions was then calculated based on the theoretical method of Urey (1947) and Bigeleisen and Mayer (1947). The β factor for liquid water was obtained by first calculating the β factor for gaseous water molecule using the same method, which was then multiplied by the experimental liquid-gas fractionation factor measured by Horita and Wesolowski (1994). Equilibrium ^{2}H/^{1}H fractionation factors (α_{eq}) were calculated as the ratio of β factors between the organic molecule in aqueous phase and liquid water.

3. RESULTS AND DISCUSSION

3.1. Isotope exchange experiments

3.1.1. Exchange kinetics

In time-series experiments, ^{2}H/^{1}H exchange profiles were measured for 2-methylcyclohexanone, 4-methylcyclohexanone, 2,6-dimethylcyclohexanone and 2,2,6-trimethylcyclohexanone at 25 and 50°C. Basic condition (pH 12.0) was exclusively applied in this study, because we have demonstrated in Chapter 1 that acid-catalysis gives the same equilibrium fractionations and is not as efficient as the base-catalysis. Exchange rates and half-lives ($t_{1/2}$) were estimated and summarized in Table 3-1.

Similar to acyclic ketones, δ^2H values of the cyclic ketones changed systematically with time, clearly recording the progress of ^{2}H/^{1}H exchange with water. Selected exchange profiles are plotted in Fig. 3-3 as the evolution of ketone δ^2H values versus time. For each substrate, incubations at a constant temperature with waters of varying δ^2H values reached equilibrium simultaneously (e.g., 2-methyl-cyclohexanone in Fig. 3-3). For 2-methyl-cyclohexanone, equilibrium was achieved in about 6 days (~$8x10^3$ min) at 25°C and within one day (~$1x10^3$ min) at 50°C. At 50°C, 2-methylcyclohexanone exchanges faster than 2,6-dimethylcyclohexanone and 2,2,6-trimethylcyclohexanone, but significantly slower than 4-

Table 3-1. Second-order rate constant and exchange half-life for base-catalyzed H_α exchange

Ketone	T (°C)	k_{OH}[a] ($M^{-1}s^{-1}$)	$t_{1/2}$[b] (hr, pH=12)	$t_{1/2}$[b] (yr, pH=7)
2-methylcyclohexanone	25	0.0032 (0.0001)	18	209
	50	0.045 (0.008)	1.3	15
4-methylcyclohexanone	50	0.150 (0.031)	0.5	5.9
2,6-dimethylcyclohexanone	25	0.0012 (0.0001)	32	361
	50	0.024 (0.002)	1.6	19
2,2,6-trimethylcyclohexanone	25	0.0004 (0.0001)	45	509
	50	0.0093 (0.0007)	2.1	24

(a) Second-order rate constant for base-catalyzed H_α substitution, corrected for the number of H_α atoms in each molecule. Uncertainties (1σ) are given in parentheses.

(b) Exchange half-life calculated at pH 12 or 7

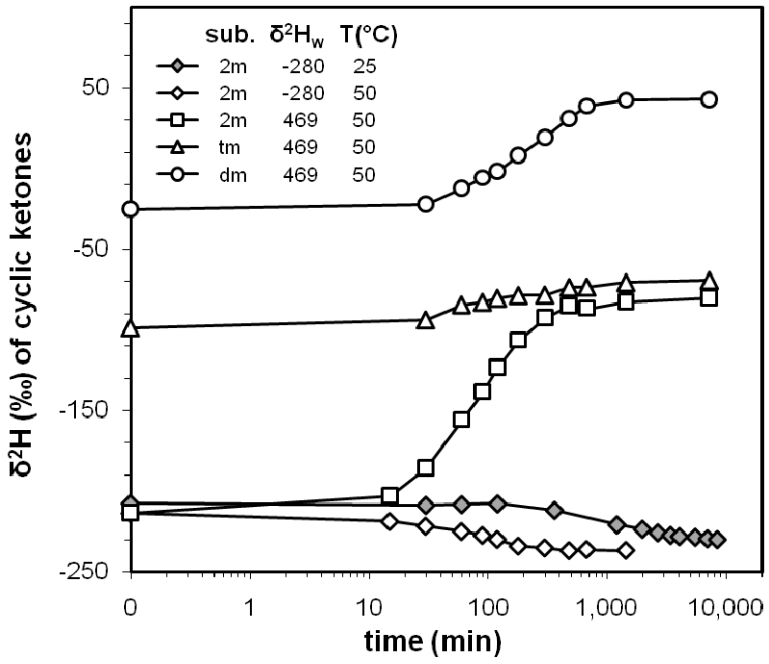

Figure 3-3. δ^2H values of the cyclic ketone substrates over time during incubations with waters of varying δ^2H values and temperature (shown in legend). Compound name abbreviations: 2-methylcyclohexanone (2m), 2,6-dimethylcyclohexanone (dm), and 2,2,6-trimethylcyclohexanone (tm). Error bars are generally smaller than the symbols.

methylcyclohexanone. This trend — H_α exchange rate decreases with increasing alkyl substitution on C_α — is consistent with the observation for acyclic ketones, and is likely due to steric hindrance of the alkyl group(s) on the H_α position. Exchange rate for secondary H_α in 4-methylcyclohexanone is 0.15±0.03 $M^{-1}s^{-1}$, comparable to that for cyclohexanone (0.11±0.01 $M^{-1}s^{-1}$), suggesting that methyl groups at non-alpha positions do not effectively affect the rate of H_α exchange.

3.1.2. Experimental measurements of equilibrium fractionation for H_α

During the second stage of experiments, incubations were carried out with all substrates at pH 12 for 6 days at 70°C, 10 days at 50°C, and 75 days at 25°C, more than 40 times longer than the estimated $t_{1/2}$ at each temperature to ensure the attainment of $^2H/^1H$ exchange equilibrium. The values of the isotopic enrichment factor ε_{eq} for H_α are derived from the regression slope between δ^2H values of the ketone and water at equilibrium (Chapter 1, Section 3.1.5.). This yields the ε_{eq} value that averages all exchanging H_α positions in each molecule.

3.1.2.1. Effect of isotopic normalization on the value of equilibrium fractionation. In the isotopic analysis of the exchanged ketones, we co-injected a series of multiple organic standards with each sample and used the normalization curve based on these standards to correct for memory effect. Detailed procedures have been described in Chapter 1, Section 3.1.3. The six cyclic ketones used in this study have very different original δ^2H values (before exchange with water), ranging from −256‰ to −148‰ for cyclohexanone, 2-methyl-cyclohexnaone, and 3-methyl-cyclohexanone, and from −99‰ to −26‰ for 4-methyl-cyclohexnaone, 2,6-dimethyl-cyclohexnaone, and 2,2,6-trimethyl-cyclohexnaone. Therefore we designed two series of organic standards to better fit the δ^2H value of each ketone. The first series (Standard 1) consists of three *n*-alkane standards, nC_{17} (−142‰), nC_{22} (−62.2‰), and nC_{25} (−256.4‰), and was co-injected with the first three cyclic ketones. The second series (Standard 2) consists of two *n*-alkane standards, nC_{17} (−142‰),

nC_{22} (−62.2‰), and two ester standards, palmitic acid methyl ester (C16M, 88.0‰) and eicosenoic n-butyl ester (C20B, 1.5‰). It was co-injected with the last three cyclic ketones.

Theoretically, both standard series should give statistically consistent normalization curves. However, the analyses using Standard 1 produced normalization curves with slope of 0.97±0.02 and intercept of 6±3, whereas those using Standard 2 produced normalization slopes of 0.88±0.02 and intercept of -9±2. For the same ketone samples, application of the second normalization gives equilibrium fractionation (ε_{eq} values) that are consistently higher by 40–60‰ than the ε_{eq} values using the first one. This offset in normalization curves could not be due to random error or system drifting, because it is observed in successive measurements during the same day. In fact, this offset is primarily caused by the large decrease in measured δ^2H values relative to the "known" values for the ester standards in Standard 2 (16–20‰ for C16M and 7–9‰ for C20B). By deleting them, the normalization of Standard 2 becomes consistent with Standard 1. Since the ester standards are synthesized via transesterification (Chapter 4, Section 2.1.) while the *n*-alkane standards are purchased pure products, it is possible that impurities during the synthesis and purification processes had biased the offline measurements for the ester standards (i.e., the "known" δ^2H values). Another possibility is the variation in memory effects. Since the measured δ^2H values are sensitive to peak size, especially for ^2H-enriched analytes (Chapter 4, Section 3.3.), we intended to maintain the same peak size for each standard and the ketone so that all of them were subject to equivalent memory effects from the preceding methane peaks. Nevertheless, small variations are still present. The peak size of C16M is smaller than *n*C_{17} by ~8%, which probably biased the measured δ^2H of C16M towards lower values.

In general, the normalization based on Standard 1 appears to be more reliable and is consistent with previous normalization records. We therefore applied this normalization to all exchanged cyclic ketone samples. R^2 values for the regressions between the water δ^2H values and the normalized ketone δ^2H values are all greater than 0.99. Complete δ^2H data are presented in Appendix Table 3-A1.

3.1.2.2. Equilibrium fractionation factors for H_α. Derived values of the equilibrium fractionation (ε_{eq} values) for H_α positions in the cyclic ketone substrates are summarized in Table 3-2 and Fig. 3-4. The uncertainties in ε_{eq} values, generally between 5–15‰, are estimated from the standard deviation of the ketone-water regressions. They are slightly smaller than the uncertainty for acyclic ketones (Table 1-2), because we used 8 waters of varying δ^2H values to exchange with each cyclic ketone, while 7 waters were used for each acyclic ketone. The relatively large uncertainty for 2,2,6-trimethylcyclohexanone is due to its low H_α content (f_{ex} = 0.063), which produces a much smaller δ^2H range after the incubations, compared to other cyclic ketones. The values of non-exchangeable H derived at different temperatures are statistically identical for each molecule. Similar to acyclic ketones, this confirms the assumption that only H_α is undergoing appreciable exchange.

The values of ε_{eq} for cyclohexanone (around −150‰) are consistent with the results measured in our previous study (Table 1-2). The two ketones that contain non-α methyl group, 3-methylcyclohexanone and 4-methylcyclohexanone, yield statistically consistent ε_{eq} values ranging between −133‰ and −154‰ with little temperature variation. They are similar to cyclohexanone, indicating that alkyl groups on non-α C atoms do not effectively change the equilibrium fractionation of H_α, consistent with the "cutoff" effect (Stern and Wolfsberg 1966a,b; Hartshorn and Shiner, 1972) and our previous results for acyclic ketones (Chapter 1). Molecules containing only tertiary H_α atoms, *cis*-2,6-dimethylcyclohexanone and 2,2,6-trimethylcyclohexanone, have similar ε_{eq} values between 7‰ and −42‰ with negative temperature dependence. The results also suggest that the measured δ^2H values for *cis*-2,6-dimethylcyclohexanone are not affected by the slight coelution with the trans-isomer in GC/P/IRMS analysis (see Section 2.1.1.). The ε_{eq} values for 2-methylcyclohexanone which contains one tertiary and two secondary H_α atoms agree well with the weighted average of tertiary H_α and secondary H_α. This trend, wherein ε_{eq} for H_α increases substantially with more alkyl substituents on C_α, is again consistent with the observation for acyclic ketones. It is caused by the electron-donating effect of alkyl groups that acts to enhance the electron density of the C_α–H_α bond and thus increases its bond stiffness.

Table 3-2. Experimental isotopic enrichment factors (ε_{eq}) for H_α and δ^2H values for non-exchangeable H (δ_N) in the six cyclic ketones

ketone substrate	25°C		50°C		70°C	
	ε_{eq} (‰)	δ_N (‰)	ε_{eq} (‰)	δ_N (‰)	ε_{eq} (‰)	δ_N (‰)
Cyclohexanone	**-148 (11)**	-196 (8)	**-158(7)**	-191 (5)	**-152 (6)**	-195 (4)
2-methylcyclohexanone	**-102(7)**	-203 (2)	**-105 (11)**	-203 (4)	**-103 (6)**	-205 (2)
3-methylcyclohexanone	**-148 (5)**	-234 (3)	**-154 (13)**	-234 (7)	**-139 (9)**	-243 (4)
4-methylcyclohexanone	**-133 (10)**	-97 (5)	**-142 (10)**	-92 (5)	**-137 (10)**	-91 (5)
2,6-dimethylcyclohexanone	**-8 (12)**	-13 (2)	**-30 (10)**	-18 (2)	**-42 (18)**	-16 (3)
2,2,6-trimethylcyclohexanone	**7 (26)**	-104 (2)	**-31 (19)**	-102 (1)	**-34 (19)**	-102 (1)

Uncertainties (1σ) are given in brackets. They are propagated from the standard error of the ketone-water regression slope and intercept.

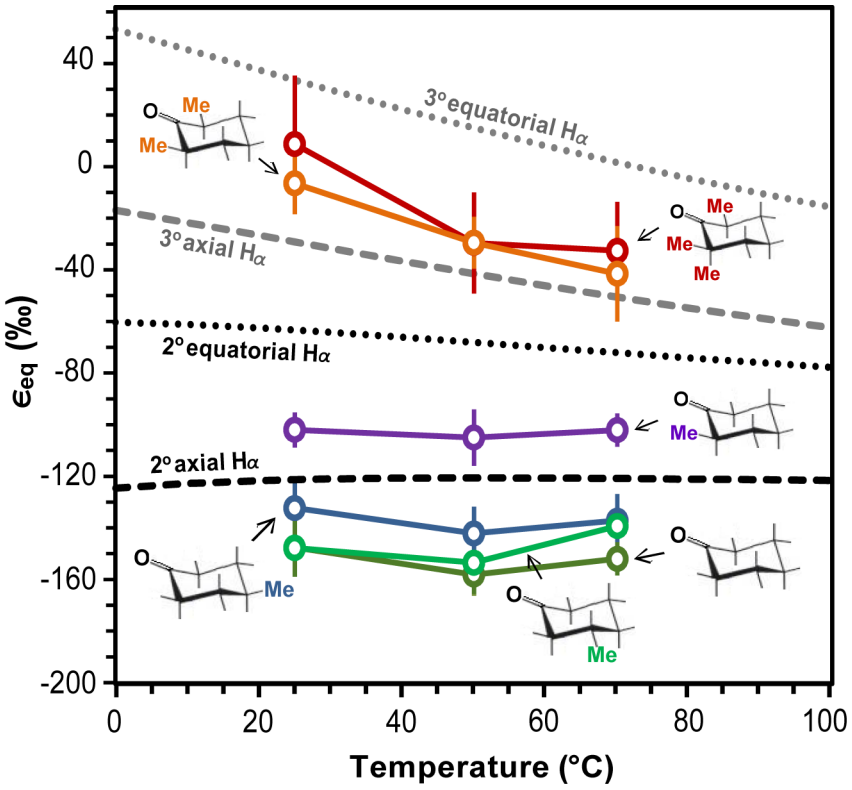

Figure 3-4. Equilibrium isotopic enrichment factors (ε_{eq}) for H_α in cyclic ketones. Symbols represent experimental results measured at 25, 50, and 70°C with error bars of ±1σ. Curves represent theoretical results from 0–100°C for secondary (2°) and tertiary (3°) H_α at the equatorial or axial position in the same molecules.

3.2. Theoretical calculations of equilibrium fractionation factors

3.2.1. Conformational change and ring flip

Optimization of the cyclic ketones generates two types of stable conformations: the chair conformation as the global minimum (optimized geometries in Fig. 3-2) and the twist-boat conformation (optimized geometries in Appendix Fig. 3-A1). To examine the effects of conformational change and ring flip on the value of ε_{eq}, we first calculated Gibbs free energy for both the chair and twist-boat conformations with the methyl group at the equatorial or axial position. The relative abundance of each conformation was then calculated according to the Boltzmann distribution based on the energy variations. Results are summarized in Table 3-3. They show that the chair form predominates for all cyclic ketones with the methyl group strongly biased to the equatorial position, regardless of its distance relative to the carbonyl group. The total effects of other conformations on the values of ε_{eq} were calculated to be less than 1‰ and thus can be safely ignored.

Table 3-3. Conformational Gibbs free energy change (ΔG) for the chair and twist-boat conformations with the methyl group at equatorial (eql.) or axial (axl.) position. ΔG (kJ/mol) is reported as the offset relative to the conformation of the highest energy. Shown in brackets are the relative abundances of individual conformations at 25°C.

Cyclic ketones	Chair		Twisted-boat	
	Eql. methyl	Axl. methyl	Eql. methyl	Axl. methyl
cyclohexanone	-8.8 (97.2%)		0 (2.8%)	
2-methylcyclohexanone	-11.8 (96.7%)	-2.7 (2.5%)	0 (0.8%)	N/A[a]
3-methylcyclohexanone	-16.5 (94.7%)	-9.2 (5.0%)	-1.2 (0.2%)	0 (0.1%)
4-methylcyclohexanone	-25.0 (96.0%)	-16.6 (3.2%)	-13.3 (0.8%)	0 (0%)
cis-2,6- dimethylcyclohexanone	-19.7 (100.0%)	N/A[b]	0 (0%)	N/A[b]
2,2,6-trimethylcyclohexanone	-15.0 (99.0%)	0 (0.2%)	-2.9 (0.7%)	N/A[b]

(a) Optimized geometry converges to the chair form with equatorial methyl group.

(b) Methyl groups at C2 and C6 are unlikely to simultaneously adopt the axial positions.

3.2.2. Theoretical estimates of equilibrium fractionation for H_α

Values of ε_{eq} are calculated as the ratio between the β factor for individual H_α positions and the β factor for liquid water. Results are statistically consistent (σ=3–7‰) for analogous H_α positions in different molecules. Thus the average values for each distinctive H_α position are plotted in Fig. 3-4. Our calculation reveals that at equilibrium a secondary or tertiary axial H_α (H_α^{axl}) would be ^{2}H-depleted by ~60‰ than the corresponding equatorial H_α (H_α^{eql}). This is very likely caused by stereochemistry. In the chair conformation, the C_α–H_α^{eql} is coplanar with the plane containing the C=O double bond, while the C_α–H_α^{axl} bond is at ~71° to this plane, a situation similar to the H's next to C=C bond in alkenes (Chapter 2, Section 3.1.2.). It would likewise facilitate σ-π hyperconjugation between the C_α–H_α^{axl} bond and the π electrons on C=O, which reduces the electron density of the C-H_α^{axl} bond because of the electron-donating effect of alkyl group and the negative inductive effect (−I) of the O atom. Beyond the C_α position, the calculated ε_{eq} values are indistinguishable between equatorial and axial H (see Section 3.2.3.). Besides, the effect of alkyl branches on C_α leads to a ^{2}H-enrichment up to 110‰ for tertiary H_α^{axl} (H_α^{eql}) relative to secondary H_α^{axl} (H_α^{eql}), slightly smaller than the corresponding offsets observed for linear ketones (~130‰ at 25‰).

3.2.3. Theoretical estimates of equilibrium fractionation for non-alpha H

We also calculated the equilibrium fractionation for non-alpha H (i.e., H_β and H_γ) in the six cyclic ketones. For these positions, the ε_{eq} values are indistinguishable between the equatorial and axial H bonded to the same C atom. The average ε_{eq} values for the same position in different cyclic ketones are plotted in Fig. 3-5. Also plotted are the theoretical ε_{eq} values for H in acyclic alkanes for comparison. It is clearly shown that primary H in the methyl group that attached to either acyclic or cyclic structures has completely overlapping ε_{eq} values. This is not surprising because methyl group appears to be a rigid moiety with ε_{eq} values hardly affected by adjacent hydrocarbon structures, even when directly attached to the C=C double bond (Chapter 2, Section 3.1.2.). The ε_{eq} values for secondary and tertiary

H_γ in the cyclic ketones are higher by about 10‰ and 20‰, respectively, than analogous positions in acyclic hydrocarbons. At equilibrium, H_β is further ^{2}H-enriched by10–20‰ than H_γ, a trend also observed in acyclic ketones and probably associated with the field inductive effect of the carbonyl group (Chapter 2, Section 3.1.3.).

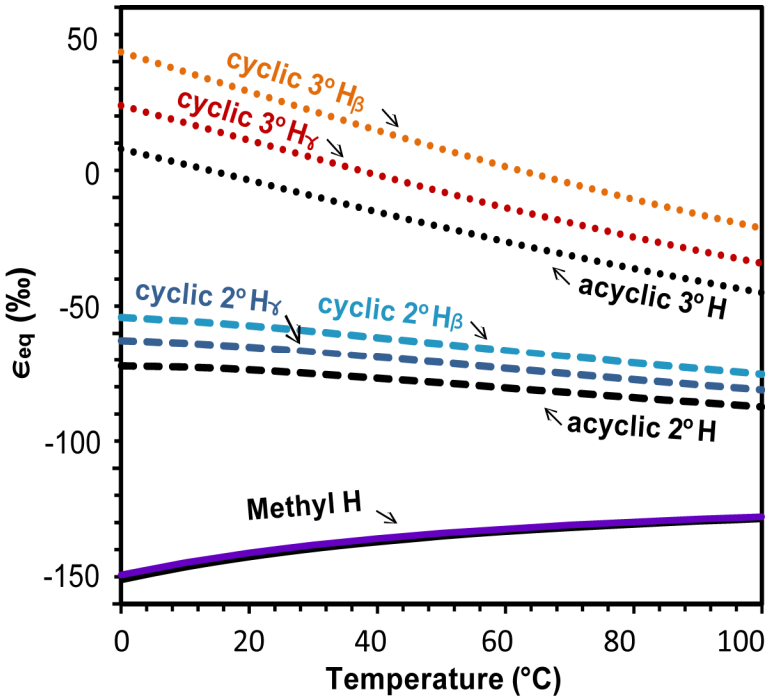

Figure 3-5. Calculated equilibrium isotopic enrichment factors (ε_{eq}) for H_β and H_γ in cyclic ketones. Theoretical ε_{eq} values for H in acyclic alkanes are also plotted for comparison. Note that H in methyl group attached to either cyclic or acyclic structures has the same ε_{eq} values.

Conclusively, theoretical calculation shows that, when free of the effects from functional groups (e.g., the H_γ positions), H in the ring system has slightly higher but generally consistent ε_{eq} values compared to analogous position in acyclic structures. This is reasonable considering that the six-membered ring in the chair conformation is free of ring strain, such that H in cyclohexane and hexane should have similar chemical environments.

3.3. Comparison of Experimental and Theoretical Equilibrium Fractionations

As shown in Fig. 3-4, the molecules containing only tertiary H_α, i.e., 2,6-dimethylcyclohexanone and 2,2,6-trimethylcyclohexanone, have ε_{eq} values close to the calculated tertiary H_α^{axl}. This is consistent with the fact that methyl groups are strongly biased to the equatorial positions (Table 3-3), leaving H_α in the axial positions. However, for the molecules having only secondary H_α, the experimental ε_{eq} values are again close to the calculated H_α^{axl} and significantly lower than H_α^{eql} by 70–90‰. It is counterintuitive, because secondary H_α atoms should be equally distributed between the axial and equatorial positions. This inconsistency for tertiary and secondary H_α in cyclic ketones are fundamentally different from acyclic ketones, where the experimental and calculated results are fairly consistent for all types of H_α. It seems to indicate that the experimental equilibrium for cyclic ketones records the fractionation associated with axial but not equatorial positions. Based on stereochemistry and the mechanism of base-catalyzed H_α substitution, we propose the following mechanism to explain the odd experiment-theory discrepancy for secondary H_α.

H_α substitution in carbonyl compounds proceeds through keto-enol tautomerism (Chapter 1, Appendix 1). Under basic conditions, the replacement of an H atom at the alpha position takes place via deprotonation by the hydroxide ion and then reprotonation by water molecules at the negatively charged C_α in the enolate ion (Fig. 3-6a). We calculated the optimized geometry of the enolate ion for cyclohexanone. The input geometries were deprotonated at either the H_α^{eql} or H_α^{axl} position. They both converged to the same geometry where the carbanion is trigonalized and coplanar with the C=O double bond (Fig. 3-6b), resulting from the resonance between the keto and enol forms of the enolate (Fig. 3-6a). Thus a proton from water should approach the C_α along the direction of the electron lone pair that is vertical to the plain and subsequently form the axial C_α–H_α bond. In fact, this process has been widely accepted to explain the lost of chirality at the C_α position during H_α substitution (Kawabata et al., 1999). As a result, reprotonation on C_α always generates the H_α^{axl} atom, and thus the measured equilibrium fractionation for secondary H_α is actually the value for H_α^{axl}, rather than the average of H_α^{eql} and H_α^{axl}. Moreover, it is

noticeable that the calculated ε_{eq} values for secondary H_{α}^{axl} in cyclic ketones (around −120‰) are almost identical to the calculated values for secondary H_{α} in acyclic ketones, consistent with the fact that they are derived via the same enolate intermediate.

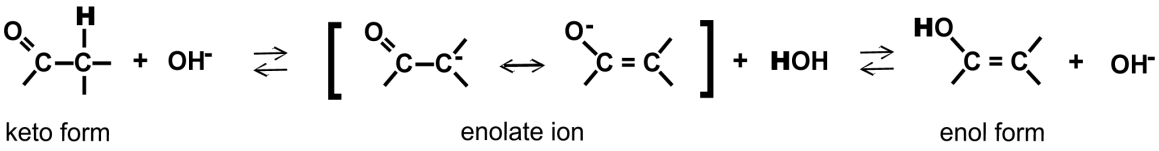

(a) Base catalyzed keto-enol tautomerism

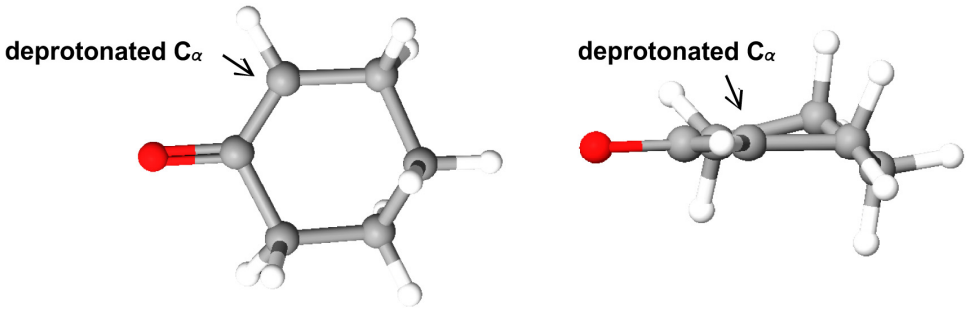

(b) Optimized enolate ion of cyclohexanone, presented in two perspectives

Figure 3-6. (a) Mechanisms of base-catalyzed H_{α} substitution. (b) Optimized geometry for the enolate ion of cyclohexanone, calculated using the B3LYP/6-311G** method

According to this mechanism, molecular equilibrium fractionations should be calculated exclusively using secondary and/or tertiary H_{α}^{axl}. The resultant ε_{eq} values for the six cyclic ketones are plotted versus the experimental results in Fig. 3-7. They give rise to a calibration curve with slope of 1.44±0.05 and intercept of 32.8±5.1. The slope slightly decreases with temperature (1.48±0.08 at 25°C, 1.43±0.10 at 50°C, and 1.39±0.09 at 70°C), similar to acyclic ketones, but the trend is inconclusive considering the relatively large regression errors. Thus the average calibration curve is used in the following section to calculate equilibrium fractionations for biomarker molecules.

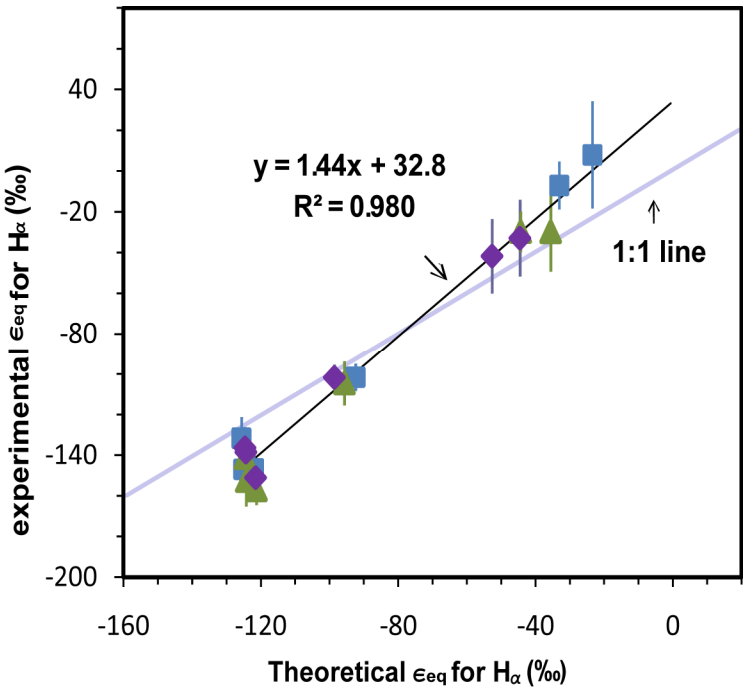

Figure 3-7. Regression between experimental and theoretical enrichment factors (ε_{eq}) for H_α in the six cyclic ketones at 25°C (squares), 50°C (triangles), and 70°C (diamonds). Error bars represent ±1σ in experimental ε_{eq} values. A 1:1 line is shown for reference.

The reason(s) for the difference from the acyclic-ketone calibration curve (slope = 0.914±0.032, intercept = −8.86±3.22) is not known. It is possible that the ring strain introduced by the planar enolate ion has affected the ε_{eq} value of H_α^{axl}, which is not present in acyclic ketones. Another possibility is that in cyclohexanone the aliphatic ring is sterically strained away, making the O atom more accessible to explicit H-bonding with water.

3.4. Application to cyclic biomarker molecules

3.4.1. Estimate of equilibrium fractionation for cyclic biomarker molecules

The most common cyclic biomarkers, steroids, and hopanoids, are polycyclic molecules primarily consisting of six-membered rings, alkyl branches, and, occasionally, five-membered rings. However, our isotope exchange experiments can only be performed on monocyclic ketones, because polycyclic ketones hardly dissolve in water. Considering that the six-membered rings predominately adopt the strain-free chair conformation and the five-membered rings take the envelope conformation where the ring strain is small, it is reasonable to estimate the equilibrium fractionation for polycyclic molecules by assembling individual H positions in monocyclic molecules. This way is much more efficient than directly calculating the large polycyclic molecules. To verify this approach, we calculated the ε_{eq} values for various H positions in 5α-cholestane (the basic sterane formed by reduction of cholesterol, see Fig. 3-8). The calculated ε_{eq} values for secondary and tertiary H in the fused rings are statistically consistent with the calculated values for H_γ in monocyclic ketones; while the calculated ε_{eq} values for H on the alkyl branches (including methyl groups) agree with the results for acyclic alkanes (Chapter 2, Section 3.1.1.). Therefore, the equilibrium fractionation for polycyclic hydrocarbons can be estimated using calculated ε_{eq} values for individual H positions in monocyclic compounds followed by applying the calibration curves, although we cannot rule out the possibility that the calibration for polycyclic compounds might be different from that based on monocyclic molecules. The estimated ε_{eq} values for secondary and tertiary H in cyclic hydrocarbons are plotted in Fig. 3-8. Uncertainties are estimated to be 8–25‰ between 0 and 100°C. They combine the standard deviation in the calibration curve with variations in ε_{eq} for analogous H positions in different molecules (typically 4–9‰).

By summing over relevant cyclic and acyclic H positions, we calculated the molecular equilibrium fractionation for 5α-cholestane (C_{27}) and hopane (C_{30}). Results between 0 and 100°C are −78‰ to −84‰ for 5α-cholestane and −94‰ to −102‰ for hopane (Fig. 3-8). The similarity in the calculated ranges is caused by the complementary ε_{eq} values for primary and tertiary Hs that cancel out in the average. Thus molecular fractionations for homologous steroids and hopanoids that vary slightly in structure are likely to fall in similar ranges. In fact, due to the same reason, the molecular fractionations are relatively insensitive to the calibration. As an example, if we apply the calibration curve for acyclic

ketones, the above ranges will be lowered by 4–8‰ for cholestane and increased by 2–6‰ for hopane, smaller than the estimated uncertainties.

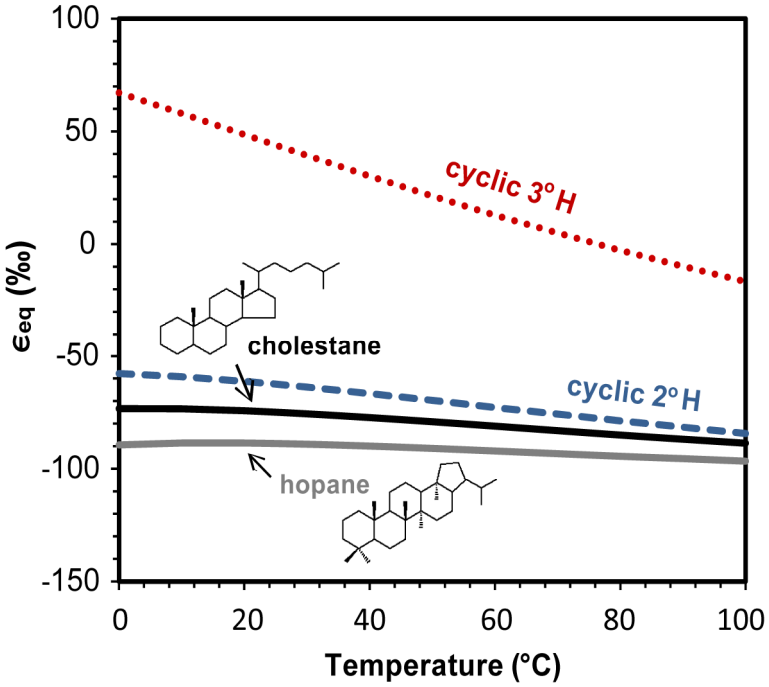

Figure 3-8. Estimated isotopic enrichment factors (ε_{eq}) for secondary (2°) and tertiary (3°) H in cyclic hydrocarbons. Also plotted are the estimated values of molecular fractionation for 5α-cholestane and C_{30} hopane.

3.4.2. Application to organic geochemical studies

The estimated range of equilibrium fractionation for cyclic biomarker molecules is substantially higher than the biosynthetic fractionation for cyclic isoprenoids (−150 to −350‰, Sessions et al., 1999). It is similar to the ranges of equilibrium fractionation for *n*-alkyl lipids (−70 to −90‰) and acyclic isoprenoids (around −100‰), and is also consistent with the field data for thermally mature hydrocarbons (δ^2H values between −80‰ and −110‰ relative to water; Schimmelmann et al., 2006). Therefore, similar to the use of

equilibrium fractionations for acyclic lipids (Chapter 2, Section 3.4.2.), our study of cyclic biomarkers provide an additional tool to evaluate the extent of H exchange in natural samples and constrain the interpretation of δ^2H data for sedimentary organic matter and oils. A good example is demonstrated by Andersen et al. (2001). They documented ~100‰ offsets between δ^2H values of 5α-cholestane and *n*-docosane in a Messinian sapropel, similar to that seen in fresh biomass. Based on our results, this is a clear evidence for the preservation of biosynthetic isotopic composition, because H isotopic exchange would lead to a convergence of δ^2H values in cyclic isoprenoids and *n*-alkyl lipids.

4. CONCLUSIONS

Equilibrium $^2H/^1H$ fractionations (ε_{eq}) between H_α in six cyclic ketones and water were measured at 25, 50, and 70°C via isotope exchange experiments, with uncertainties typically between 5–15‰. The values of ε_{eq} for secondary H_α are in the range of −130‰ to −150‰ with little temperature variation; ε_{eq} values for tertiary H_α are in the range of 10‰ to −40‰ with negative temperature dependence. Equilibrium fractionations were also calculated for the same cyclic ketones in chair and twist-boat conformations using vibrational frequencies from ab initio calculations (B3LYP/6-311G**). The calculated ε_{eq} values for secondary H_α is higher than the experimental results by ~60‰, whereas the experiment-theory discrepancy for tertiary H_α is only ~10‰. Based on stereochemistry and the mechanism of base-catalyzed H_α substitution, we propose that the measured equilibrium fractionation is the value for axial H_α rather than the average of axial and equatorial H_α, because reprotonation on C_α in the enolate intermediate always takes place along the axial direction. According to this mechanism, regression between experimental and theoretical ε_{eq} values produces a calibration curve with slope of 1.44±0.05 and intercept of 32.8±5.1.

Applying this calibration, we estimated the ε_{eq} values for individual H positions in cyclic structures and hereby calculated the molecular fractionations for cyclic biomarkers. The results are in the range of −75 to −100‰ for steroids and hopanoids between 0 to

100°C, similar to *n*-alkyl lipids and acyclic isoprenoids. Thus post-burial H exchange will remove the ~50–100‰ biosynthetic fractionations between cyclic and *n*-alkyl lipids, which can be used to evaluate the extent of H exchange in sedimentary organic matter and oils.

ACKNOWLEDGEMENTS

The authors thank Arndt Schimmelmann for the analysis of ^{2}H-enriched organic standards employed here. This work was supported by the National Science Foundation (NSF) grant #EAR-0645502.

REFERENCES

Andersen N., Paul H. A., Bernasconi S. M., McKenzie J. A., Behrens A., Schaeffer P. and Albrecht P. (2001) Large and rapid climate variability during the Messinian salinity crisis: Evidence from deuterium concentrations of individual biomarkers. *Geology* **29**, 799-802.

Becke A. D. (1993) Density-functional thermochemistry. 3. The role of exact exchange. *J. Chem. Phys.* **98**, 5648-5652.

Bigeleisen J. and Mayer M. G. (1947) Calculation of equilibrium constants for isotopic exchange reactions. *J. Chem. Phys.* **15**, 261-267.

Brocks J. J. and Summons R. E. (2003) Sedimentary hydrocarbons, biomarkers for early life. In: *Treatise in geochemistry*. (D. H. H., Ed.). Elsevier.

Chikaraishi Y. and Naraoka H. (2003) Compound-specific delta D-delta C-13 analyses of n-alkanes extracted from terrestrial and aquatic plants. *Phytochemistry* **63**, 361-371.

Farrimond P., Fox P.A., Innes H.E., Miskin I.P. and Head I.M. (1998). Bacterial sources of hopanoids in recent sediments: improving our understanding of ancient hopane biomarkers. *Ancient Biomol.* **2**, 147-166.

Eisenreich W., Schwarz M., Cartayrade A., Arigoni D., Zenk M. H., and Bacher A. (1998) The deoxyxylulose phosphate pathway of terpenoid biosynthesis in plants and microorganisms. *Chem. Biol.* **5**, R221–R233.

Hartshorn Sr. and Shiner V. J. (1972) Calculation of H/D, c-12/c-13, and c-12/c-14 fractionation factors from valence force fields derived for a series of simple organic-molecules. *J. Am. Chem. Soc*. **94**, 9002-9012.

Horita J. and Wesolowski D. J. (1994) Liquid-vapor fractionation of oxygen and hydrogen isotopes of water from the freezing to the critical-temperature. *Geochim. Cosmochim. Acta* **58**, 3425-3437.

Kawabata T., Yahiro K., and Fuji K. (1991) Memory of chirality — enantioselective alkylation reactions at an asymmetric carbon adjacent to a carbonyl group. *J. Am. Chem. Soc*. **113**, 9694-9696.

Lee C. T., Yang W. T. and Parr R. G. (1988) Development of the colle-salvetti correlation-energy formula into a functional of the electron-density. *Phy. Rev. B*, **37**, 785-789.

Qureshi, N. and Porter, J.W. (1981). Conversion of acetyl-coenzyme A to isopentenyl pyrophosphate. In *Biosynthesis of lsoprenoid Compounds* Vol. 1. (Porter, J.W. & Spurgeon, S.L., eds.). John Wiley, New York, pp. 47-94.

Rohmer M., Bouviernave P., and Ourisson G. (1984) Distribution of hopanoid triterpenes in prokaryotes. *J. Gen. Microbiol.* **130**, 1137-1150.

Sauer P. E., Eglinton T. I., Hayes J. M., Schimmelmann A., and Sessions A. L. (2001) Compound-specific d/h ratios of lipid biomarkers from sediments as a proxy for environmental and climatic conditions. *Geochim. Cosmochim. Acta.* **65**, 213-222.

Schimmelmann A., Sessions A. L. and Mastalerz M. (2006) Hydrogen isotopic composition (D/H) of organic matter during diagenesis and thermal maturation. *Ann. Rev. Earth Planet. Sci.* **34**, 501-533.

Sessions A. L. and Hayes J. M. (2005) Calculation of hydrogen isotopic fractionations in biogeochemical systems. *Geochim. Cosmochim. Acta* **69**, 593-597.

Sessions A. L., Burgoyne T. W., Schimmelmann A. and Hayes J. M. (1999) Fractionation of hydrogen isotopes in lipid biosynthesis. *Org. Geochem.* **30**, 1193-1200.

Sessions A. L. (2001) *Hydrogen isotope ratios of individual organiccompounds.* Ph.D. dissertation, Indiana University.

Stern M. J. and Wolfsberg M. (1966a) On absence of isotope effects in absence of force constant changes. *J. Chem. Phys.* **45**, 2618.

Stern M. J. and Wolfsberg M. (1966) Simplified Procedure for Theoretical Calculation of Isotope Effects Involving Large Molecules. *J. Chem. Phys.* **45**, 4105.

Tannor D. J., Marten B., Murphy R., Friesner R. A., Sitkoff D., Nicholls A., Ringnalda M., Goddard W. A. and Honig B. (1994) Accurate first principles calculation of molecular charge-distributions and solvation energies from ab-initio quantum-mechanics and continuum dielectric theory. *J. Am. Chem. Soc*. **116**, 11875-11882.

Urey H. C. (1947) The thermodynamic properties of isotopic substances. *J. Chem. Soc*. MAY, 562-581.

Volkman J. K. (2003) Sterols in microorganisms. *Appl. Microbiol. Biotechnol.* **60**, 495-506.

Zhang Z. and Sachs J. P. (2007) Hydrogen isotope fractionation in freshwater algae: I. Variations among lipids and species. *Org. Geochem.* **38**, 582-608.

APPENDIX

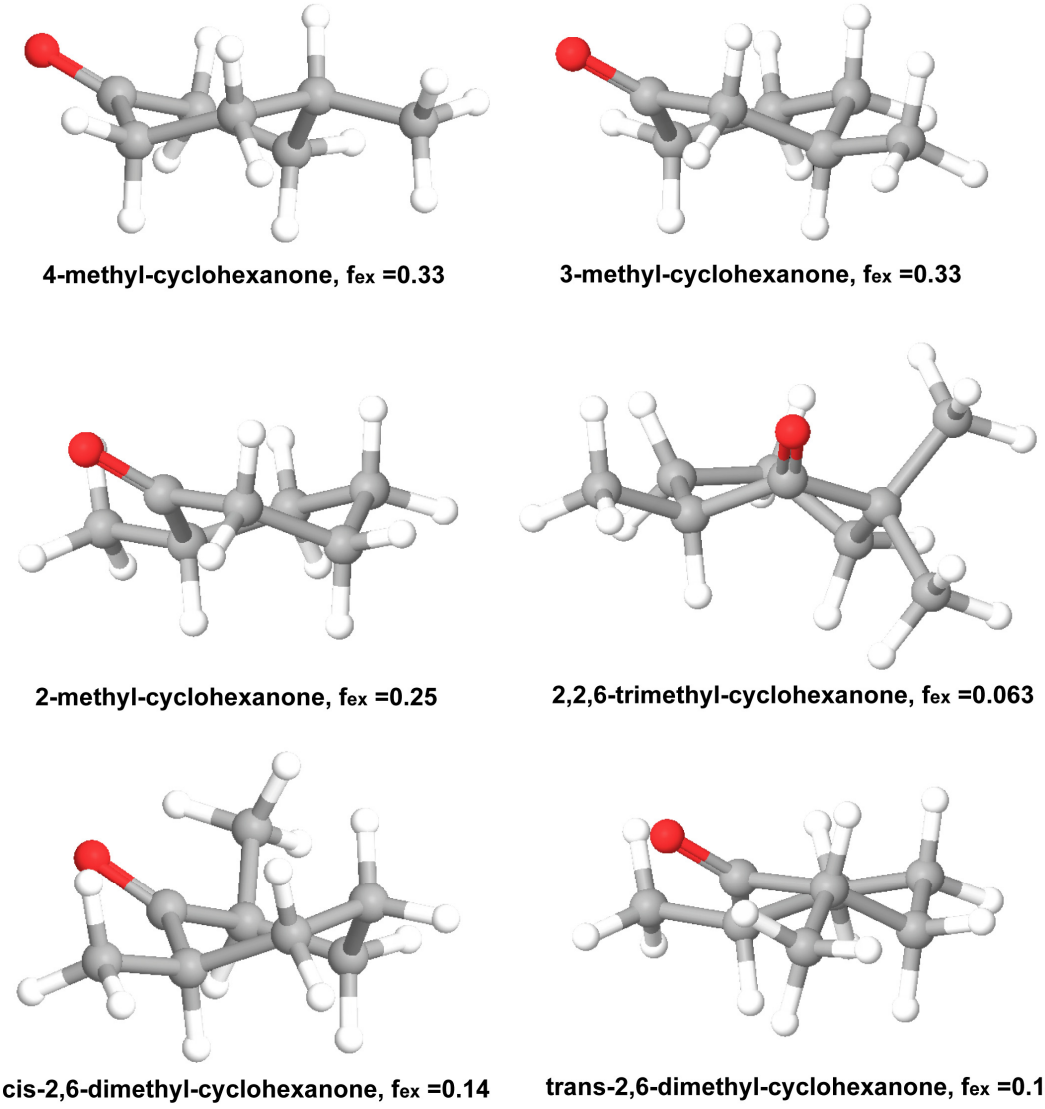

Figure 3-A1. Optimized geometries of the substrate ketone molecules (● = O, ● = C, ○ = H) in the twisted-boat conformation (see 3.2.1.). f_{ex} is the fraction of exchangeable H in each molecule, assumed to be exclusively H_{α}. Note that 2,6-dimethyl-cyclochexanone is a mixture of the cis- and trans- isomers, but only the cis-isomer is investigated in this study.

Table 3-A1. Measured hydrogen isotopic compositions of each cyclic ketone substrate (δ^2H_K) and the corresponding water (δ^2H_W) at equilibrium[a]

ketone	δ^2H (‰)	1	2	3	4	5	6	7	8
2-Methyl-cyclohexanone	δ^2H_W	473.8	362.1	264.0	150.9	43.2	-63.2	-172.6	-279.7
	25°C δ^2H_K	-71.5	-96.2	-120.0	-144.5	-167.3	-192.1	-218.7	-239.6
	50°C δ^2H_K	-71.0	-98.2	-122.7	-145.6	-168.7	-190.8	-216.2	-243.0
	70°C δ^2H_K	-73.5	-97.5	-120.0	-147.8	-169.3	-193.3	-219.4	-241.6
3-Methyl-cyclohexanone	δ^2H_W	474.4	364.1	262.2	145.3	43.7	-66.4	-168.4	-283.3
	25°C δ^2H_K	-70.2	-102.8	-132.6	-163.3	-191.8	-224.6	-252.4	-287.2
	50°C δ^2H_K	-70.2	-104.7	-136.8	-165.2	-195.4	-228.1	-257.1	-282.9
	70°C δ^2H_K	-72.1	-104.1	-131.0	-168.1	-197.3	-225.4	-259.4	-287.6
4-Methyl-cyclohexanone	δ^2H_W	472.9	363.7	263.5	150.4	47.9	-64.1	-166.8	-286.2
	25°C δ^2H_K	26.0	-0.2	-33.2	-63.4	-97.8	-128.5	-158.2	-189.4
	50°C δ^2H_K	29.8	-6.1	-36.8	-65.1	-93.6	-128.5	-157.6	-188.4
	70°C δ^2H_K	28.6	1.4	-31.5	-63.0	-91.9	-125.1	-157.8	-185.4
2,6-Dimethyl-cyclohexanone	δ^2H_W	474.1	367.7	260.5	156.4	51.0	-59.7	-165	-285.6
	25°C δ^2H_K	53.3	40.7	25.2	8.8	-5.7	-19.8	-37.4	-52.8
	50°C δ^2H_K	45.6	32.3	15.2	1.8	-12.2	-26.9	-41.8	-60.4
	70°C δ^2H_K	44.5	28.3	17.4	3.8	-14.3	-30.2	-43.3	-58.2
2,2,6-Trimethyl-cyclohexanone	δ^2H_W	472.7	366.5	264.1	150.9	44.4	-59.9	-174.2	-281.7
	25°C δ^2H_K	-67.7	-73.0	-81.2	-88.2	-92.8	-100.6	-109.8	-114.0
	50°C δ^2H_K	-70.1	-74.8	-81.5	-89.0	-95.2	-101.6	-107.2	-116.0
	70°C δ^2H_K	-68.7	-76.6	-83.2	-88.9	-95.9	-100.7	-109.4	-114.9
Cyclohexanone	δ^2H_W	469.0	368.2	265.1	153.8	43.8	-56.1	-162.2	-279.6
	25°C δ^2H_K	-13.9	-49.7	-90.0	-126.2	-158.5	-199.3	-231.5	-269.5
	50°C δ^2H_K	-19.3	-55.0	-88.0	-126.3	-162.1	-198.8	-235.6	-269.1
	70°C δ^2H_K	-20.2	-50.0	-89.4	-125.8	-162.2	-199.1	-232.5	-272.1

(a) The standard deviations from 2–3 replicates of each ketone sample and from 3–4 replicates of each water sample are shown in brackets.

Table 3-A2. Calculated β factors from 0°C to 100°C for H_α in cyclic ketones

T	2-Methyl-cyclohexanone			3-Methyl-cyclohexanone		4-Methyl-cyclohexanone		*Cis*-2,6-Dimethyl-cyclohexanone	2,2,6-Trimethyl-cyclohexanone
(°C)	$2°H_\alpha^{eql}$	$2°H_\alpha^{axl}$	$3°H_\alpha^{axl}$	$2°\ H_\alpha^{eql}$	$2°\ H_\alpha^{axl}$	$2°H_\alpha^{eql}$	$2°H_\alpha^{axl}$	$3°\ H_\alpha^{axl}$	$3°\ H_\alpha^{axl}$
0	18.303	16.970	18.692	18.159	16.818	18.159	16.804	18.875	19.082
10	16.050	14.928	16.349	15.928	14.798	15.928	14.787	16.502	16.676
20	14.206	13.252	14.436	14.101	13.140	14.103	13.132	14.566	14.713
25	13.408	12.525	13.610	13.311	12.421	13.312	12.414	13.730	13.866
30	12.680	11.861	12.858	12.590	11.764	12.591	11.758	12.969	13.095
40	11.404	10.695	11.541	11.326	10.611	11.327	10.605	11.637	11.746
50	10.328	9.709	10.433	10.259	9.635	10.261	9.631	10.516	10.611
60	9.412	8.868	9.491	9.351	8.802	9.353	8.799	9.564	9.648
70	8.626	8.145	8.686	8.573	8.087	8.574	8.084	8.750	8.824
80	7.948	7.520	7.991	7.900	7.467	7.902	7.465	8.049	8.114
90	7.358	6.975	7.389	7.315	6.927	7.317	6.926	7.440	7.498
100	6.842	6.497	6.862	6.803	6.454	6.805	6.454	6.908	6.961

(a) Listed β factors are for the chair conformations with methyl group(s) at equatorial position(s).

(b) 1° = primary, 2° = secondary, 3° = tertiary

(c) Superscript "eql" or "axl" denotes the equatorial or axial H_α.

C h a p t e r 4

MEMORY EFFECTS IN COMPOUND-SPECIFIC $^{2}H/^{1}H$ ANALYSIS BY GAS CHROMATOGRAPHY/PYROLYSIS/ISOTOPE-RATIO MASS SPECTROMETRY

Ying Wang and Alex L. Sessions

Division of Geological and Planetary Sciences,
California Institute of Technology, Pasadena, CA, USA

(Published in *Analytical Chemistry*, 2008, 80 (23), 9162–9170)

ABSTRACT

Compound-specific analyses of lipid $^{2}H/^{1}H$ ratios often encounter ranges of 300‰ or more, and experiments using ^{2}H-enriched water to study fractionations often extend the range up to 1000‰. Here we show that for such large dynamic ranges in $^{2}H/^{1}H$ ratio, isotopic ”memory” between adjacent peaks can be significant. Memory effects have not been previous reported for GC/P/IRMS systems, but can have a significant impact on many measurements, even those exploring only natural-abundance variations in $^{2}H/^{1}H$. To quantitatively evaluate these effects, we synthesized two series of organic standards with $\delta^{2}H$ values varying from -230 to +800‰. We then analyzed chromatograms in which analyte $\delta^{2}H$ values, retention times, or relative abundances were independently varied. For two sequential GC peaks, isotopic memory is measured to be typically 2–4% of the difference in $\delta^{2}H$ values between the two. Roughly half of this effect can be attributed to unknown processes within the GC itself, and the other half to surface adsorption processes in the pyrolytic conversion of analytes to H_2. Isotopic memory increases with decreasing time separation between peaks, with decreasing analyte abundance, and with increasing age of pyrolysis reactors. A simple numerical model that simulates dynamic adsorption of H_2 on pyrolytic carbon can reproduce many aspects of the experimental data, suggesting that this is likely to be an important mechanism in isotopic memory. Several steps to mitigate memory effects in routine analyses are suggested.

1. INTRODUCTION

Gas chromatography coupled to isotope-ratio mass spectrometry via a pyrolysis interface (GC/P/IRMS; also 'thermal conversion', GC/TC/IRMS) provides a convenient analytical route to high-precision analysis of the hydrogen-isotopic composition ($^2H/^1H$, or $^2H/^1H$) of individual organic compounds (Begley and Scrimgeour, 1997; Tobias and Brenna, 1997; Burgoyne and Hayes, 1998; Hilkert et al., 1999; Sessions, 2006). Over the past decade the methodology has been rapidly adopted in geochemistry (Xiong et al., 2005), environmental chemistry (Sauer et al., 2001), biochemistry (Chikaraishi et al., 2004), and the petroleum and food/flavor industries (Hor et al., 2001a; Hor et al., 2001b; Li et al., 2001). In contrast to ^{13}C, whose natural abundance typically varies over ~50‰, the natural abundance of ^2H in organic materials often ranges over 300‰ or more (Sessions and Hayes, 2005). Moreover, studies using ^2H-enriched tracers or water often extend this range to beyond 1000‰. This large range, coupled with the tendency of many materials to absorb and/or adsorb H_2, make compound-specific $^2H/^1H$ analyses particularly susceptible to memory effects. We use the term 'memory' here to indicate any situation in which the isotopic composition of a given chromatographic peak affects that of the following peak (or peaks), regardless of mechanism.

Isotopic memory effects are well known during the conversion of H_2O to H_2 in vacuum lines using metal reductants, especially uranium (Bigeleisen et al., 1952). Such effects are generally due to the absorption of hydrogen by hot metals, and are typically overcome by repeated injections of each sample until a stable δ^2H value is reached. Memory effects have also been reported for the pyrolysis of water over metal catalysts in continuous-flow analyses. Using an alumina pyrolysis reactor packed with C-coated Ni and operated at 1050°C, Begley and Scrimgeour (1997) showed that memory for successive injections of water amounted to ~1.6% of the difference in isotope ratios between the injections (~2600‰ for δ^2H and ~150‰ for $\delta^{18}O$). In a similar system using reduced Cr in the pyrolysis reactor, Morrison et al. (2001) reported ~1% memory between successive injections of water differing in δ^2H values by up to 1500‰. In an early GC/P/IRMS system with a pyrolysis reactor containing no metal catalyst and operated at 1200°C, Scrimgeour et al. (1999) tested for isotopic memory by alternately measuring *n*-alkane and fatty acid

peaks that differed in δ^2H values by 200‰. They concluded that no memory effects were observable above analytical precision (~5‰). A similar conclusion was reached by Sessions et al. (2001a) using a series of *n*-alkanes with δ^2H values ranging from −256‰ to −42‰.

In both of these latter cases, memory effects of 1-2% would be very hard — if not impossible — to observe given typical analytical precision for δ^2H values of 2–4‰. It thus remains uncertain if such effects exist in compound-specific $^2H/^1H$ analyses. Although likely small, they are nevertheless potentially very significant. As a concrete example, in one study microorganisms are grown in waters with δ^2H values ranging from near 0‰ up to 500‰ or higher (Zhang and Sachs, 2007). The fractionation factor associated with lipid biosynthesis is then derived from the slope of a regression of lipid δ^2H values on water δ^2H values. A memory effect of 2% in the system used to analyze lipids from these samples would lead to a systematic bias of 20‰ in the estimated fractionation factor.

In the study described here, we synthesized multiple lipid standards with δ^2H values varying by up to 1000‰, allowing us to demonstrate conclusively that isotopic memory effects do exist for GC/P/IRMS systems. These memory effects are typically 2–3% of the difference in δ^2H values between successive peaks, can reach ~5% for an aging pyrolysis reactor, and would result in significant errors for many types of natural samples if not accounted for. Mechanisms responsible for the memory effects are explored, and we present a model of hydrogen adsorption on graphite that can reproduce many aspects of the experimental observations. The results suggest several ways in which memory effects can be quantified and/or minimized in routine analytical operations.

2. METHODS

2.1. Materials

Tests utilized three types of materials for isotopic analyses: synthetic fatty acid esters, CH_4 (C.P. grade), and H_2 (ultra high purity). Fatty acid esters were prepared as follows. ^2H-

labeled ethyl palmitate (EP) and *n*-propyl palmitate (PP) were synthesized by reacting hexadecanoic acid (2,2-d_2, 98%; C/D/N ISOTOPES) with a mixture of the appropriate anhydrous alcohol and acetyl chloride (20:1) at 100ºC for 25 min. After cooling to room temperature, each ester was extracted in hexane, purified over silica gel, and the purity was checked by GC/MS. Each ^{2}H-labeled ester was then mixed quantitatively with a stock solution of the same unlabeled ester (Sigma-Aldrich) in varying ratios to yield 6 standards each for EP and PP with δ^2H values ranging between -230 and +800‰. Different combinations and amounts of the two esters were then further mixed and diluted to produce the sample solutions analyzed by GC/P/IRMS.

Values of δ^2H for CH_4 and H_2 reference gases were determined using the GC/P/IRMS system by comparison to a series of *n*-alkanes with known δ^2H values (Sessions et al., 2001a). Importantly, the δ^2H values of the *n*-alkanes — determined independently by offline combustion/reduction — and CH_4 and H_2 gases are similar, such that memory effects will have little influence on the measurements. The approximate δ^2H values of synthetic esters were then measured relative to the CH_4 reference gas. Because they differ considerably in ^{2}H/^{1}H ratio they are, of course, subject to the same memory affects that we are attempting to measure. There are no certified isotopic standards (organic, water, or otherwise) with δ^2H values above 0‰, so our measurements of δ^2H values for these ^{2}H-enriched materials are highly precise but of unknown accuracy. To avoid this complication, all of our tests focused on apparent changes in measured δ^2H values, independent of the "true" δ^2H values for these standards.

2.2. Isotopic Analyses

Compound-specific ^{2}H/^{1}H analyses were performed on a ThermoElectron Trace GC coupled to a Delta^{plus}XP IRMS via a ThermoElectron Thermal Conversion interface, consisting of an Al_2O_3 pyrolysis tube (0.8 mm I.D. and 305 mm long) operated at 1440ºC and an open split. No Nafion drier was employed. The GC was equipped with a programmable temperature vaporization (PTV) injector operated at a split ratio of 1:10,

with a 2.0 mm I.D. metal liner (Siltek deactivated) packed with ~ 7 cm of silanized glass wool. An EC-1 analytical column (30 m long, 0.32 mm I.D., 1.0 μm stationary phase; Alltech Associates, IL) was used with helium carrier gas at 1.4 mL/min. The GC oven temperature was 100°C for 3 min, 20°C/min to 180°C, then 5°C/min to 280°C for all analyses. All connections within the GC and pyrolysis interface were made with methyl-deactivated fused silica tubing (SGE), and stainless steel fittings (Valco Instruments)

To provide peaks of an organic reference gas in sample chromatograms, CH_4 (δ^2H = −148‰) or H_2 (δ^2H = −171‰) reference gas was diluted into a stream of helium which then filled a 20 μL sample loop on a 6-port sampling valve (Valco Instruments). This valve was used to deliver discrete peaks of the reference gas into the GC system at a point immediately downstream from the analytical column (Fig. 4-1). Peak heights were varied by changing dilution of the sample gas. Peak widths are approximately the same as for GC analyte peaks. This approach allowed us to insert peaks of known size and isotopic composition at any point in the chromatogram, such that they are still subject to pyrolytic conversion. In addition, another H_2 reference gas (δ^2H = -150‰) was diluted into a second helium gas stream and flowed directly into the IRMS ion source (Fig. 4-1) using the stock ThermoFinnigan GC II/III interface. These peaks, which are also variable in size and timing, do not experience any of the potential memory effects associated with the GC and pyrolysis systems.

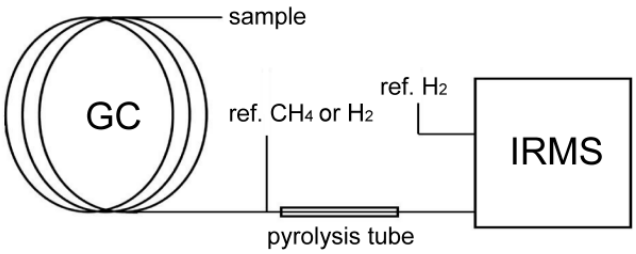

Figure 4-1. Simplified instrument schematic showing the pathways for delivery of sample, CH_4, and H_2 to the IRMS

Mass-2 and -3 signals were processed using ISODAT NT 2.5 software (ThermoElectron), and data are reported as δ^2H values relative to VSMOW in permil units. To correct for H_3^+ interference (Sessions et al., 2001a; Sessions et al., 2001b), the H_3^+

factor was determined daily by measuring the mass 3/2 signal ratio of 10 injections of H_2 reference gas at varying peak height. The value of the H_3^+ factor was very stable at 2.9–3.2 ppm/mV, and all H_3^+ corrections were performed via the ISODAT software. To minimize variations in δ^2H values due to changing background conditions between GC runs, the following protocol was used for all sample analyses. Each chromatogram consisted of four peaks of CH_4 reference gas, followed at a 100 s interval by the analytes to be measured. A second series of two CH_4 peaks followed those of the analytes. All peak sizes were kept constant at 16 ± 2 Vs for CH_4 and 20 ± 2 Vs for the esters (expressed as the integrated mass-2 peak area), except where noted below. The final CH_4 peak from the first set — before the esters — was used as the calibration peak for all experiments with an assigned value of -148‰.

2.3. Raman spectroscopy

Thin layers of carbonaceous material were obtained from the inner wall of used pyrolysis tubes. Raman spectroscopy of this material was performed using a Renishaw RM1000 Micro-Raman Spectrometer, operating with a 514.5 nm Ar ion laser with spectral resolution of 1 cm^{-1}. An optical microscope was used to focus the excitation laser beam on a sample area of 20 μm in diameter. Acquisition time was 30 s and 10 spectra were recorded for each sample.

2.4. Numerical model

To quantitatively explore the effect of hydrogen adsorption in the pyrolysis reactor on memory effects, we developed a simple numerical model to simulate the flow of analyte peaks through a pyrolysis reactor. The key feature of this model is explicit treatment of hydrogen adsorption on graphite lining the reactor. Gas residence times within a hot pyrolysis reactor are much shorter than typical analyte peak widths, and the thermal decomposition of analytes to H_2 is in turn faster than gas residence time. The input flow to

the reactor was therefore simulated as a sequence of discrete H_2 gas parcels, with no concentration or isotopic gradient within the reactor. The concentrations and $^2H/^1H$ ratios of gas parcels in the input stream are varied sequentially to simulate chromatographic peaks. H_2 in the input stream is allowed to interact with adsorption sites evenly coated on the inner wall of the pyrolysis reactor during its transit. The concentration and $^2H/^1H$ ratio of H_2 gas exiting the reactor are calculated and recorded as the output "signal" (see Appendix for details of the model and algorithm). Model output is then used to calculate δ^2H values, as described by Ricci et al. (1994) and Sessions (2006).

Parameters required by the model include: (i) the number of adsorption sites lining the reactor tube, which is estimated as the product of available carbonaceous material (typically 0.8–1.0 mg) in used pyrolysis tubes and the concentration of strong (~20 appm) or weak (~200 appm) adsorption sites in pyrolytic carbon (Kanashenko et al., 1996); (ii) desorption rate constant for hydrogen adsorbed to these sites, estimated to be ~1.1 s^{-1} based on the relevant C-H bond dissociation energy (see Theory and Model section); (iii) the average concentration of H_2 in a typical chromatographic peak, which is estimated as ~ 890 Pa using typical carrier gas flow rate, dimensions and temperature of the reactor tube, peak shape (assumed to be Gaussian with σ = 5s), and the amount of injected analyte (50 nmol H_2); and (iv) the concentration and $^2H/^1H$ ratio of background hydrogen in the carrier gas. This last quantity is impossible to measure directly because of isobaric interferences from $^4He^{2+}$ and $^3He^+$. Based on experimental data, we estimated the hydrogen background to be ~20 pA (20 mV measured signal) with a δ^2H value between −200 and −300‰. An average δ^2H value of −250‰ is adopted for background hydrogen in the model.

3. EXPERIMENTAL SECTION

Memory effects were investigated experimentally by analyzing multiple combinations of fatty acid esters, CH_4 reference gas, and/or H_2 reference gas. Each analysis (i.e., a single GC/P/IRMS chromatogram containing multiple peaks) contained the same analytes, typically 2 esters plus multiple reference gas peaks. The abundance and δ^2H values of

esters in any given chromatogram were manipulated by altering the composition of the solution injected into the GC. The timing of CH_4 and H_2 reference gas peaks relative to these esters was manipulated in each chromatogram directly via the ISODAT software. Multiple chromatograms were then analyzed in series that were arranged such that individual chromatograms differed systematically in either (*i*) δ^2H values, (*ii*) retention times, or (*iii*) relative abundances. A single "experiment" (as defined in Table 4-1) consisted of one such series of multiple chromatograms.

Table 4-1. Summary of experimental conditions.

Exp.	n[a]	Peak 1		Peak 2		Δt (s)[c]	A_2/A_1[d]
		ID[b]	δ^2H (‰)	ID[b]	δ^2H (‰)		
A	6	EP	-225 to +730	PP	-204	100	1.0
B	6	EP	-225 to +730	CH_4	-148	100	0.8
C[e]	5	EP	-225 to +730	CH_4	-148	100	0.8
D	6	EP	-225 to +730	H_2	-171	100	0.8
E	8	EP	639	CH_4	-148	100 – 800	0.8
F	5	CH_4	-148	EP	639	100 – 500	1.2
G	8	CH_4	-148	EP	672	100	0.22-2.23
H	5	EP	-238 to 526	PP	179	100	0.67
I	6	EP	-238 to 742	PP	179	100	1.24
J	6	EP	-238 to 742	PP	179	100	1.90

(a) Number of different chromatograms analyzed in the experiment

(b) EP = ethyl palmitate; PP = *n*-propyl palmitate

(c) Time separation between peaks 1 and 2

(d) Abundance ratio for peaks 1 and 2, defined by mass-2 peak area

(e) H_2 peak added midway between peaks 1 and 2

Because accurate δ^2H values for the ^2H-enriched esters could not be readily determined, we instead looked for correlations between the measured δ^2H values of peaks and the systematic differences between chromatograms. Those correlations allow us to quantitatively document the existence of memory effects, their functional dependence on different operating parameters, and their likely source(s) within the analytical system. Experimental results are summarized first, followed by a discussion of probable mechanisms leading to the observed effects.

3.1. Variations in $^2H/^1H$ ratios

Two initial experiments were conducted to look for memory effects, each consisting of 6 chromatograms. In the first experiment (A in Table 4-1), each chromatogram contained ethyl palmitate (EP) and propyl palmitate (PP) at equal concentrations and constant time separation. The δ^2H values of peak 1 (EP) varied between chromatograms, while that of peak 2 (PP) was held constant. Measured δ^2H values for peak 2 were found to vary systematically with those of peak 1, with a correlation slope of 0.046 and R^2 value of 0.99 (Fig. 4-2). In the second experiment (B), peak 2 consisted of CH_4 reference gas instead of PP. Again, the measured δ^2H values for peak 2 varied systematically with those for peak 1, although this time with a lower correlation slope (0.011; Fig. 4-2). Both results clearly demonstrate the existence of an isotopic memory effect.

In these experiments, the slope of the correlation line is a quantitative measure of how much the isotopic composition of one peak affects that of the next peak. It thus serves as a convenient metric for the size of the memory effect, which we denote as M ($= \Delta\delta_2/\Delta\delta_1$). It is also conceptually equivalent to the fraction of H_2 from one peak that is carried over to the next peak, though that need not be the physical mechanism by which memory exerts its influence. The value of M depends strongly on the specific test conditions used to determine it, including choice of compounds, time separation, peak size, and potentially instrument conditions. When these parameters are held constant, such as by using the EP +

PP or EP + CH_4 test series, the values of M could be used for quantitative comparison of memory effects over time or between analytical systems.

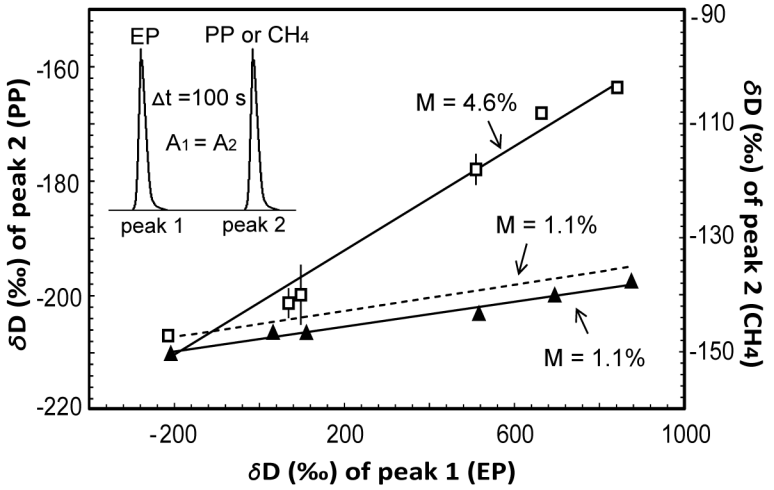

Figure 4-2. Demonstration of isotopic memory between two peaks of differing δ^2H values. Specific test conditions are illustrated by the inset chromatograph, and are summarized in Table 4-1. □, exp. A, (EP + PP); ▲, exp. B, (EP + CH_4). Standard deviations from 2–3 replicates are shown on measured data points, and are usually smaller than the symbols. M is the slope of the correlation and indicates the size of the observed memory effect. Dashed line is the modeled memory effect using conditions of exp. B (shifted upwards from exp. B data for clarity), as discussed in the Theory and Model section.

The value of M was found to be systematically higher in experiments employing EP + PP compared to those using EP + CH_4 (Table 4-2). The only substantive difference between the experiments was that CH_4 peaks did not go through the GC injector or column, while PP peaks did. We thus infer that part of the memory effect is localized within one or both of those components. The magnitude of M attributable to the GC is estimated to be 0.5–3.5%. To further pinpoint other sources of memory, a third experiment (C) introduced peaks of H_2 reference gas midway between peaks 1 and 2, with all other conditions identical to exp. B. The measured values of M were identical both with and without H_2 peaks (data not shown), indicating that these H_2 peaks did not contribute to isotopic memory. We conclude that the IRMS itself does not cause any detectable memory, consistent with previous investigations using dual-inlet techniques (Bigeleisen et al., 1952).

The remaining memory effect (1.1–3.7%) must then be attributed to the pyrolysis reactor itself. Indeed, the value of M is roughly correlated with the age of pyrolysis reactor tubes (Table 4-2), consistent with the expectation that memory increases as pyrolytic carbon accumulates in the reactor tube. In a fourth experiment (D), peak 2 consisted of H_2 reference gas (δ^2H = -171‰) inserted using the same peak generator as for CH_4 (Fig. 4-1). In this experiment, the value of M was measured to be about two times larger than that measured in the EP + CH_4 test during the same period of the reactor (Table 4-2). This result suggests that some sources or sites of isotopic memory are accessible to H_2 but not to CH_4 (see Theory and Model Section).

Table 4-2. Summary of memory effects measured between adjacent pairs of peaks with differing δ^2H values.

EP+PP tests		**EP+CH_4 tests**		**EP+H_2 test**		**Tube age[b]**
M (%)	**σ_M[a]**	**M (%)**	**σ_M[a]**	**M (%)**	**σ_M[a]**	
3.1	0.1	1.2	0.1	N/A		10-50
N/A		0.80	0.05	2.1	0.1	40-70
1.6	0.2	1.1	0.1	N/A		20-90
4.7	0.2	1.2	0.1	N/A		150-220
4.6	0.7	3.7	0.2	N/A		250-340

(a) Standard error of the regression slope at 95% confidence level

(b) Cumulative number of analyses using that reactor tube

3.2. Variation in time separation

The dependence of memory effects on the time separation (Δt) between two peaks was investigated in two further experiments. In exp. E, each chromatogram contained ^2H-enriched EP (peak 1; 639‰) followed by CH_4 (peak 2; -148‰) with Δt varying between 100–800 s. As Δt increased, the measured δ^2H value of peak 2 decreased systematically

toward the "true" value (Fig. 4-3a). The data are consistent with a simple decrease in memory as the time separation between peaks increases.

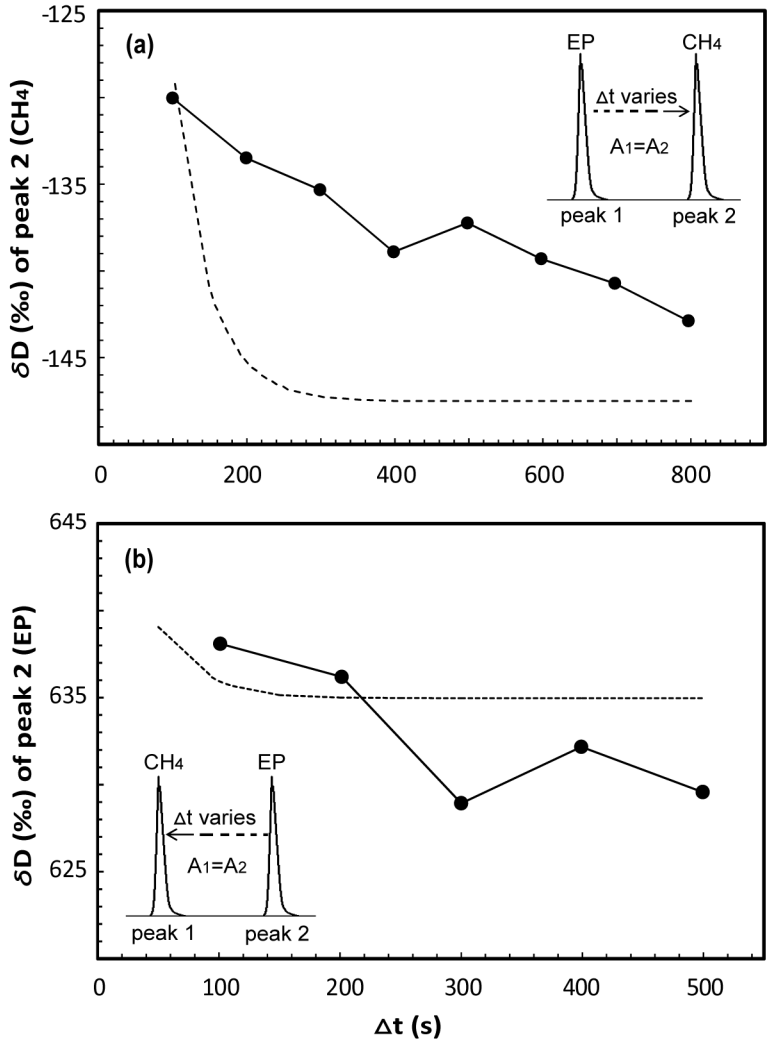

Figure 4-3. Dependence of isotopic memory on the time separation between adjacent peaks. (a) exp. E (EP + CH_4); (b) exp. F (CH_4 + EP). Symbols are experimental data, dashed lines are model results.

However, as a further test the order of these two peaks was reversed (exp. F), with CH_4 (peak 1) appearing 100–500 s before EP (peak 2). Surprisingly, as Δt increased the measured δ^2H value of peak 2 decreased, just as before (Fig. 4-3b). A plausible explanation is that there is second component of isotopic memory, namely background hydrogen in the helium carrier gas. The source of this background could be any species that yields H_2 on pyrolysis, including H_2O. As Δt between peaks increases, the isotopic composition of

background hydrogen should exert a progressively greater influence on whatever pool of stored H is causing the memory effects. Thus if background hydrogen is more ^{2}H-depleted than peak 1, then the δ^2H value of peak 2 will appear to decrease with increasing Δt, consistent with data of both exp. E and F. This idea is explored further in the Theory and Model section.

3.3. Variation in relative abundance

The effect of analyte abundance on memory was investigated in exp. G. Each chromatogram in the series contained CH_4 reference gas (peak 1; -148‰) followed by ^{2}H-enriched EP (peak 2; 672‰), with EP present in gradually increasing amounts. In Fig. 4-4a, measured δ^2H values for peak 2 are plotted against its abundance relative to peak 1, expressed as the ratio of peak areas (A_2/A_1). As the abundance ratio increases from 0.22 to 2.23, measured δ^2H values of peak 2 systematically increased from 583‰ to 712‰ and tended toward a constant value at still higher ratios. These results are consistent with a decrease in memory with increasing analyte abundance.

Three further experiments (H, I, J) employed EP (peak 1) with variable δ^2H values, followed by ^{2}H-enriched PP (peak 2) with δ^2H value fixed at 179‰. These experiments are identical to exp. A, except that the A_2/A_1 ratio was 0.67, 1.24, and 1.90 in exp. H, I, and J, respectively (Table 4-1). Values of M were calculated as before. As the A_2/A_1 ratio tripled, the value of M decreased from 3.4% to 2.1% (Fig. 4-4b), consistent with exp. G. However, if memory effects manifested in peak 2 were solely due to hydrogen contained in peak 1, there should be no observable memory when the δ^2H values of the two peaks are equal. Thus the three curves in Fig. 4-4b would be expected to intersect at a δ^2H value near 179‰. This is clearly not the case, and the participation of background hydrogen in the memory phenomenon offers a potential explanation. If background hydrogen is always ^{2}H-depleted relative to peak 1, its presence will tend to shift the measured δ^2H values for peak 2 downward. This effect will be more pronounced when peak 2 is smaller, leading to the position of the three curves in Fig. 4-4b.

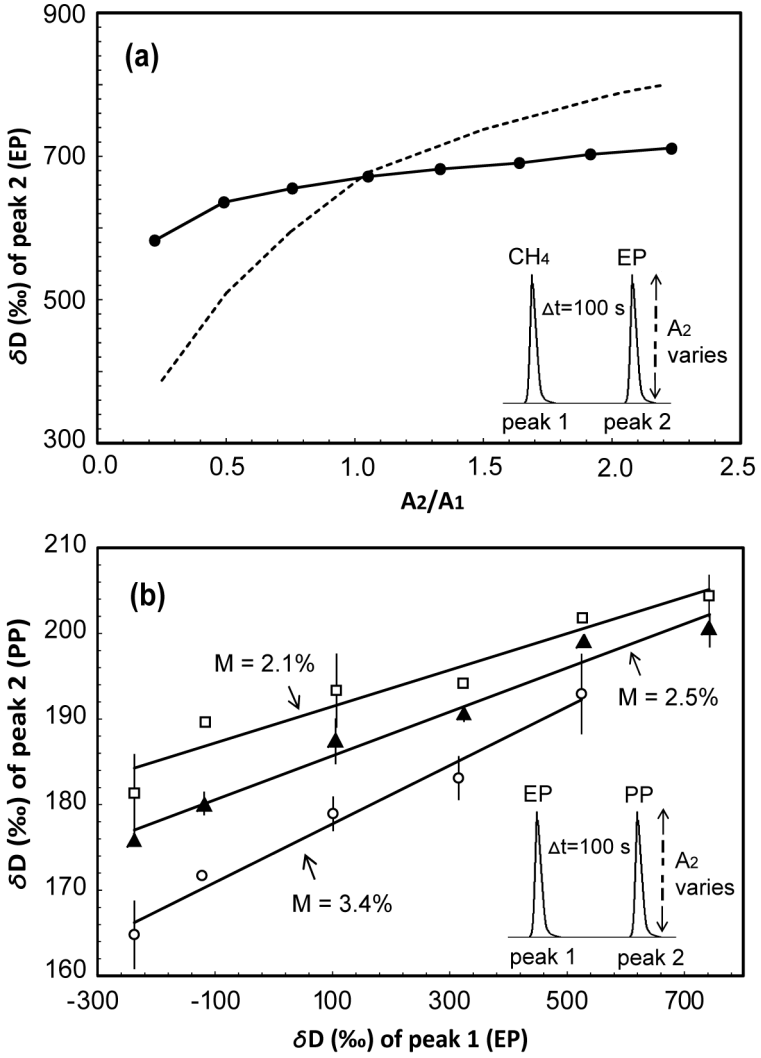

Figure 4-4. Dependence of isotopic memory on analyte abundance. (a) Changing abundance of peak 2 with constant δ^2H value (exp. G). (b) Changing δ^2H values of peak 1 for three different A_2/A_1 ratios. ○, exp. H (A_2/A_1 = 0.67); ▲, exp. I (A_2/A_1 = 1.24); □, exp. J (A_2/A_1= 1.90). Error bars are standard deviations from duplicate analyses. Symbols are experimental data, dashed line is model result.

4. THEORY AND MODEL SECTION

4.1. Physical basis for memory effects

Numerous physical and chemical mechanisms could lead to isotopic memory effects in GC/P/IRMS systems. The most obvious candidates are those that result in physical transfer of hydrogen from one peak to the next. Alternatively, certain system conditions might systematically change as a result of interactions with organic analytes, such that the conversion or analysis of a given peak is subtly altered by the presence of those preceding it. As a concrete example, pyrolysis of an organic analyte will deposit fresh carbonaceous material within the pyrolysis tube, and might alter its reactivity for some short time span. While such phenomena might lead to the observed changes in δ^2H with Δt or A_2/A_1, they cannot plausibly produce the systematic changes observed between peaks differing only in δ^2H values given that δ^2H changes of several hundred permil represent changes in absolute ^2H content of only a few parts per million. We therefore believe that the observed memory effects are caused primarily by molecule-surface interactions that lead to hydrogen storage and thus hydrogen transfer, specifically: (i) adsorption of hydrogen on surfaces, (ii) absorption of hydrogen into solid materials such as tubing or fittings, and/or (iii) direct isotopic exchange between gas-phase molecules and hydrogen that is covalently bound in solid materials.

Mechanism 3 (direct isotopic exchange) seems most likely to cause memory effects that are localized within the GC system, which represent roughly half of all those observed here. When a highly ^2H-labeled (~98% ^2H) analyte is injected into the GC, the $^2H/^1H$ ratios of all subsequent peaks — even in subsequent chromatograms following extensive bakeout — are substantially increased (A. Sessions, unpublished data). This effect can be reversed only by replacing the analytical column. Surface-bound methyl groups are of course abundant in the stationary phase of the GC column employed here (100% dimethylpolysiloxane) and in the capillaries made of methyl-deactivated fused silica. However, isotopic exchange of C-bound H in gas-phase molecules at temperatures below 300°C has not to our knowledge been previously reported. Very slow isotopic exchange has been reported in condensed (liquid or adsorbed) phases, but only under activation by strong catalysts (Larcher et al., 1986; Sessions et al., 2004). Direct H exchange could occur in the injector, but would affect all analytes equally because they are not yet separated. This could not produce the memory effects observed here, in which the δ^2H value of one peak

depends on that of the previous one. We are thus unable to suggest a specific mechanism to explain the phenomenon. Nevertheless, the observation suggests that there is indeed exchange within the GC column via some unknown mechanism. A systematic comparison of memory associated with stationary phases and analytes of varying chemistry would help to elucidate the mechanism.

In contrast, mechanisms 1 and 2 (adsorption and absorption) are more likely to cause memory effects that are localized in the pyrolysis reactor and associated fittings and tubing. This reactor consists of a narrow-bore, 99.8% alumina tube heated to 1440°C (measured near its midpoint), connected to fused-silica capillary tubing at both ends, through which chromatographic effluents continuously flow. Connections in this system are made with stainless-steel fittings, which can be considered as a potential source for memory. The solubility of hydrogen in Fe has been measured at ~0.03 nmol H_2/g metal at 400 K in equilibrium with 101 kPa H_2 (Sieverts, 1911). The solubility decreases exponentially with temperature and pressure. At typical GC/P/IRMS operating conditions ($10–10^3$ Pa H_2 and < 50 ºC), hydrogen absorption in metal fittings is therefore negligible. Many oxides, including Al_2O_3, SiO_2, and Fe_2O_3, can acquire surface hydroxyl groups from ambient water (Wang et al., 2000) which might then undergo hydrogen exchange with gas-phase H_2. While we have no specific data regarding H_2-OH exchange rates, the equilibration of H_2 with H_2O occurs very slowly at room temperature without Pt catalysts, and takes several days even with them (Coplen et al., 1991). Surface OH groups within the hot alumina pyrolysis tube itself might also be considered. However, these surface hydroxyl groups tend to desorb as water according to the equilibrium $Al_2O_3 + 3H_2O \leftrightarrow 2Al(OH)_3$ at temperatures above 1000°C (Ahn and Rabalais, 1997; Woll, 2004), so the size of this exchangeable reservoir is likely small.

Dissection of used alumina reactor tubes reveals that pyrolysis deposits carbonaceous material over a 5–8 cm length near the upstream end of the tube, while the rest of the tube remains bare. He-atom scattering experiments (Woll, 2004), in which alumina surfaces were exposed to molecular or atomic hydrogen both at room temperature and at 1200 K, show that there is virtually no hydrogen retained on bare surfaces. At room temperature, H_2 molecular adsorption on alumina surfaces is negligible (Nijkamp et al., 2001) while

dissociative adsorption (i.e., as H atoms) is limited by the large bond dissociation energy for H_2 (Woll, 2004). At high temperatures, it is proposed that H atoms adsorb onto the surface as OH species, but then quickly react with other impinging H atoms to form water molecules which desorb. This process can lead to hydrogen etching of the alumina surface, and might contribute to the observed increase in porosity of pyrolysis tubes as they age (Burgoyne & Hayes, 1998; Sessions, 2006). While we are not aware of similar experimental data for hydrogen adsorption on silica surfaces, that process seems equally unlikely for all the same reasons.

Many carbonaceous materials have high gas-storage capacity (i.e., absorption) due to their relatively high porosity. Assuming a typical pore volume of ~0.5 ml/g for activated carbon (Nijkamp et al., 2001), and typical operating conditions for GC/P/IRMS of 1440°C, 1 mg pyrolytic carbon and P_{H2} = 900 Pa, hydrogen storage within the entire pyrolysis reactor would be ~0.06 nmol H. This represents only about 0.1% of the H_2 in a typical analyte peak, and so is unlikely to be a major source of the observed memory effects. In contrast, carbonaceous materials also have a high affinity for surface adsorption of H_2, to an extent that could quantitatively explain the memory effects we observe. We therefore focus specifically on hydrogen adsorption onto graphite surfaces as a model for the processes responsible for isotopic memory in the pyrolysis reactor.

4.2. Hydrogen-graphite interactions

Hydrogen can adsorb onto graphite surfaces in a variety of ways. On the surface of the aromatic plane, adsorption occurs both through molecular or dissociative adsorption. Adsorption enthalpies (ΔE) for these two mechanisms are 0.04 eV (Ghio et al., 1980) and 0.7 eV (Sha and Jackson, 2002; Zecho et al., 2002). Carbon atoms at the truncated edges of the aromatic plane are known to have dangling bonds that can form very strong C-H bonds (ΔE = 4.45 eV) (Atsumi & Iseki, 2000; Kanashenko et al., 1996), while nearby dangling bonds can interact with one another to form a "relaxed" structure which lowers the bond energy by ~1 eV. For carbon atoms at the edge of interstitial loops and in-plane defects,

this relaxation is prevented by the surrounding carbon lattice. ΔE for hydrogen adsorption at relaxed and unrelaxed edge carbon atoms can thus be estimated to be 2.4 eV (weak sites) and 4.4 eV (strong sites), respectively (Kanashenko et al., 1996).

Fig. 4-5 shows the Raman spectrum of carbonaceous material recovered from a used pyrolysis tube. The band of highest frequency (1580 cm^{-1}) is the G band corresponding to stretching vibrations in aromatic layers. The 1350 cm^{-1} band (D1 band) is attributed to in-plane defects and heteroatoms, and a weak wide band at 1500 cm^{-1} (D3 band) is attributed to defects outside the plane of aromatic layers (e.g., tetrahedral units; Beyssac, 2003). They indicate that the pyrolytic carbonaceous material is composed of poorly organized aromatic sheets and tetrahedral fragments that expose abundant edges and in-plane defects, potential sites for hydrogen adsorption.

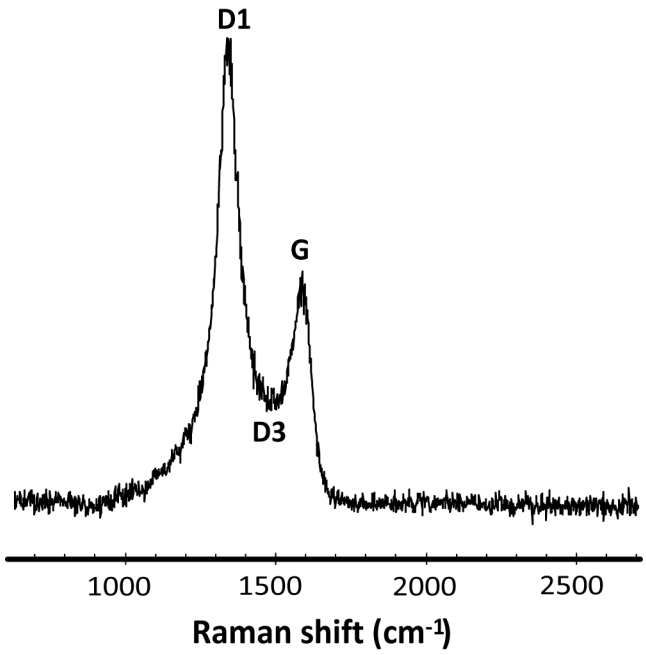

Figure 4-5. Raman spectrum of pyrolytic carbon

To evaluate the possibility that hydrogen adsorption produces isotopic memory effects, we first calculate the equilibrium surface coverage (θ, the ratio of occupied to total adsorption sites) as a function of adsorption enthalpy based on a Langmuir Isotherm (Billing, 2000; Fig. 4-6). This relationship is in accordance with hydrogen-graphite

adsorption experiments at high temperatures (600–1800K) and a wide range of hydrogen pressures (0.66~10^5 Pa; Kanashenko et al., 1996; Atsumi and Iseki, 2000). The calculation is presented in the Appendix.

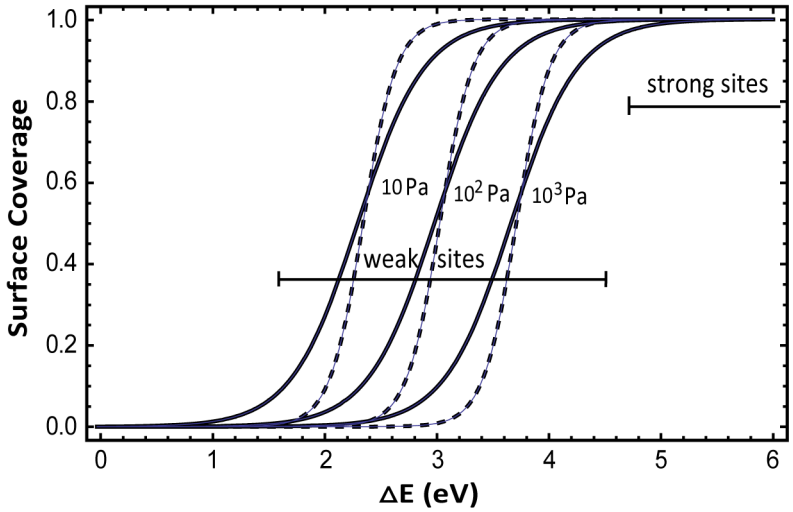

Figure 4-6. Calculated surface coverage (θ) vs. adsorption enthalpy (ΔE) at 1440ºC and P_{H2} = 10, 10^2, and 10^3 Pa. Solid lines are for dissociative adsorption; dashed lines are for molecular adsorption.

Three characteristic situations can be identified from Fig. 4-6. When ΔE > 4.5 eV, corresponding to strong adsorption sites at in-plane defects and interstitial loops, the sites are nearly fully occupied regardless of P_{H2}. In this case, the amount of hydrogen adsorbed on these sites will remain constant even as each analyte peak passes and P_{H2} fluctuates significantly. But while there will be no net transfer of hydrogen, $^2H/^1H$ exchange between adsorbed and gaseous hydrogen will still proceed at the desorption rate, $t_{1/2}$ estimated via the Arrhenius equation to be $>10^0$ s. Kinetic isotope effects accompanying this exchange are expected to be negligible at such a high temperature. Equilibrium isotope effects may well exist, but they would affect all peaks equally and thus could not contribute to memory.

Hydrogen adsorbed to strong sites can thus be viewed as a pool of constant size but varying isotopic composition. It is continuously equilibrating with H_2 in the gas phase, but on a timescale similar to that of the chromatographic separation. It will initially be in isotopic equilibrium with background hydrogen, but as an analyte peak passes through the

reactor the $^{2}H/^{1}H$ ratio of the adsorbed hydrogen pool will shift towards that of the analyte. If a second peak arrives before the adsorbed pool has fully re-equilibrated with background, then a memory effect will be induced. The size of the adsorbed pool, and thus the resulting memory effect, is governed by the amount and structure of carbonaceous material in the pyrolysis reactor.

The second situation arises when 1.5 eV < ΔE < 4.5 eV, corresponding to weak adsorption sites at relaxed edges of the graphite plane. In this case, equilibrium surface coverage varies substantially and rapidly with P_{H2}. There will be net transfer of hydrogen into the adsorbed pool when an analyte peak is present and P_{H2} is high, followed by net transfer of hydrogen into the gas phase once that peak passes. The speed of this equilibration (10^{-7} s < $t_{1/2}$ < 10^{0} s) precludes it from producing memory effects that can span tens of seconds, but it can result in peak tailing. An analogous situation familiar to chromatographers occurs when analytes are weakly and reversibly adsorbed onto bare silica or metal surfaces. The third situation, in which ΔE < 1.5 eV, includes molecular and dissociative adsorption onto aromatic planes. Hydrogen adsorption on these sites is negligible at 1440ºC, and can be ignored.

In a real pyrolysis reactor, there is a temperature gradient from GC oven temperature at the inlet up to 1440°C in the middle. Because pyrolytic conversion of organic compounds to H_2 is incomplete at the lower temperatures (Burgoyne and Hayes, 1998), as analytes traverse this zone they may deposit partial pyrolysis products on the reactor walls. H atoms on these organic fragments are conceptually equivalent to chemisorbed H. They can undergo exchange with gaseous H_2 according to the same mechanisms, but with slower kinetics due to the lower temperatures. This process might also explain the extra memory effect observed when the reference H_2 gas instead of CH_4 is used as peak 2 (Exp. D), if the temperature in this zone is sufficient to promote exchange with H_2 but insufficient to pyrolyze CH_4. Hydrogen exchange in the form of CH_4 molecules seems unlikely because the adsorption heat of CH_4 on graphite is only 0.14 eV (Albesa et al., 2008), resulting in negligible surface coverage at the relevant temperatures.

4.3. Model of memory effects

As the preceding discussion demonstrates, only strong-site adsorption is capable of producing memory effects spanning tens of seconds. To understand whether the experimentally observed memory effects can be quantitatively described by this phenomenon, we constructed a numerical model that simulates hydrogen isotopic exchange between gas-phase and adsorbed hydrogen. A detailed description of the model algorithm and choice of relevant parameters is provided in the Appendix. Model results indicate that memory effects due to changes in δ^2H between pairs of otherwise identical peaks (i.e., exp. A and B) can be fully explained by strong-site adsorption (dashed line in Fig. 4-2). Parameters used in the model were tuned to match the data from exp. B, and the same values were then used for simulation of subsequent experiments. So while the near-perfect agreement of model and experiment in Fig. 4-2 is the result of model tuning, the prediction of a linear dependence of the δ^2H value for peak 2 on the δ^2H value of peak 1 is robust regardless of chosen parameters.

In model simulations of experiments in which Δt varies (Fig. 4-3 a & b), the model produces a drop in δ^2H values for peak 2 with increasing Δt as in the experiments, but the change is much faster. The rate of change in the model results is controlled primarily by the choice of desorption rate constant and adsorption pool size, which are derived from published data for pyrolytic carbon (Kanashenko et al., 1996). Our model could closely replicate the shape of the experimental data in Fig. 4-3, but doing so requires an unrealistically strong C-H bond dissociation energy (e.g., > ~5 eV), resulting in slow desorption, and a huge number of strong adsorption sites in the pyrolytic carbon (concentration > 500 appm). Similarly, model simulations of experiments in which analyte abundance varies (Fig. 4-4a) reproduce the general trend of increasing δ^2H value for peak 2 with increasing A_2/A_1 ratio, but rise more rapidly than the observations. Modeled δ^2H of peak 2 was enriched by 430‰ over a 10-fold increase of analyte abundance, which is much more sensitive than the observation. In this case, the rate of rise in δ^2H value of peak 2 with changing A_2/A_1 ratio depends mainly on the choice of background δ^2H value. A background δ^2H value of +250‰ yields model results that accurately reproduce the slope

of experimental data (not shown), but this value is unrealistically high for the true hydrogen background. Possible causes for these discrepancies are discussed below.

5. DISCUSSION

5.1. Model simulations of experimental data

Our model for hydrogen adsorption on graphite reproduces many of the general features of the experimental data, suggesting that this mechanism is an important component of isotopic memory in GC/P/IRMS systems. There are, however, significant differences in detail. This is perhaps not surprising given that many other processes are not accounted for in the model. For example, hydrogen exchange within the GC system, which accounts for up to half of the memory affecting organic analytes, is not considered and the kinetic characteristics of this process are essentially unknown. Moreover, the carbonaceous material lining the pyrolysis reactor is a 3-dimensional structure and so diffusion of H_2 into and out of the carbonaceous material will affect exchange rates. Reported values of the hydrogen diffusion coefficient in carbonaceous materials range from 10^{-12} to 10^{-17} m^2/s at 1440˚C (Atsumi, 2003). Assuming a thickness for the pyrolytic carbon to be 10 μm, the characteristic diffusion time for H_2 will be minutes to years. This process may explain much of the difference between model and experiment when Δt is varied (e.g., Fig. 4-3), wherein observed memory effects are sustained much longer than predicted by model simulations. Indeed, our model most accurately simulates these experiments using unrealistically slow desorption rates. Additionally, hydrogen exchange near the ends of the pyrolysis reactor that are <<1440°C might also result in slower kinetics.

Other potential differences between model and experiment include the pressure dependence of several hydrogen seclusion mechanisms, such as gas storage within porosity or molecular flow through microfractures in the pyrolysis tube. Because P_{H2} varies significantly with peak size, these effects may partially explain differences between model and observation when A_2/A_1 abundance ratios are varied (Fig. 4-4a). Finally, the model assumes background hydrogen with fixed abundance and δ^2H value. Background hydrogen

likely derives from a combination of column bleed, water in the carrier gas and/or air leaks, and a slow release of absorbed hydrogen from wall materials, all of which are likely to vary over the course of a single GC analysis.

5.2. Impact and mitigation of memory effects in complex samples

The number of different parameters contributing to isotopic memory in GC/P/IRMS systems makes it impractical to predict, or correct for, memory in all but the simplest of chromatograms. For complex chromatograms with closely spaced peaks, uncertainty contributed by memory effects can be approximately estimated as follows. Assuming an average value for M of 4%, the added error in the δ^2H value of each peak will be roughly 0.04 times the difference in δ^2H value between that peak and the preceding peak. Differences in peak spacing, height, background size and composition, pyrolysis tube age, and other factors will all affect this estimate, but are second-order effects. Given a typical analytical precision for δ^2H values of ~4‰, we suggest that — as a rule of thumb — memory effects will become significant when peaks vary in δ^2H values by more than 100‰. This threshold is frequently exceeded when comparing, for example, *n*-alkyl and isoprenoid lipids (Sessions et al., 1999), or when measuring ^2H-enriched samples against natural abundance standards (Sessions et al., 2002; Zhang & Sachs, 2007).

Our results further suggest several ways in which the impact of isotopic memory can be mitigated. First, decreasing the amount of pyrolytic carbon in the reactor, either by replacing the reactor frequently or by heating in an oxidizing atmosphere, should help minimize memory. However, this needs to be balanced against the necessity of "conditioning" new pyrolysis reactors to achieve quantitative pyrolysis (Bilke & Mosandl, 2002). Second, we emphasize the importance of comparing unknown analytes to reference peaks of similar δ^2H value to minimize systematic errors due to memory. This recommendation is currently problematic due to the lack of ^2H-enriched standards. We are therefore making nine of our ^2H-enriched fatty acid ester standards, with δ^2H values ranging from +1.5 to +552‰, available to the community at nominal cost. They may be

obtained from Arndt Schimmelmann at Indiana University (http://php.indiana.edu/~aschimme/hc.html). Third, the insertion of peaks of constant δ^2H value into a chromatogram — either by coinjection of standards or via an organic reference gas such as described here — will help to stabilize the isotopic composition of pools of exchangeable hydrogen that lead to memory effects. This procedure does not reduce the amount of memory, but does help to ensure a more consistent offset due to memory. In samples where differences in δ^2H between analytes are more important than absolute δ^2H values, this approach will be beneficial. Finally, our model simulations suggest that a higher hydrogen background will serve a similar function, rapidly returning the pool of exchangeable hydrogen to a constant $^2H/^1H$ ratio. We have not yet tested this prediction.

A further difficulty is encountered in the common "normalization" procedure used to ensure that δ^2H data from different laboratories are comparable. For example, the procedure recommended by Sessions et al. (2001a) is based on measuring a series of 15 *n*-alkanes with δ^2H values ranging from -46‰ to -260‰. However, because these materials were obtained from natural sources, they tend to follow a pattern in which even carbon numbers are ^2H-enriched (near -50‰), and odd carbon numbers are ^2H-depleted (< −120‰). The resulting chromatogram thus has large differences in δ^2H values between most pairs of adjacent peaks. Memory effects will tend to reduce measured differences in δ^2H values between these peaks, leading to the appearance of scale compression. Over 500 analyses of this *n*-alkane standard in our laboratory over the past four years reveal a systematic pattern in which the slope and intercept of the normalization line (calculated as the regression of measured δ^2H on "true" δ^2H) systematically decrease from ~1 to < 0.92 and from ~2 to < -10, respectively, as the pyrolysis reactor ages. A simple calculation estimating the impact of memory effects on these analyses indicates that the trend can derive almost entirely from isotopic memory, rather than true scale compression. We therefore recommend that the normalization procedure of Sessions et al. (2001a) not be employed as described. A simple and robust strategy to separately assess memory effects and scale compression is currently lacking.

6. CONCLUSIONS

We have conclusively demonstrated the existence of memory effects in compound-specific $^{2}H/^{1}H$ analyses of organic analytes by GC/P/IRMS. The magnitude of these effects can be quantified as the apparent change in $\delta^{2}H$ value of a given peak relative to the change in $\delta^{2}H$ value of the preceding peak ($\Delta\delta_2/\Delta\delta_1$), and is typically 1–5%. In general, memory decreases with increased time separation between peaks and with increased analyte abundance. Roughly half of this memory appears to originate within the GC system itself, while the other half arises during the pyrolytic conversion of analytes to H_2. Adsorption of hydrogen on carbonaceous material lining the pyrolysis reactor is likely an important mechanism in this latter source of memory. A model for hydrogen adsorption on graphite sites can reproduce many, though not all, of our experimental data using experimentally relevant parameters. As a rule of thumb, these memory effects become significant when adjacent peaks differ in $\delta^{2}H$ value by >100‰. The results emphasize the need to match analytes with reference standards of similar $\delta^{2}H$ value to minimize systematic biases due to isotopic memory effects.

ACKNOWLEDGEMENTS

The authors acknowledge Magnus Eek and Chao Li for experimental assistance and helpful discussions, and Arndt Schimmelmann for analyses of ^{2}H-enriched standards by dual-inlet IRMS. We thank George Rossman for access to the Raman Spectrometer, and Nathan Dalleska for assistance analyzing ^{2}H-enriched standards by GC/MS. This work was supported by grants to ALS from the Petroleum Research Fund of the ACS (PRF#43746-G2) and from NSF (EAR-0645502).

REFERENCES

Ahn J. and Rabalais J. W. (1997) Composition and structure of the Al_2O_3 {0001}-(1x1) surface. Surf. Sci. **388**, 121–131.

Albesa A. G., Llanos J. L. and Vicente J. L. (2008) Comparative Study of Methane Adsorption on Graphite. Langmuir **24**, 3836–3840.

Atsumi H. (2003) Mechanism of hydrogen trapping and transport in carbon materials. Phys. Scripta **T103**, 77–80.

Atsumi H. and Iseki M. (2000) Hydrogen absorption process into graphite and carbon materials. J. Nucl. Mater. **283**, 1053–1056.

Begley I. S. and Scrimgeour C. M. (1997) High-precision delta H-2 and delta O-18 measurement for water and volatile organic compounds by continuous-flow pyrolysis isotope ratio mass spectrometry. Anal. Chem. **69**, 1530–1535.

Beyssac O. (2003) On the characterization of disordered and heterogeneous carbonaceous materials by Raman spectroscopy. Spectrochim. Acta Part A, **59**, 2267–2276.

Bigeleisen J., Perlman M. L. and Prosser H. C., (1952) Conversion of hydrogenic materials to hydrogen for isotopic analysis. Anal. Chem. **24**, 1356–1357.

Bilke S. and Mosandl A. (2002) Measurements by gas chromatography/pyrolysis/mass spectrometry: fundamental conditions in H-2/H-1 isotope ratio analysis. Rapid Commun. Mass Sp. **16**, 468–472.

Billing G. D. (2000) *Dynamics of molecular surface interactions.* John Willy & Sons, Inc.

Burgoyne T. W. and Hayes J. M., (1998) Quantitative production of H-2 by pyrolysis of gas chromatographic effluents. Anal. Chem. **70**, 5136–5141.

Chikaraishi Y., Suzuki Y. and Naraoka H. (2004) Hydrogen isotopic fractionations during desaturation and elongation associated with polyunsaturated fatty acid biosynthesis in marine macroalgae. Phytochem. **65**, 2293–2300.

Coplen T. B., Wildman J. D. and Chen J. (1991) Improvements in the gaseous-hydrogen water equilibration technique for hydrogen isotope ratio analysis. Anal. Chem. **63**, 910–912.

Ghio E., Mattera L., Salvo C., Tommasini F. and Valbusa U. (1980) Vibrational-spectrum of h and d on the (0001) graphite surface from scattering experiments. J. Chem. Phys. **73**, 556–561.

Hilkert A. W., Douthitt C. B., Schluter H. J. and Brand W. A. (1999) Isotope ratio monitoring gas chromatography mass spectrometry of $^{2}H/^{1}H$ by high temperature conversion isotope ratio mass spectrometry. Rapid Commun. Mass Sp. **13**, 1226–1230.

Hor K., Ruff C., Weckerle B., Konig T. and Schreier P. (2001) Flavor authenticity studies by H-2/H-1 ratio determination using on-line gas chromatography pyrolysis isotope ratio mass spectrometry. J. Agricul. Food Chem. **49**, 21–25.

Hor K., Ruff C., Weckerle B., Konig T. and Schreier P. (2001) H-2/H-1 ratio analysis of flavor compounds by on-line gas chromatography pyrolysis isotope ratio mass spectrometry (HRGC-P-IRMS): citral. Flav. and Frag. J. **16**, 344–348.

Kanashenko S. L., Gorodetsky A. E., Chernikov V. N., Markin A. V., Zakharov A. P., Doyle B. L. and Wampler W. R. (1996) Hydrogen adsorption on and solubility in graphites. J. Nucl. Mater. **237**, 1207–1212.

Larcher A. V., Alexander R., Rowland S. J. and Kagi R. I. (1986) Acid catalysis of alkyl hydrogen-exchange and configurational isomerization-reactions — acyclic isoprenoid acids. Org. Geochem. **10**, 1015–1021.

Li M. W., Huang Y. S., Obermajer M., Jiang C. Q., Snowdon L. R. and Fowler M. G. (2001) Hydrogen isotopic compositions of individual alkanes as a new approach to petroleum correlation: case studies from the Western Canada Sedimentary Basin. Org. Geochem. **32**, 1387–1399.

Morrison D. J., Dodson B., Preston T. and Weaver L. T. (2001) Rapid quality control analysis of C-13-enriched substrate synthesis by isotope ratio mass spectrometry. Rapid Commun. Mass Sp. **15**, 1279–1282.

Nijkamp M. G., Raaymakers J. E., van Dillen A. J. and de Jong, K. P. (2001) Hydrogen storage using physisorption — materials demands. Appl. Phys. A: Mater. Sci. Proc. **72**, 619–623.

Ricci M. P., Merritt D. A., Freeman K. H. and Hayes J. M. (1994) Acquisition and processing of data for isotope-ratio-monitoring mass-spectrometry. Org. Geochem. **21**, 561–571.

Sauer P. E., Eglinton T. I., Hayes J. M., Schimmelmann A. and Sessions A. L. (2001) Compound-specific $^{2}H/^{1}H$ ratios of lipid biomarkers from sediments as a proxy for environmental and climatic conditions. Geochim. Cosmochim. Acta **65**, 213–222.

Scrimgeour C. M., Begley I. S. and Thomason M. L. (1999) Measurement of deuterium incorporation into fatty acids by gas chromatography isotope ratio mass spectrometry. Rapid Commun. Mass Sp. **13**, 271–274.

Sessions A. L. (2006) Isotope-ratio detection for gas chromatography. J. Separ. Sci. **29**(12), 1946–1961.

Sessions A. L., Burgoyne T. W. and Hayes J. M., (2001) Correction of H-3(+) contributions in hydrogen isotope ratio monitoring mass spectrometry. Anal. Chem. **73**, 192–199.

Sessions A. L., Burgoyne T. W. and Hayes J. M. (2001) Determination of the H-3 factor in hydrogen isotope ratio monitoring mass spectrometry. Anal. Chem. **73**, 200–207.

Sessions A. L., Burgoyne T. W., Schimmelmann A. and Hayes J. M. (1999) Fractionation of hydrogen isotopes in lipid biosynthesis. Org. Geochem. **30**, 1193–1200.

Sessions A. L. and Hayes J. M. (2005) Calculation of hydrogen isotopic fractionations in biogeochemical systems. Geochim. Cosmochim. Acta **69**, 593–597.

Sessions A. L., Jahnke L. L., Schimmelmann A. and Hayes J. M. (2002) Hydrogen isotope fractionation in lipids of the methane-oxidizing bacterium Methylococcus capsulatus. Geochim. Cosmochim. Acta **66,** 3955–3969.

Sessions A. L., Sylva S. P., Summons R. E. and Hayes J. M. (2004) Isotopic exchange of carbon-bound hydrogen over geologic timescales. Geochim. Cosmochim. Acta **68**, 1545–1559.

Sha X. W. and Jackson B. (2002) First-principles study of the structural and energetic properties of H atoms on a graphite (0001) surface. Surf. Sci. **496**, 318–330.

Sieverts A. (1911) The solubility of hydrogen in copper, iron and nickel. Zeitschrift Fur Physikalische Chemie — Stochiometrie Und Verwandtschaftslehre. **77,** 591–613.

Tobias H. J. and Brenna J. T. (1997) On-line pyrolysis as a limitless reduction source for high-precision isotopic analysis of organic-derived hydrogen. Anal. Chem. **69**, 3148–3152.

Wang X. G., Chaka A. and Scheffler M. (2000) Effect of the environment on alpha-Al2O3 (0001) surface structures. Phys. Rev. Lett. **84**, 3650–3653.

Woll C. (2004) Hydrogen adsorption on metal oxide surfaces: a reinvestigation using He-atom scattering. J. Phys. — Conden. Matter, **16**, S2981–S2994.

Xiong Y. Q., Geng A. S., Pan C. C., Liu D. Y. and Peng P. A. (2005) Characterization of the hydrogen isotopic composition of individual n-alkanes in terrestrial source rocks. Appl. Geochem. **20**, 455–464.

Zecho T., Guttler A., Sha X. W., Jackson B. and Kuppers J. (2002) Adsorption of hydrogen and deuterium atoms on the (0001) graphite surface. J. of Chem. Phys. **117**, 8486–8492.

Zhang Z. and Sachs J. P. (2007) Hydrogen isotope fractionation in freshwater algae: I. Variations among lipids and species. Org. Geochem. **38**, 582–608.

APPENDIX

1. Model description and typical output

The reactor is modeled as a linear series of discrete gas parcels moving past and interacting with a single, stationary box representing surface adsorption sites in graphitic carbon (Fig. 4-A1). Each gas parcel equilibrates with the graphite surface for one residence time (τ, typically 0.5 s), after which the gas parcels shift sequentially and the next gas parcel equilibrates. The molar amount and isotopic composition of hydrogen in the graphite phase are retained from one gas parcel to the next. Our model is thus conceptually similar to simple models of chromatographic partitioning between mobile and stationary phases (Peters, 1974). Concentrations and isotopic compositions are assumed to be homogeneous within each gas parcel, and within the graphite "box". This approach is justified because at a typical GC flow of 1.2–1.5 ml/min, each gas parcel takes < 0.5 s to go through a pyrolysis reactor of 30 cm length, in which the pyrolytic carbon covers only 5–8 cm near the upstream end. Thus the timescale for interaction between H_2 gas and adsorption sites within the reactor is much shorter than typical peak width (~20 s). For similar reasons, diffusion within and between gas parcels and the graphite surface is ignored in the model. Potential consequences of these simplifications are discussed in the paper.

In the model, the molar amount of hydrogen (n) and fractional deuterium abundance ($F = [^2H]/[^2H+^1H]$) are tracked for each gas parcel (n_g, F_g) and for the graphite surface (n_a, F_a). n_g is calculated from the product of the parcel volume (each equal to the pyrolysis reactor volume) and P_{H2} due to analytes plus background hydrogen. These parameters can be adjusted to simulate GC peaks of varying size, shape, and temporal separation superimposed on a background of fixed size. F_g is calculated by mass balance from the stipulated δ^2H values of the analyte (assuming no chromatographic separation of isotopes) and background hydrogen. The number of total graphite adsorption sites (N_a) is constant in the model, and is calculated from typical parameters for graphite as described in the Methods section. As each gas parcel equilibrates with the graphite surface, partitioning of both ^1H and ^2H between adsorbed and gaseous phases is calculated as a function of residence time (τ) using one of two algorithms, depending on whether the model is

simulating weak or strong adsorption sites on the graphite, as described below. Adsorptions on the two types of sites are not modeled simultaneously. We assume no isotopic fractionation during the partitioning of H_2 between adsorbed and gaseous phases.

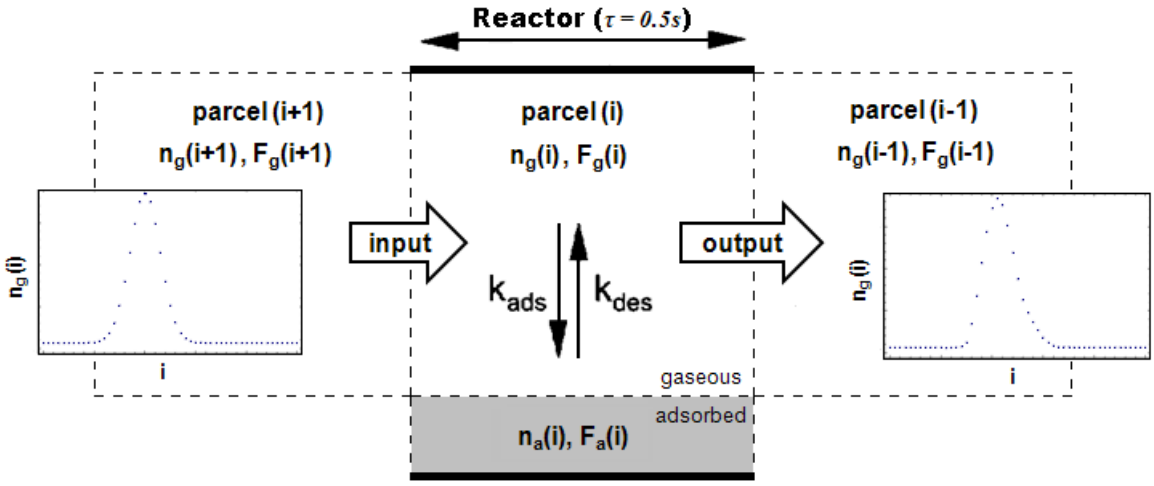

Figure 4-A1. Schematic description of the model, showing the equilibration of discrete gas parcels with the graphite surface pool. Also shown are sample input and output chromatograms, plotted as $n_g(i)$ vs. i.

The model produces two characteristic types of results depending on whether strong or weak adsorption sites are modeled. In the case of strong adsorption sites, graphite surface coverage remains virtually complete and so n_g and n_a do not change during equilibration. The result is that the shape of the chromatographic peak changes very little, while its isotopic composition (and that of the following background) changes substantially as a result of isotopic exchange with the pool of adsorbed hydrogen (Fig. 4-A2). In contrast, for weak adsorption sites the surface coverage of graphite changes with varying P_{H2} across a chromatographic peak, but quickly re-equilibrate with the background hydrogen once the peak has passed. As a result, chromatographic peaks are both broadened and delayed, while their isotopic compositions after background subtraction change very little (Fig. 4-A3). In effect, weak adsorption sites serve as a source of peak broadening but not of isotopic memory.

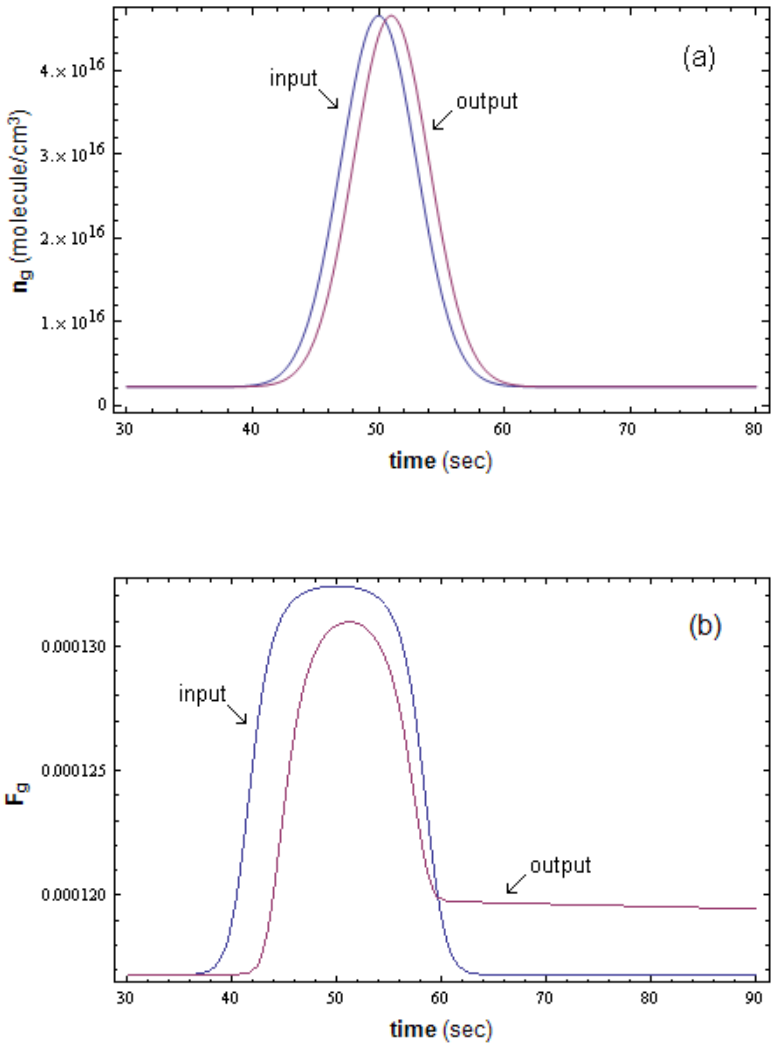

Figure 4-A2. Simulated input and output trace of (a) H_2 concentration and (b) $^2H/^1H$ ratio for strong sites

The chromatograms produced by the model were processed according to Ricci et al. (1994) and Sessions (2006) to obtain δ^2H values for each peak. Specifically, peak integration intervals were evaluated based on the mass-2 chromatogram and then applied to the mass-3 chromatogram. Background was determined by the point immediately before the start of the peak and was then subtracted on a point-by-point basis across the integration interval. Because the model does not simulate the chromatographic process or the formation of H_3^+, no correction for isotope chromatography or isobaric interference is necessary. Finally, the integrated mass-2/mass-3 ratio was normalized to that of a peak

(δ^2H = -148‰) introduced 100 s before the first analyte peak, simulating the use of the CH_4 reference peak in experimental measurements.

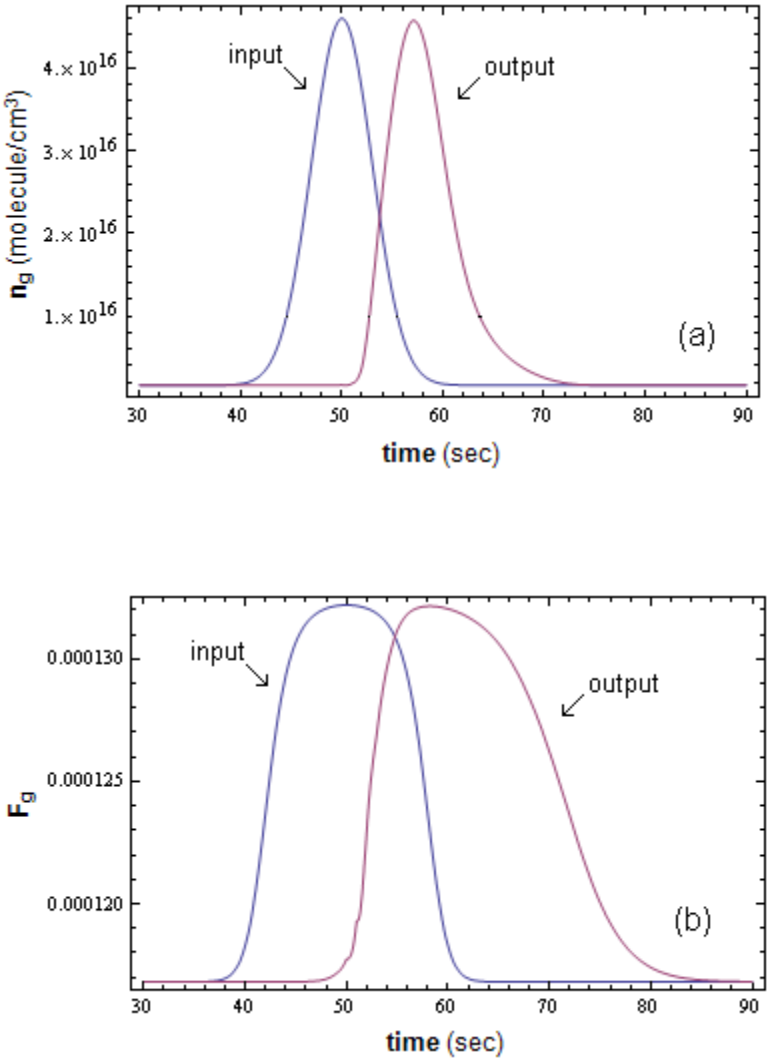

Figure 4-A3. Simulated input and output trace of (a) H_2 concentration and (b) $^2H/^1H$ ratio for weak sites

2. Mathematical derivation of partitioning algorithms

A mathematical description for partitioning of hydrogen between the gas phase and adsorption on graphite is derived from statistical thermodynamics as follows. Assuming no

chemical reactions in the vapor phase or on graphite surfaces, and that adsorption enthalpy is independent of surface coverage, the amount of adsorbed hydrogen at equilibrium obeys the Langmuir Isotherm. Equilibrium surface coverage for molecular adsorption (θ_m) and dissociative adsorption (θ_d) is expressed as:

$$\theta_m = \frac{KP}{KP + 1} \qquad (4 - \text{A1a})$$

$$\theta_d = \frac{\sqrt{KP}}{\sqrt{KP} + 1} \qquad (4 - \text{A1b})$$

where P is H_2 partial pressure at equilibrium and K is the equilibrium constant ($K = k_{ads}/k_{des}$) (Billing, 2000). Because K reflects equilibrium partitioning, it can be calculated from statistical thermodynamics apart from reaction kinetics (Fowler, 1935; Fowler, 1936; Hoinkis, 1991). For the dissociative adsorption H_2 + 2S ↔ 2S-H (where S denotes a generic surface site), the value of K is given by (Hoinkis, 1991)

$$K = h^3(2\pi m k_B T)^{-\frac{3}{2}}\left(\frac{kT}{P}\right)^{-1}\left(\frac{T}{\sigma\theta_{rot}}\right)^{-1}\frac{(1 - e^{-h\nu_H/kT})}{(1 - e^{-h\nu_{SH}/kT})^2}e^{-\frac{\Delta E}{kT}} \qquad (4 - \text{A2})$$

where h and k_B are Planck and Boltzmann constants, T is the temperature, m is molecular mass, θ_{rot} is the characteristic temperature of rotation (θ_{1H1H} = 88 K, θ_{1H2H} = 66 K; CCCBDB, 2006), σ is the symmetry factor (σ_{1H1H} = 2, σ_{1H2H} = 1), and E is the adsorption enthalpy. The parameters υ_H and υ_{SH} represent the vibrational frequencies for gaseous H_2 molecules (υ_{1H1H} = 4401 cm^{-1}, υ_{1H2H} = 3813 cm^{-1}; CCCBDB, 2006) and for surface-bound hydrogen, respectively. The value of υ_{SH} for normal and parallel vibrations is reported as 2900 to 1450 cm^{-1} for chemisorbed hydrogen on pyrolytic graphite (Zecho et al., 2002) and 1000 to 2000 cm^{-1} for hydrogen adsorbed on various surface sites of copper (Lee & Plummer, 2002; McCash et al., 1989). Since the calculation is relatively insensitive to υ_{SH}, average frequencies were adopted. K for molecular adsorption has the same formulation, except that the change in vibrational entropy is assumed to be negligible. Combining eqns. 4-A1 and 4-A2, the equilibrium surface coverage can be calculated as a function of temperature, pressure, and adsorption enthalpy (Fig. 4-6 in the paper). Two characteristic

regions are recognized. When adsorption enthalpy is high ($\Delta E > 4.5$ eV, corresponding to **"strong" adsorption sites**), surface coverage is virtually complete regardless of P_{H2}. When adsorption enthalpy is lower ($1.4 < \Delta E < 4.5$ eV, corresponding to **"weak" adsorption sites**), surface coverage varies as a function of P_{H2}. Because of these different behaviors, the two types of adsorption sites are modeled separately.

Our model seeks to reproduce time-dependent equilibration of gas and adsorbed phases, so the kinetics of this exchange must also be considered. According to Langmuir theory, adsorption is a second-order process and its rate is proportional to the number of gaseous molecules and number of unoccupied adsorption sites:

$$\frac{dn_a}{dt} = k_{ads} n_g (1 - \theta) N_a \qquad (4 - \text{A3})$$

where θ is the fractional surface coverage at time t. The desorption process is considered as a first-order process with the rate proportional to the number of occupied surface sites:

$$-\frac{dn_a}{dt} = -k_{des} \theta N_a \qquad (4 - \text{A4})$$

k_{ads} (s^{-1}molecule^{-1})and k_{des} (s^{-1}) are the adsorption and desorption rate constants. Setting eqn. 4-A3 equal to Eq. 4-A4, the fractional surface coverage at equilibrium can be obtained as (Billing, 2000):

$$\theta_e = \frac{k_{ads} n_g}{k_{ads} n_g + k_{des}} \qquad (4 - \text{A5})$$

At any time, the molecular adsorption (f_{ads}) and desorption (f_{des}) fluxes are given by Eqs. 4-A3 and 4-A4, and the corresponding adsorption and desorption fluxes of ^{2}H are simply $F_g f_{ads}$ and $F_a f_{des}$, respectively. The net transfer of ^{2}H between gas phase and adsorbed phase is then given by:

$$F_g f_{ads} + F_a f_{des} = F_g k_{ads} n_g (1-\theta) N_a - F_a k_{des} \theta N_a \qquad (4-\text{A6})$$

where a positive value represents a net transfer of ^{2}H into the adsorbed phase, and negative value represents a net transfer into the gas phase. Alternatively, the net change in ^{2}H content of the adsorbed phase can be written as the derivative

$$\frac{d(F_a n_a)}{dt} = n_a \frac{dF_a}{dt} + F_a \frac{dn_a}{dt} \qquad (4-\text{A7})$$

Eqs. 4-A6 or 4-A7 could in theory be evaluated directly. Unfortunately, the calculation of k_{ads} contains a number of significant uncertainties, so we adopted several further simplifications.

(i) Strong adsorption sites. For strong adsorption sites, surface sites are nearly saturated regardless of P_{H2}. Thus n_a is constant and $dn_a/dt = 0$. Combining 4-A6 and 4-A7, we get:

$$\frac{d(F_a n_a)}{dt} = n_a \frac{dF_a}{dt} = F_g k_{ads} n_g (1-\theta) N_a - F_a k_{des} \theta N_a \qquad (4-\text{A8})$$

which, by substituting $n_a = N_a \times \theta$, can be simplified to

$$\frac{dF_a}{dt} = F_g k_{ads} n_g \left(\frac{1}{\theta} - 1\right) - F_a k_{des} \qquad (4-\text{A9})$$

Although the pool of adsorbed hydrogen equilibrates very slowly with H_2 in the gas phase due to the large desorption energy ($t_{1/2} > 10^0$ s), both θ_e and θ are very close to 1 and thus $\theta \approx \theta_e$. Therefore Eq. 4-A5 can be applied to further simplify the above equation to:

$$\frac{dF_a}{dt} = k_{des}\left(F_g - F_a\right) \qquad (4-\text{A10})$$

Following a similar approach, the net change in fractional abundance of ^{2}H in the gas phase

can be obtained as

$$\frac{dF_g}{dt} = -\frac{n_a}{n_g} k_{des}\left(F_g - F_a\right) \qquad (4-\text{A}11)$$

Combining deferential Eqs. 4-A10 and 4-A11, F_g and F_a can be solved as functions of time:

$$F_g(t) = \frac{\left(F_g^0 - F_a^0\right)n_a}{n_a + n_g} e^{-k_{des}\left(1+\frac{n_a}{n_g}\right)t} + \frac{F_g^0 n_g + F_a^0 n_a}{n_g + n_a} \qquad (4-\text{A}12)$$

$$F_a(t) = \frac{\left(F_a^0 - F_g^0\right)n_g}{n_a + n_g} e^{-k_{des}\left(1+\frac{n_a}{n_g}\right)t} + \frac{F_g^0 n_g + F_a^0 n_a}{n_g + n_a} \qquad (4-\text{A}13)$$

in which a superscript "0" reflects the fractional abundance prior to equilibration. In the model, Eqs. 4-A12 and 4-A13 are used to calculate changes in the isotopic composition of gaseous and adsorbed hydrogen at time $t = \tau$. There is no change in the abundance of hydrogen in either phase because — for strong adsorption sites — surface coverage remains complete. The rate of isotopic exchange is controlled by k_{des} and the relative sizes of the two hydrogen pools.

(ii) Weak adsorption sites. For weak adsorption sites, n_a varies substantially with P_{H2} as a result of changing surface coverage, and thus the above simplifications for strong sites don't apply. We therefore took an approach to circumvent Eqs. 4-A6 and 4-A7, based on the kinetic feature of weak adsorption sites. Because the desorption half-life is much shorter than τ, hydrogen exchange between the gas and graphite phases achieves equilibrium almost instantaneously. Thus for each gas parcel we can first calculate the equilibrium partitioning of hydrogen between adsorbed and gas phases (i.e., θ_e) using n_g^0 as input to Eq. 4-A5. The superscript "0" again indicates the value prior to equilibration. In this case, application of Eq. 4-A5 is approximate because n_g^e (i.e., at equilibrium) will vary with θ_e, and vice-versa, as there is a net transfer of hydrogen to or from the adsorbed phase.

Although an exact solution for n_g^e and θ_e is possible through an iterative calculation, such an approach is not warranted here because the errors introduced are negligible given that changes in n_g^0 from one gas parcel to the next are quite small. The new (equilibrium) hydrogen amount in the adsorbed phase can then be computed as $n_a^e = \theta_e N_a$, and the equilibrium amount of hydrogen in the gas phase computed as

$$n_g{}^e = n_g{}^0 + (n_a{}^0 - n_a{}^e) \qquad (4-\text{A14})$$

Calculation of the fractional abundance of ^{2}H in the adsorbed and gas phases is based on isotopic mass balance. The total abundance of ^{2}H in the gas + adsorbed phases must remain constant during equilibration:

$$n_g{}^0 F_g{}^0 + n_a{}^0 F_a{}^0 = n_g{}^e F_g{}^e + n_a{}^e F_a{}^e \qquad (4-\text{A15})$$

Recognizing that $F_g^e = F_a^e$ at equilibrium because we assume no isotopic fractionation during the partitioning, and that $n_g^0 + n_a^0 = n_g^e + n_a^e$, Eq. 4-A15 can be rearranged to give the equation employed by the model:

$$F_g{}^e = F_a{}^e = \frac{F_g^0 n_g + F_a^0 n_a}{n_g{}^0 + n_a{}^0} \qquad (4-\text{A16})$$

REFERENCE

Billing G. D. (2000) *Dynamics of molecular surface interactions*. John Willy & Sons, Inc.

National Institute of Standards and Technology (2006) *Computational Chemistry Comparison and Benchmark DataBase*.

Fowler R. H. (1935) A statistical derivation of Langmuir's adsorption isotherm. *Proceedings of the Cambridge Philosophical Society* **31**, 260–264.

Fowler R. H. (1936) Adsorption isotherms — Critical conditions. *Proceedings of the Cambridge Philosophical Society* **32**, 144–151.

Hoinkis E. (1991) The chemisorption of hydrogen on porous graphites at low-pressure and at elevated-temperature. *J. Nucl. Mater.* **182**, 93–106.

Lee G. and Plummer E. W. (2002) High-resolution electron energy loss spectroscopy study on chemisorption of hydrogen on Cu(111). *Surf. Sci.* **498**, 229–236.

McCash E. M., Parker S. F., Pritchard J. and Chesters M. A. (1989) The adsorption of atomic-hydrogen on cu(111) investigated by reflection-absorption infrared-spectroscopy, electron-energy loss spectroscopy and low-energy electron-diffraction. *Surf. Sci.* **215**, 363–377.

Peters D. G. H. and Hieftje G. M. (1974) *Chemical Separations and Measurements: Theory and Practice of Analytical Chemistry*. W.B. Saunders Company.

Ricci M. P., Merritt D. A., Freeman K. H. and Hayes J. M. (1994) Acquisition and processing of data for isotope-ratio-monitoring mass-spectrometry. *Org. Geochem.* **21**, 561–571.

Sessions A. L. (2006) Isotope-ratio detection for gas chromatography. *J. Separ. Sci*. **29**(12), 1946–1961.

Zecho T., Guttler A., Sha X. W., Jackson B. and Kuppers J. (2002) Adsorption of hydrogen and deuterium atoms on the (0001) graphite surface. *J. Chem. Phys.* **117**, 8486–8492.